8622269

Berger, Philip S.

ANALYSIS OF BED-DUPLICATION FOLDING

University of Cincinnati PH.D. 1986

University
Microfilms
International 300 N. Zeeb Road, Ann Arbor, MI 48106

PLEASE NOTE:

In all cases this material has been filmed in the best possible way from the available copy. Problems encountered with this document have been identified here with a check mark __√__.

1. Glossy photographs or pages ____
2. Colored illustrations, paper or print ____
3. Photographs with dark background ____
4. Illustrations are poor copy ____
5. Pages with black marks, not original copy ____
6. Print shows through as there is text on both sides of page ____
7. Indistinct, broken or small print on several pages __√__
8. Print exceeds margin requirements ____
9. Tightly bound copy with print lost in spine ____
10. Computer printout pages with indistinct print ____
11. Page(s) ________ lacking when material received, and not available from school or author.
12. Page(s) ________ seem to be missing in numbering only as text follows.
13. Two pages numbered ____. Text follows.
14. Curling and wrinkled pages ____
15. Dissertation contains pages with print at a slant, filmed as received ______
16. Other ____

University
Microfilms
International

ANALYSIS OF BED-DUPLICATION FOLDING

A dissertation submitted to the
Division of Graduate Studies and Research
of the University of Cincinnati
in partial fulfillment of the
requirements for the degree of

DOCTOR OF PHILOSOPHY

in the Department of Geology of the
College of Arts and Sciences

August, 1986
by
Philip S. Berger

B.S., University of Maryland, 1976
M.S., West Virginia University, 1978

UNIVERSITY OF CINCINNATI

May 30, 1986

I hereby recommend that the thesis prepared under my supervision by Philip S. Berger

entitled Analysis of Bed-Duplication Folding

be accepted as fulfilling this part of the requirements for the degree of Doctor of Philosophy

Approved by:

ANALYSIS OF BED-DUPLICATION FOLDING

Abstract

John L. Rich introduced the revolutionary concept that many folds in the Appalachian Mountains can be explained as superficial structures formed by passive translation of thrust blocks over ramps in detachment surfaces. The amount of layer-parallel shortening can be negligible in the formation of these bed-duplication folds. Rich primarily was concerned with an explanation for the Powell Valley anticline, in the southern Appalachians, but the essential kinematic features of his model of folding have been verified in other folds in the Appalachians, in the Canadian Rockies, in the Idaho-Wyoming thrust belt, and in the Pyrenees.

In this dissertation I solve boundary-value problems for an idealized thrust block moving over a detachment surface and ramp, and produce theoretical bed-duplication folds in the thrust block that closely resemble those in Rich's idealized model. The anticline is

narrow and rounded if the translation is small, and broad and flat-topped if the translation is large. The limbs of the anticline are symmetric if drag is zero. Drag along the ramp part of the detachment surface can explain the asymmetry of dips of the two limbs of the Powell Valley anticline, particularly if drag between relatively competent rocks in opposition at the ramp causes an initial anticline to form as the thrust block begins to move, and then drag reduces markedly as relatively soft shales at the base of the block were thrust over competent rocks in the ramp.

The Burning Spring anticline in West Virginia appears to have formed at the termination of a detachment surface. Investigation of the translation of an homogeneous, viscous material above a flat detachment surface that terminates laterally indicates that the termination produces a broad, low-amplitude anticline in passive layering as a result of thickening induced by a gradient of shear stresses in the vertical direction. This thickening above the termination of a detachment is a mechanism of folding. If the viscous fluid contained mechanical layering, the fold would become amplified by buckling. The Burning Springs anticline probably was initiated by termination of a detachment surface and subsequently amplified by buckling.

Bed-duplication folding has been studied mechanically and geometrically during the last few years. In order to bridge between geometrical constructions of Suppe (1983) and one of the mechanical models of Chapter I, two kinematical models are introduced. In this way, results of the two methods of determining deformations and geometry of bed-duplication folding can be compared. One kinematical model is required for early stages and the other for later stages of bed-duplication folding, but each involves a simple, domainal, velocity distribution. The kinematical models produce the type of bed-duplication fold Suppe has termed "fault-bend fold," and the models provide new insights into the essence of the type.

The velocity distributions assumed in the kinematical models are similar to those predicted by the first-order, mechanical model for thrust ramps with low slopes (less than about 20°) and zero drag introduced in Chapter I. The fold forms computed for the two sets of models are also similar, so the Suppe (1983) geometrical construction produces a reasonable approximation to a simple, low-amplitude, bed-duplication fold.

The approximation is poorer for steeper thrust ramps. The upper limit of the Suppe model is 30° and at that ramp angle, the dip of the distal limb of the fold is twice the dip of the thrust ramp. Results of the mechanical analysis of steeper ramps, carried to second-order accuracy, indicates that the dip of the distal limb should be less than the dip of the thrust ramp, and that the block being thrusted is subjected to general simple shearing, which is absent in the kinematical models. Nevertheless, both the kinematical and mechanical models predict asymmetry of fold limbs.

TABLE OF CONTENTS

Page No.:

CHAPTER II FOLDING OF PASSIVE LAYERS AND FORMS OF MINOR STRUCTURES NEAR TERMINATIONS OF BLIND THRUST FAULTS- APPLICATION TO THE CENTRAL APPALACHIAN BLIND THRUST

CHAPTER III KINEMATICS OF FAULT-BEND FOLDING

LIST OF FIGURES

Figure No.: Page No.:

CHAPTER 1

INTRODUCTION

In 1934, John L. Rich proposed ramp folding or bed-duplication folding as a new mechanism for producing folds in fold-and-thrust belts. Using the combination of the Powell Valley anticline and Middlesboro syncline in Kentucky and Tennessee as his example, Rich proposed that these folds formed with a flat crest as a result of translation of the hanging wall over steps in the Pine Mountain thrust surface. Rich assumed that the Pine Mountain thrust surface had a ramp that connected a lower detachment in the Cambrian Rome shale with an upper detachment in the Devonian Chattanooga shale. Given sufficient translation, such that beds cut off at the thrust ramp are translated over the ramp and along the upper detachment, a flat-crested fold will form. He suggested that dips of the fold limbs will equal the dip of the thrust ramp.

In Chapter I, a theoretical model is proposed to reproduce the essential features of Rich's idealized model of a thrust sheet being translated over a thrust ramp, satisfying, as closely as posssible, the general conditions assumed in the Rich concept. The model investigates translation of a viscous material over a thrust ramp, thereby producing a bed-duplication fold. The overburden is assumed to be an infinite half-space, so buckling cannot occur. The footwall is modeled as rigid material so no deformation can occur there.

In Chapter II, the theoretical model is modified so that deformation results from a combination of bed-duplication folding and termination of easy slip at the top of a thrust ramp. A frictionless thrust ramp connects a lower detachment surface with zero drag with an upper detachment surface with high adhesive drag.

The Powell Valley anticline has the distinct flat crest of a bed-duplication fold, but has profound asymmetry of fold limbs. A possible explanation for the asymmetry is that the hanging wall is deformed as a result of drag along the ramp fault surface. Thus, in Chapter I, the theoretical model also incorporates adhesional drag on the thrust ramp as well as translation.

A theoretical model that incorporates translation and drag may be utilized to investigate other mechanisms for producing folds. The analysis appears relevant to the Burning Springs anticline in western

West Virginia which may have formed partly as a result of termination of a detachment surface (Woodward, 1959). The late Silurian rocks of the upper Salina Group contain a thick salt horizon that pinches out distally in the vicinity of the Burning Springs anticline. In Chapter II, I investigate folding of passive layering in an homogeneous, viscous material near the termination of a flat detachment surface. The detachment surface is flat and along part of it adhesional drag is large and along part of it drag is zero.

In Chapter II, I also investigate deformation produced by a combination of bed-duplication folding and termination of easy slip at the top of a thrust ramp. The frictionless thrust ramp connects a lower detachment surface with zero drag with an upper detachment surface with high adhesive drag.

Thus, in Chapters I and II, I use a combination of geometric information obtained from field studies and theoretical analyses of folding processes in order to investigate several types of fault-related folding.

In 1983, John Suppe developed a geometrical construction that produces a bed-duplication fold closely resembling the construction proposed by John L. Rich (1934). The new geometrical construction is more restrictive than the model suggested by Rich, because it requires constant length and thickness of beds. In Chapter III, I examine the effect of the additional restrictions on the form of the folds and compare Suppe's geometrical construction with the mechanical model developed in Chapter I, by using a kinematical model of material particle paths to bridge between the two. The impetus for comparing the geometrical construction and the mechanical model is that the geometrical construction makes predictions about fold form that are testable with the mechanical model.

CHAPTER 1

MECHANICAL ANALYSIS OF BED-DUPLICATION FOLDING IN A THRUST SHEET MOVING OVER A RAMP

(Published in essentially this form in Tectonophysics, 1980, volume 70, p. T9-T24)

Introduction

Two general views of folding processes in the central and southern Appalachian Mountains of the eastern United States are that folding is primarily a result of layer-parallel shortening of a stack of sedimentary layers with contrasting properties, and that folding is primarily a result of repetition of sedimentary layers above ramp faults which connect thrust detachment zones at different horizons.

Bailey Willis (1893) assumed that the folds represent buckling caused by layer-parallel compression, and identified several basic mechanisms of folding, including the importance of "strut" members in controlling the sizes of folds (Currie et al., 1962; Nickelsen, 1963), and the importance of stratigraphic controls, particularly of initial dips of layering, in determining the locations of large folds (Cooper, 1964). Willis recognized that faulting is at least as obvious as folding in the southern Appalachians, but he imagined that the faulting followed the folding, and in a sense was a result of folding. This view of the faults in the southern Appalachians was largely based on structural interpretations of the Saltville thrust and associated fold by Willard Hayes (1891), who suggested that the Saltville thrust fault changed level by a ramp fault cutting through the northwestern limb of an anticline formed earlier.

Willis' basic idea, that Appalachian folds are a result of buckling, has several modern proponents. Low-amplitude folds on the Allegheny Plateau of Pennsylvania may have resulted from buckling of relatively competent rocks over a detachment zone of salt or shale (Sherwin, 1972; Wiltschko and Chapple, 1977). The folds in Silurian and Devonian rocks of central Pennsylvania may also be buckle folds (Currie et al., 1962; Nickelsen, 1963; Faill, 1969, 1973).

John L. Rich (1934), however, revolutionized concepts of folding in the Appalachians by showing that several large folds, including those in the Pine Mountain overthrust block of Virginia, Kentucky and Tennessee, and the Sequatchie Valley anticline of Tennessee and Alabama, can be explained without recourse to shortening of layers, but rather by lateral translation of thrust blocks over ramp faults. His concept of folding originated through study of cross sections of the Pine Mountain block prepared by Charles Butts (1927), who showed that a shallow thrust fault must underlie the syncline and anticline within the block.

The most important contribution by Rich was to explain the Middlesboro syncline and the Powell Valley anticline (Fig. 1D) as natural consequences of transport of the thrust block over ramps (Figs. 1A, 1B, and 1C) producing <u>bed-duplication folds</u>, rather than by buckling or by subsequent warping of the surface of thrusting (Rich, 1934, p. 1589).

Rich also noted that: "If the forward movement is slight, a narrow anticline is formed [Fig. 1B], whereas greater movement produces a broad, flat-topped anticline [Fig. 1C]" (Rich, 1934, p. 1590). He indicated that the Powell Valley anticline illustrates both narrow, rounded forms and broad, flat-topped forms along its length. Rich (1934, p. 1594) indicated that the anticlines and synclines appearing with a thrust block are superficial and do not extend below the level of the thrust surface.

Rich imagined that the thrust surface followed a zone of easy sliding, within the Chattanooga Shale, until the frictional resistance became too great, then stepped upward by shearing across bedding to another zone of easy sliding, and repeated the stepping and sliding

Figure 1. Cross sections of the Pine Mountain thrust block, Tennessee (after Harris and Millici, 1977, plate 2 and fig. 9). A, B, and C show idealized sequence of stages in the development of the Powell Valley anticline and the Middlesboro syncline.

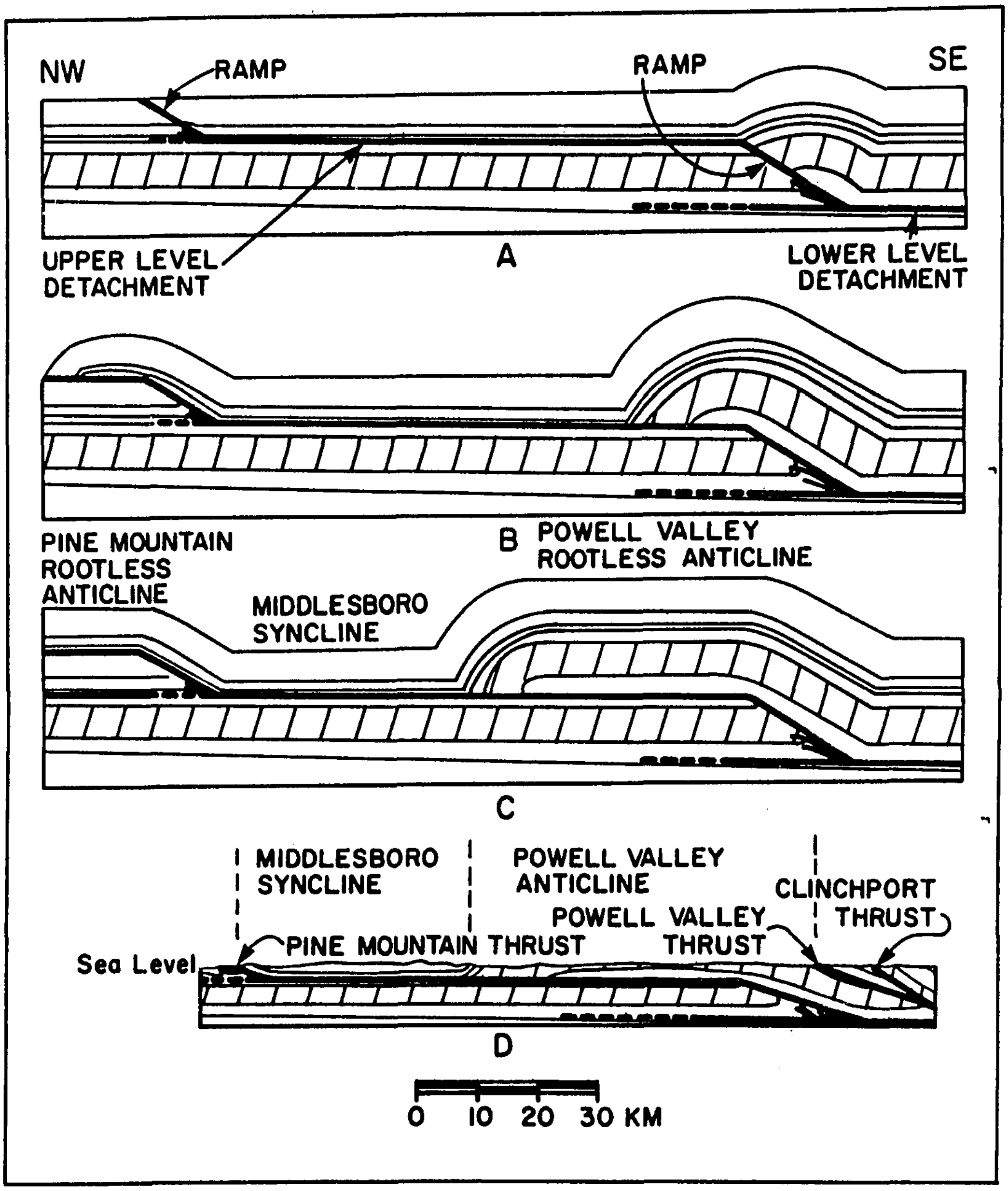
NW
RAMP
RAMP
SE
UPPER LEVEL
DETACHMENT
A
LOWER LEVEL
DETACHMENT
PINE MOUNTAIN
ROOTLESS
ANTICLINE
B
POWELL VALLEY
ROOTLESS ANTICLINE
MIDDLESBORO
SYNCLINE
C
MIDDLESBORO
SYNCLINE
POWELL VALLEY
ANTICLINE
CLINCHPORT
THRUST
POWELL VALLEY
THRUST
PINE MOUNTAIN THRUST
Sea Level
D
0 10 20 30 KM

until the ground surface was reached (e.g., Fig. 1B).

Chamberlin and Miller (1918) were able to produce analogous ramps between zones of detachment in experiments with multilayers comprised of plaster and clay, where the competency contrasts among layers were low. Morse (1977) experimentally produced symmetric folds over ramps in layers of various rocks.

Subsequent field work, deep drilling, and seismic-reflection profiling have verified the essential features of Rich's mechanism of bed-duplication folding in the Appalachians (Rodgers, 1949, 1963; Gwinn, 1964, 1970; Harris, 1970; Harris and Milici, 1977), and the kinematic framework of Rich's mechanism of folding has been adopted to describe structures in the Idaho-Wyoming thrust belt (Berger, 1984; Royse et al., 1975), in the Canadian Rockies (Douglas, 1950), in the Pyrenees (Seguret, 1972), and in a fold and thrust belt presently forming in Taiwan (Suppe, 1979; Suppe, 1983).

One purpose of this chapter is to reproduce the essential features of Rich's idealized model of a thrust sheet being translated over a ramp structure, satisfying, as closely as possible, the general conditions assumed in the model. I assume a low-amplitude ramp of sinusoidal form (Fig. 2), and impose the boundary conditions that there is zero drag along the surface of thrusting and that the rocks beneath the ramp are effectively rigid. The thrust sheet is represented by a simple viscous material, containing passive markers which initially are flat and become deformed by translation over the ramp.

Most of my calculations have been made assuming an infinitely thick thrust sheet because preliminary calculations indicated that, if the thickness of the thrust sheet is at least twice the height of the ramp, and the top of the sheet remains flat as a result of erosion and deposition, the finite thickness of the sheet has insignificant effect on the pattern of deformation.

My solution is quite general and can be used for the deformation over a ramp of any shape that can be described in terms of a Fourier sinusoidal series. The particular series I select describes an infinite number of ramps connected by horizontal detachment surfaces, so that the ramps alternately step upward and downward rather than continually climb by a series of up-ramps. However, the solution is approximate, because it is valid to first order in the maximum slope

Figure 2. Shape of detachment surface and distribution of drag assumed in theoretical analyses. A. Symbols used to describe the detachment surface, which is comprised of sinusoidal ramp segment connecting upper and lower flat segments. B. Magnitudes of drag parallel to detachment surface. Drag parallel to ramp segment is constant, k Drag on flat segments is zero.

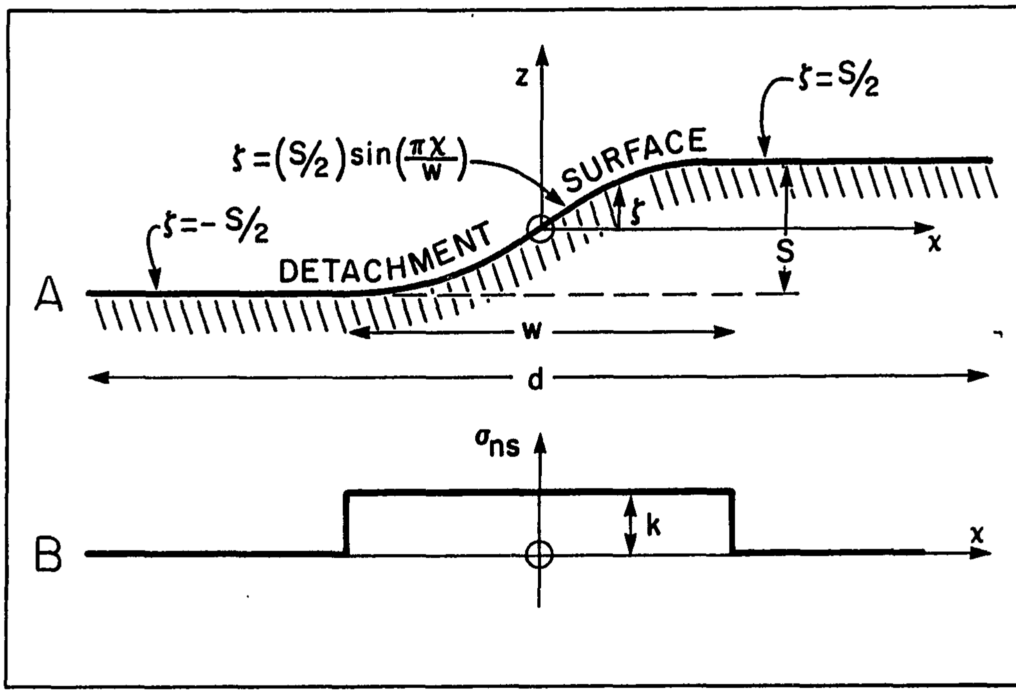
z
ζ=S/2
ζ=(S/2)sin(πx/w)
SURFACE
ζ=- S/2
DETACHMENT
A
ζ
x
S
w
d
σns
k
B
x

of the surface of thrusting. The first-order solution is valid for maximum slope angles up to about 15 or 20 degrees (corresponding to errors in the sine and cosine of 5-7%). According to a cross section presented by Harris (1970), the maximum slope angle of the ramp beneath the Powell Valley anticline is about 20 degrees. I have selected a maximum angle of about 17 degrees for the solution presented here. A solution to second order has been developed and the results are presented in Chapter IV. This solution should be valid for slope angles up to 30 or 35 degrees.

There is zero drag to the order of approximation of my solution, so that the distinctive asymmetry of the Powell Valley anticline does not appear in the theoretical forms. The asymmetry has been known since the field work by Keith (1896, 1901), and is shown in Fig. 1D but has remained unexplained. According to Wiltschko (1979a, p. 1093) dips of the northwestern limb are as high as 70 degrees. The dips of the southeastern limb are about 20 degrees.

A possible explanation can be deduced by examination of the structural cross-sections representing the idealized development of the folds on the Pine Mountain thrust block by Harris and Milici

(1977), as shown in Fig. 1A. Figure 1A shows folding next to a ramp before the thrust sheet is pushed over the ramp; folding before thrusting was suggested by Hayes (1891) and by Milici (1970). Then, if the folded sheet is passively pushed over the ramp, as Rich envisioned, the asymmetry develops, as shown schematically in Fig. 1C. In this case the asymmetry is interpreted to be a result of buckle-folding followed by ramp-folding.

An alternative explanation for the asymmetry of the Powell Valley anticline is that it is a result of drag induced by the ramp. For example, frictional drag between rocks initially connected across the ramp might be much higher than that along the flat sections of the surface of thrusting. I chose not to investigate here the effect of drag on the flat segments, reasoning that the flat segments were zones of easy sliding and therefore should have low resistance to sliding. In order to investigate effects of drag along the ramp, I introduce shearing resistance of any form that can be represented by a Fourier cosine series. I specifically evaluate the effect of constant shear stress along the ramp. The analysis indicates that the asymmetry of the Powell Valley anticline could have been caused by drag on the ramp when relatively competent rocks (sandstones and limestones) opposed each other across the ramp. Further, incorporation of drag along the ramp into the theoretical analysis leads to a form that strikingly resembles early stages of the formation of nappes, according to conceptions by Argand, Heim and Trumpy (references in Rutten, 1969, pp. 185, 186, 190 and 195).

Most of the theoretical analyses of thrust sheets have focused on the critical problem of explaining mechanically how it is possible for massive blocks of rock to translate laterally over detachment surfaces (Hubbert and Rubey, 1959; Raleigh and Griggs, 1963; Hsu, 1969; Kehle, 1970; Chapple, 1978). Deformation in ramp regions has been analysed by Elliott (1976a, 1976b) and by Wiltschko (1979a, 1979b) whose primary aim was to estimate the driving and resisting forces acting on idealized thrust sheets. Wiltschko (1979b) showed, using plate theory, that thrusting of viscous sheets requires both a horizontal push and a topographic slope toward the distal end of the thrust sheets. None of these previous studies focuses on the subjects of my study.

Solution

A detailed treatment of the boundary-value problem will not be presented here; it is presented in the dissertation appendix. The general method has been well documented (Kamb, 1970; Budd, 1970; Fletcher, 1977; Reches and Johnson, 1979; Johnson, 1977). My solution for uniform translation, with zero drag, of a thrust block over a ramp is analogous to that of Barclay Kamb (1970), who was examining viscous flow and regelation associated with slip at the base of a glacier. He noted, incidentally, that the analysis is relevant to thrust sheets. Kamb was primarily interested in the form drag caused by a rough, adhesionless surface; this type of drag is zero to the level of approximation of the first-order solution. I consider drag due to adhesional resistance to slip at the ramp. I also incorporate effects of layer-parallel compression in my general solution, but effects of such compression are negligible in inhomogeneous, isotropic materials. The solutions for drag and layer-parallel compression are original.

Let ζ represent the position (in z-direction) of the detachment surface relative to a coordinate system centered at mid-height on the ramp (Fig. 2A). I represent the detachment surface by means of the Fourier, sine series:

$$\zeta = \sum_{m=1}^{\infty} A_m \sin(m\pi x/d) = \sum_{m=1}^{\infty} A_m \sin(l_m x) \qquad (1a)$$

in which x is the horizontal coordinate, m is an integer, and d is the spacing of adjacent ramps (Fig. 2A). In the problem I am solving, that of an isolated ramp, d is selected to be large compared to the height of the ramp.

Here l_m is the wave number

$$l_m = m\pi/d \qquad (1b)$$

and A_m is amplitude of a sine wave.

One of the boundary conditions is that the position of the detachment surface is fixed:

$$\partial\zeta/\partial t = 0 \qquad (2a)$$

(or that the velocity normal to the detachment surface is zero). This requires that the vertical velocity, v_z, and the horizontal velocity, v_x, at the detachment surface satisfy the relation (Kamb, 1970):

$$[v_z]_\zeta = [v_x]_\zeta(\partial\zeta/\partial x) \qquad (2b)$$

The other boundary condition is that the shear stress, σ_{ns}, parallel to the detachment surface is of the form of a Fourier cosine series:

$$\sigma_{ns} = \sum_{m=1}^{\infty} R_m \cos(m\pi x/d) \qquad (3)$$

in which R_m is determined by the shear-stress distribution at the detachment surface. The Fourier series in (3) expresses constant adhesional drag of magnitude k along the surface of the ramp and zero drag elsewhere. The remaining boundary conditions are that the velocities become equal to the mean velocities at large distances from the ramps.

With boundary conditions (2b) and (3) I eliminate the arbitrary constants in the solution for viscous flow of a half-space. Skipping all remaining steps, the solution for the velocities within the thrust sheet is:

$$V_X = (V_X)_{\bar{v}_x} + (V_X)_{\tau} + (V_X)_{\varepsilon} \tag{4a}$$

$$V_Z = (V_Z)_{\bar{v}_x} + (V_Z)_{\tau} + (V_Z)_{\varepsilon} \tag{4b}$$

in which subscript ($_x$) identifies the component of velocity associated with uniform translation of the thrust block, subscript τ identifies the component associated with drag along the detachment surface, and subscript ε identifies the velocity component associated with uniform extension or compression of the thrust block. The components are as follows.

Uniform translation:

$$(v_x)_{\bar{v}_x} = \bar{v}_x[1 + \sum_{m=1}^{\infty} A_m l_m(l_m z)\exp(-l_m z)\sin(l_m x)] \tag{5a}$$

$$(v_z)_{\bar{v}_x} = \bar{v}_x \sum_{m=1}^{\infty} A_m l_m(1+l_m z)\exp(-l_m z)\cos l_m x) \tag{5b}$$

Uniform extension or compression:

$$(v_x)_\varepsilon = -D_{xx}\sum_{m=1}^{\infty} A_m[(2-(l_m z)^2)\cos(l_m x)$$

$$-(l_m z)(l_m x)\sin(l_m x)]\exp(-l_m z) + D_{xx}x \tag{6a}$$

$$(v_z)_\varepsilon = D_{xx}\sum_{m=1}^{\infty} A_m[(1-(l_m z)-(l_m z)^2]\sin(l_m x)$$

$$+(1+l_m x)\cos(l_m x)]\exp(-l_m z) - D_{xx}z \tag{6b}$$

in which D_{xx} is the rate of deformation ("strain rate") caused by overall shortening or lengthening of the thrust block. D_{xx} is negative if compressive.

Shear along detachment surface:

$$(v_x)_\tau = -\sum_{n=1}^{\infty}(R_n/2\mu l_n)[(l_n z-1)\exp(-l_n z)\cos(l_n x)$$

$$-\sum_{m=1}^{\infty}(A_m/2)\,[[l_q+l_r(l_q z-1)]\exp(-l_q z)\sin(l_q x)$$

$$\pm[l_r \pm l_q(l_r z \mp 1)]\exp(\mp l_r z)\sin(l_r x)]] \qquad (7a)$$

$$(v_z)_\tau = \sum_{n=1}^{\infty}(R_n/2\mu l_n)[(l_n z)\exp(-l_n z)\sin(l_n x)$$

$$+\sum_{m=1}^{\infty}(A_m/2)\,[[l_q+l_r l_q z]\exp(-l_q z)\cos(l_q x)$$

$$+[l_r \pm l_q l_r z]\exp(\mp l_r z)\cos(l_r x)]] \qquad (7b)$$

in which the upper sign is selected if $m \geq n$ and the lower sign is selected if $m < n$ and:

$$r = [(m/n)-1]; \qquad q = [(m/n)+1] \qquad (7c)$$

$$l_r = r l_n \qquad l_q = q l_n \tag{7d}$$

Here m and n are both odd.

As indicated above, these solutions are valid if the position of the detachment surface can be expressed in the form of Fourier, sine series, eq. 1a, and if the shear stress along the detachment surface can be expressed in the form of a Fourier, cosine series, eq. (3).

For the particular problem I have selected, the shear stress is constant along the ramp (Fig. 2B). The form of the detachment surface is a sine curve joining horizontal lines (Fig. 2A); the steps are alternately upward and downward so that the mean position of the interface is the horizontal axis. Thus:

$$A_n = (2S/\pi)[[(1/n)/(1-(nw/d)^2)]\cos(n\pi w/2d)-\cos(n\pi/2)];$$

$$n \text{ is odd} \tag{8a}$$

in case $n = d/w$,

$$A_n = -(2S/n\pi)\cos(n\pi/2) \tag{8b}$$

in which S is the step height of the ramp, w is the width of the ramp, and d is a distance much greater than S and w, for an isolated ramp. Also:

$$R_m = (4k / m\pi)\sin(m\pi\, w/2d); \qquad m \text{ is odd} \tag{8c}$$

in which k is the constant shear resistance to movement of the thrust block over the ramp.

In evaluating the solution I normalize all distances by the height of the ramp, and determine displacements of points by numerically integrating over time. I introduce a dimensionless drag parameter, K, which ranges in value from zero for zero drag ($k = 0$), eq. 8c), to one for perfect drag such that a point in the thrust block at position (0, 0) remains there. It is a measure of the ratio of adhesional drag, k, to a representative viscous shear stress, $\mu(\bar{V}_x / w)$. I derive K by equating the horizontal velocity, $\bar{V}_x$, at point (0, 0) caused by the mean flow, with the negative of the horizontal velocity caused by adhesional drag, $kw/\mu F$, where F is a function of the width and spacing of the ramps (Fig. 3);

$$F = 1/\left[\sum_{m=1}^{\infty}(2d/w)(1/n\pi)^2\sin(n\pi w/2d)\right]; \qquad \text{odd n} \tag{9a}$$

Thus:

$$K = k/\mu(\bar{V}_x/w)F, \qquad 0 \le K \le 1 \tag{9b}$$

For all my numerical results, w/d=0.1 and w/S= 5.

Results

Patterns of deformation in idealized thrust blocks are determined by numerically integrating the velocity equations, eqs. (4), (5), (6), and (7), using small increments. In this way points along passive markers within the thrust blocks become displaced (Figs. 4 and 5). Markers that were originally horizontal become deformed into folds, and markers that were originally vertical display distortions. In all the solutions the ramp segment is five units long and one unit high, and reaches a maximum slope angle of 17 degrees.

Figure 3. Relation between a factor, F, and the ratio of the width, w, of the ramp segment and the spacing, d, of adjacent ramps in the Fourier series expression for the shape of the detachment surface. Here $\overline{V}_x$ is the uniform velocity of the thrust block far from the detachment surface. F is a factor that determines the effect of shape of detachment surface on the drag parameter, K, and it depends on w/d

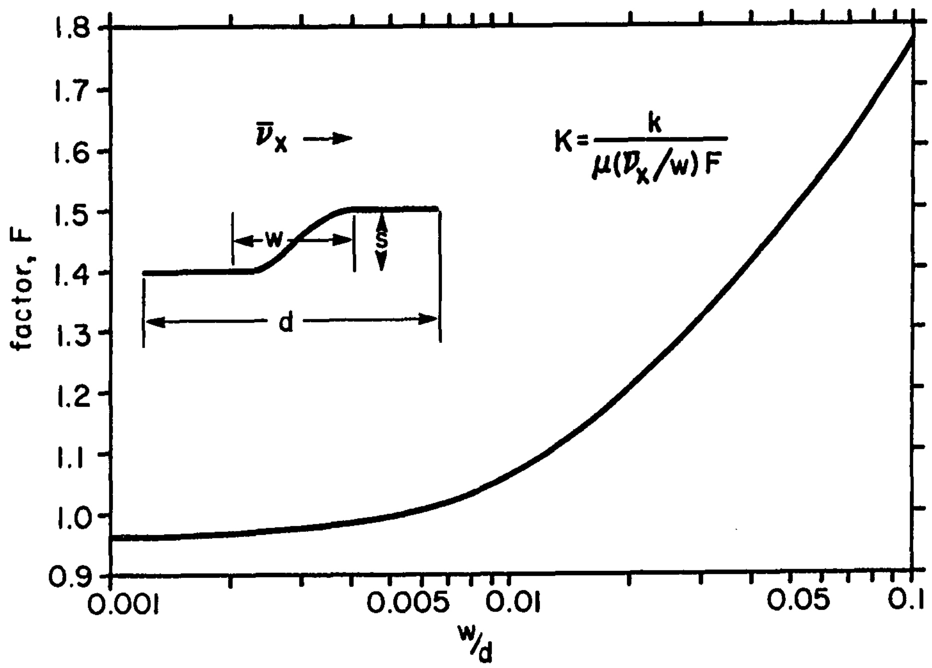

1.8
1.7
1.6
1.5
1.4
1.3
1.2
1.1
1.0
0.9
factor, F
0.001
0.005
0.01
0.05
0.1
w/d
$\bar{v}_x$
w
s
d
$K = \frac{k}{\mu(\bar{v}_x/w)F}$

Figure 4. Deformation of passive markers by uniform translation of one unit (equal to ramp height). Markers with low dips originally horizontal; those with high dips originally vertical. A. Thrust block subjected solely to uniform translation (zero drag). B. Thrust block subjected to uniform translation and high drag along the ramp segment of the detachment surface.

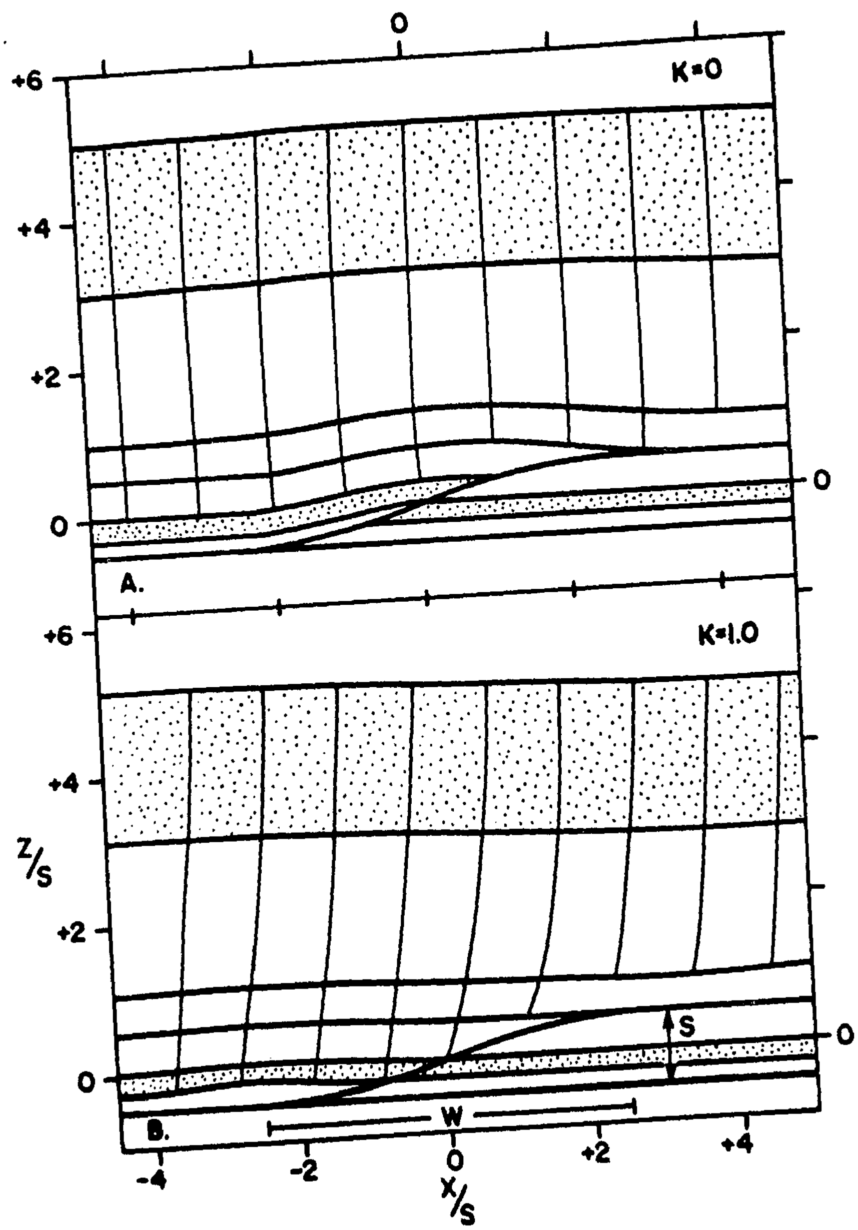
K=0
+6
+4
+2
0
0
0
A.
K=1.0
+6
+4
Z/S
+2
0
0
S
B.
W
-4
-2
0
+2
+4
X/S

Figure 5. Thrust blocks subjected to ten units of uniform translation and various amounts of drag along the ramp. Markers originally horizontal. A. Zero drag. B, C. Moderate drag (K less than one). D. High drag. Dotted lines indicate approximate configurations of markers near ramp. Exact positions could not be determined because of error.

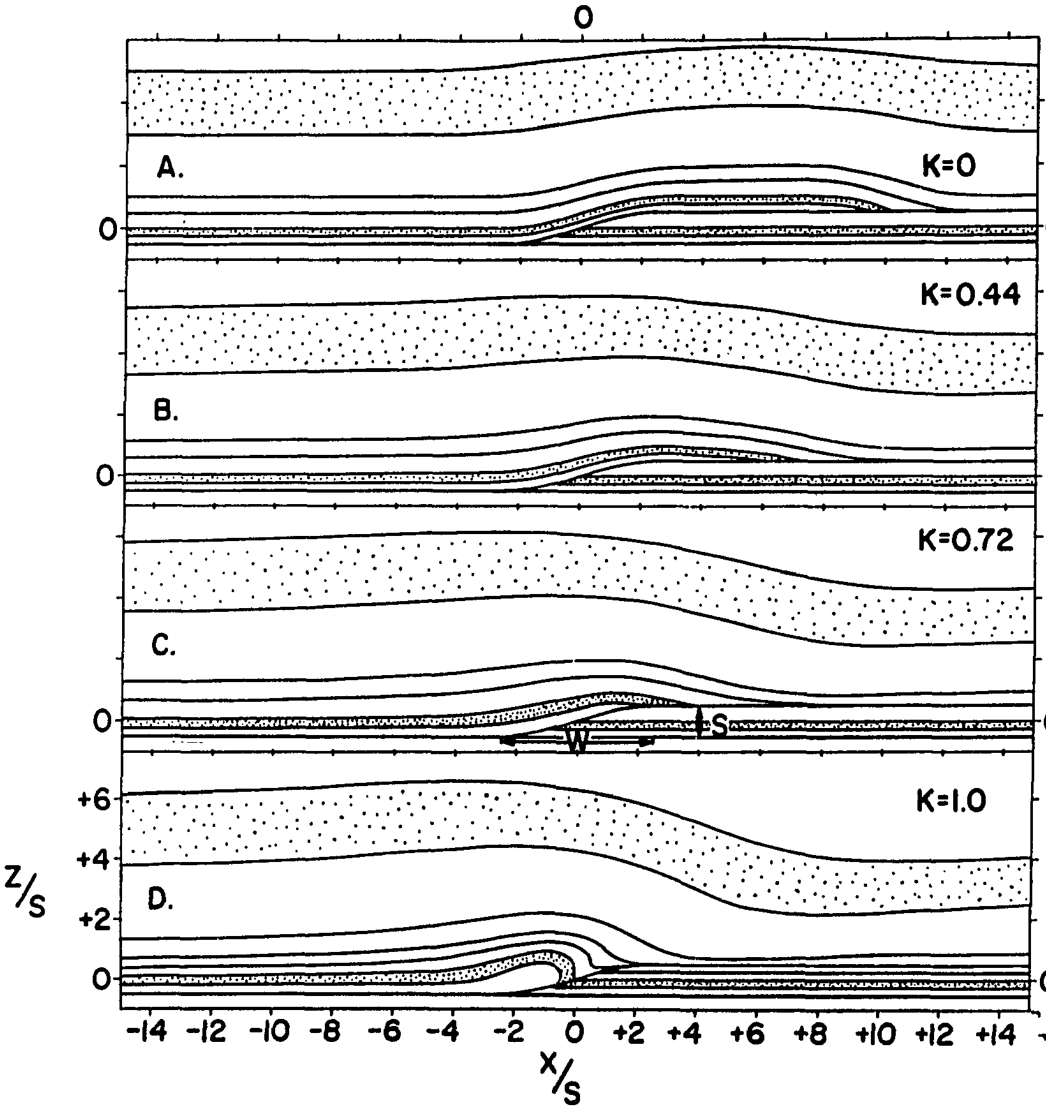

A.
K=0
B.
K=0.44
C.
K=0.72
S
W
D.
K=1.0
Z/S
X/S
-14 -12 -10 -8 -6 -4 -2 0 +2 +4 +6 +8 +10 +12 +14
+6
+4
+2
0

Of the many possible boundary-value problems that the equations solve, the problems of most interest are those involving various amounts of adhesional drag at the ramp and various amounts of translation of the thrust block over the ramp. I will not present results where there are compression and extension because preliminary calculations indicate that effects of compression and extension are insignificant in the absence of mechanical layering.

Translation

Figure 4A shows the deformation of passive markers within a thrust block subjected solely to uniform horizontal translation, far from the ramp, equal to the height of the ramp (one unit), and Fig. 5A is for horizontal translation of ten times the height of the ramp (10 units). In both examples the passive markers are deformed into symmetric folds. For translation of one unit (Fig. 4A), the fold has a rounded crest and the amplitude of the fold is less than the height of the ramp. The leading edge of the thrust is wedge-shaped, and is similar in form to individual imbricate thrust slices shown in cross-sections of the foothills in the Canadian Rockies (Thompson, 1979) and of the central Appalachians (Perry, 1975).

For translation of ten units (Fig. 5A), the amplitude of the fold in a marker directly above the detachment surface increases to the height of the step at the ramp, the width of the fold increases, and the fold becomes a flat-topped anticline. As indicated by Rich, the width of the anticline increases with the translation. The beds that were initially disrupted at the ramp become truncated by the flat part of the detachment surface, and form the distal limb of the fold. The dip angles of both limbs are equal.

A characteristic of the anticlines produced by either one or ten units of translation is that the anticlines broaden and flatten with distance above the detachment surface. Thus the width of an anticline produced by bed-duplication folding is a function of the stratigraphic level as well as of the amount of translation. Each limb of the anticline resembles a monoclinal flexure.

The forms derived analytically correspond with the principal elements of the kinematical model John L. Rich proposed for explaining bed-duplication folds.

Translation and Drag

The existence of drag at the ramp has a marked effect on the shape of the fold produced by translation of the thrust block over a ramp. Let us consider extreme examples where drag is large enough to prevent the thrust sheet, at the steepest part of the ramp, from moving. Figure 4B shows the form if there are high drag and one unit of uniform translation, and Fig. 5D shows the form if there are high drag and ten units of uniform translation. The major effect of high drag is to thicken the layers proximally, behind the ramp; the ramp with drag acts much as a dam, retarding flow of viscous material over the ramp. Further, high drag and high uniform translation result in a nappe-like structure (Fig. 5D).

Effects of intermediate amounts of drag and ten units of horizontal displacement are illustrated in Figs. 5B and 5C. The drag inhibits translation near the ramp and therefore the development of the flat-topped fold, and it imparts asymmetry to the fold. The gradual change with increasing drag, from a flat-topped anticline to a round-crested anticline, is apparent in Figs. 5. As the amount of drag increases, thrust displacement decreases near the ramp, the anticline becomes more rounded, and asymmetry increases. The amplitude of the folds, as shown by passive markers far above the detachment surface, decreases due to the increased thickening at the proximal end of the ramp. In the extreme, as shown in Fig. 5D, the fold dies out upward into a single, monoclinal form. The amplitude of the folds and the dip of the passive markers increase, near the detachment surface, with increasing drag.

Figures 4A and 4B illustrate differences of internal deformation of the thrust block where there is free slip (4A) and high drag (4B). The steeply dipping lines are passive markers that originally were vertical and evenly spaced. These lines remain nearly vertical where there is uniform translation (Fig. 4A) and zero drag; they are sharply bent near the detachment surface where there is high drag along the ramp (Fig. 4B).

Discussion

I have shown that one readily can produce the anticline with a symmetric form and a flat top that is the central feature of the model of bed-duplication folding of Rich (1934), and elaborated upon by Harris (1970) and by Harris and Milici (1977). The development of such a form in an isotropic, viscous thrust block with passive bedding planes, riding over a detachment surface with a ramp, is shown in Figs. 4A and 5A.

In many ways the theoretical model resembles the structural cross section of part of the Pine Mountain thrust block (Fig. 1D), particularly the idealized cross-section drawn by Harris and Milici (1977), shown in Fig. 1C. The most obvious difference is the marked asymmetry reflected by different dips of the limbs of the Powell Valley anticline. I can imagine at least three ways in which the asymmetry could have developed. They all depend upon the formation of a low-amplitude fold in hanging-wall rocks adjacent to the ramp before the thrust block moved over the ramp, as illustrated in Fig. 1A. The layers in the hanging wall may have folded by buckling, that is, as a result of layer-parallel compression, as suggested by Hayes (1891). The layers may have folded passively as a result of splay-faulting, as envisioned by Harris and Milici (1977), and as indicated by the short faults beneath the ramp in Fig. 1A.

In previous paragraphs we have illustrated yet another mechanism, involving drag between the thrust block and the footwall rocks at the ramp, as shown for example in Fig. 4B. The initial fold produced in this way can be highly asymmetric, as shown in Fig. 5D. According to this interpretation, an initial fold developed when relatively competent sandstones and limestones opposed each other across the ramp, and then the broad form developed when the initial fold was thrust upward and over the ramp as the relatively incompetent shales were thrust into contact with the ramp surface. I have simulated this sequence of events in constructing Fig. 6.

First, I assumed high drag and produced the form shown in Fig. 5D. Then, I assumed free slip all along the detachment surface, and supplied ten units of additional translation over the ramp. The amount of asymmetry could be reduced somewhat by reducing the amount of drag during the first stage, for example by assuming an initial fold as in Fig. 4B. However, the essential elements are shown in Fig. 6. The dip of the layers over most of the anticline will be in the proximal direction and there will be a bulge at the distal edge of the anticline.

Figure 6. Form of anticline produced by first subjecting a thrust block to ten units of translation and to high drag and then to ten addditional units of translation and zero drag. Marker lines originally horizontal

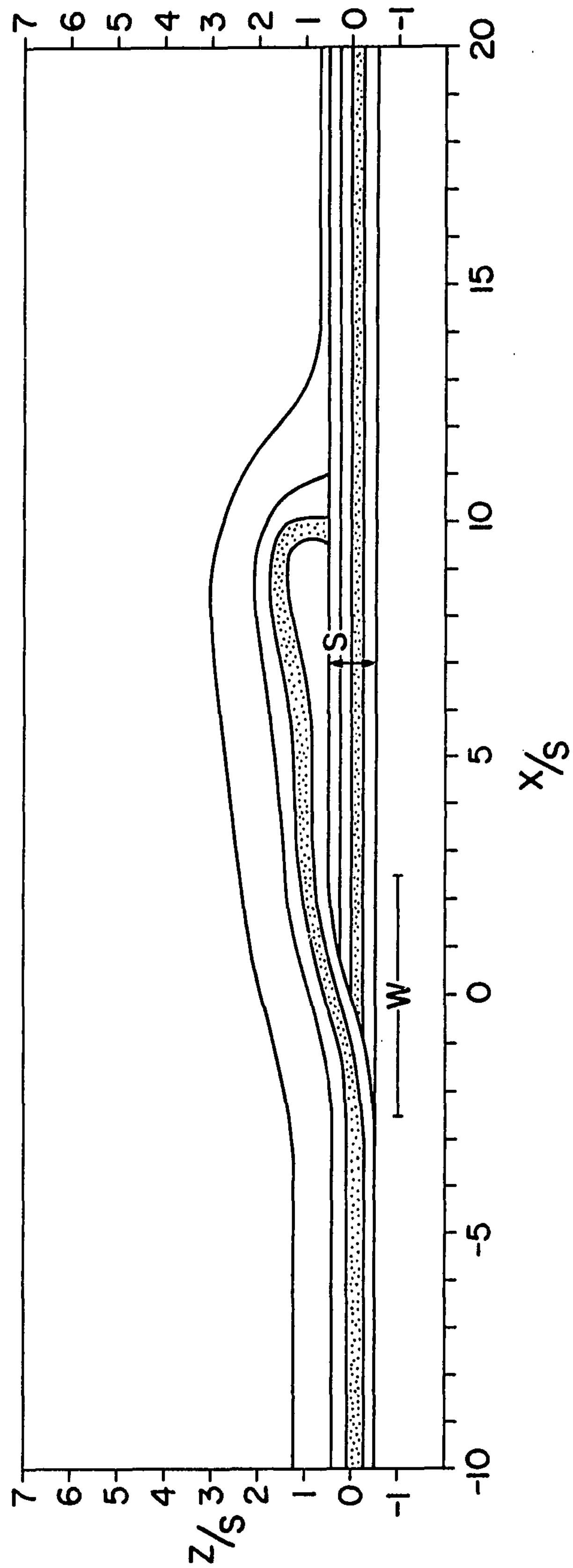
Z/S
X/S
S
W
-10
-5
0
5
10
15
20
7
6
5
4
3
2
1
0
-1

The bulge will develop whether the initial folding was a result of buckling, of splay faulting, or of drag at the ramp. Perhaps the Powell Valley anticline had a bulge at its distal edge rather than the flat crest indicated in the idealized diagram shown in Fig. 1C.

CHAPTER II

FOLDING OF PASSIVE LAYERS AND FORMS OF MINOR STRUCURES NEAR TERMINATIONS OF BLIND THRUST FAULTS - APPLICATION TO THE CENTRAL APPLACHIAN BLIND THRUST

(Published in essentially this form in Journal of Structural Geology, 1982, vol. 4, p. 343-353)

Introduction

In this chapter, I investigate folding of passive layering in an homogeneous viscous material near the termination of a flat detachment surface (blind thrust, Thompson, 1979). A motivation for the study is that such a mechanism of folding has not been investigated analytically, although it has been suggested to be responsible for some folds.

For example, the Burning Springs anticline in western West Virginia and eastern Ohio may have formed partly as a result of termination of a detachment surface (Woodward, 1959). The Burning Springs anticline is somewhat different from many folds on the Plateau; it trends north-south, rather than about N 45° E as is typical, and it has higher structural relief at the ground surface, about 500 m, than folds nearby (Woodward, 1959; Rodgers, 1963). According to Rodgers (1963), the Burning Springs anticline is a flat-topped fold with steep sides; however, cross-sections by Cardwell et al. (1968) show the anticline to be a rounded, asymmetric form, with the steeper limb facing eastward.

According to Woodward (1959), a well drilled through the fold showed a normal stratigraphic section to a depth of about 1.2 km, near the top of the Oriskany Sandstone; but below that depth, several units, comprising the interval between Onondaga and Helderberg formations, were repeated by imbricate thrusting, producing an increase of section of about 500 m in excess of normal thickness of units. Below the faulted zone the Lower Devonian rocks apparently are flat-lying. The Late Silurian rocks of the upper Salina Group encountered in the well contain anhydrite, but no salt.

According to Rodgers (1963, p. 1533), a well drilled about 6 km east of the Burning Springs anticline encountered about 30 m of salt in the upper Salina Group, and evidence from wells west and north of the anticline indicate that the salt pinches out in the vicinity of the anticline. Rodgers attributed the thrusting in the core of the anticline to lateral pinching out of the salt. Gwinn (1964, p. 878) suggested that, "...increase of frictional resistance along the decollement west of the salt wedge-out impeded westward movement of the upper part of the plateau cover, producing imbricate thrust faulting; the ...anticline was produced as an incidental effect of the thrusting at depth." Rodgers (1963) suggested essentially the same mechanism of folding. Thus, the fold apparently was initiated by termination of a detachment surface or a zone of soft salt, and subsequent faulting was the mechanism by means of which rocks in the core of the anticline were thickened.

In this chapter I show that terminations of detachment surfaces can produce passive folds by thickening the section locally. My analysis should be relevant to early stages of formation of folds similar to the Burning Springs anticline. However, it is possible that, once initiated, most of the growth of the Burning Springs anticline was a result of buckle folding. As suggested by Sherwin (1972) for the Chestnut Ridge anticline, the faulting in the core of the Burning Springs anticline may have been a mechanism of thickening of the section there during buckle folding of overlying rock, rather than the cause of the folding as suggested by Rodgers (1963) and by Gwinn (1964).

The analysis presented here is similar to that developed in Chapter I to describe folding of passive layers over idealized ramp faults. There I considered the effect of adhesional drag, represented by constant shear stress, on a ramp connecting a lower detachment surface to a higher detachment surface. Drag was assumed to be zero along the flat detachment surfaces. Here, I investigate deformation in viscous material above a flat detachment surface along part of which adhesional drag is large and along part of which drag is zero (Fig. 1a).

I compare the folding caused by the termination of a flat detachment surface with the folding caused by bed-duplication folding at a ramp fault connecting frictionless detachment surfaces at two different levels. I examine deformation associated with a more complicated detachment surface that terminates at the top of a ramp fault (Fig. 1b), where folding is caused both by drag and by repetition of strata. The ramp fault connects a lower detachment surface with zero drag to an upper detachment surface with high adhesive drag.

Solution

In order to determine velocities and stresses near the termination of a detachment surface, I analyse a model that assumes rigid material below the detachment and viscous material above (Fig. 1a). The detachment surface is assumed to be frictionless so that the horizontal shear stress is zero here. The viscous material over the extension of the detachment surface (dashed line in Fig. 1a) is assume to adhere to the rigid base, and the maximum shear stress the base can exert onto the contacting viscous fluid is the adhesional strength, k.

I use Fourier series in order to solve this problem, so that the detachment surface and the adhesional surface, both of width d are repeated cyclically along the x-axis. I present results of calculations for a small area, ABCD (Fig. 1a), of the body; so, for translations that are a small fraction of d the results are similar to those one would obtain for infinitely long detachment and adhesional surfaces. The method of solution of such problems has been well documented (Kamb, 1970; Fletcher, 1977; Reches and Johnson, 1978; McClung, 1981), so I will omit discussion of the method here, but I present the derivation in the dissertation appendix.

The solution for the velocities is,

Figure 1. Shape of detachment surface and distribution of drag assumed in theoretical analyses. (a) Symbols used to describe the flat detachment surface. Area ABCD denotes region near the termination of the detachment surface shown in Figure 2. Solid heavy line is segment with free slip. Dashed line is segment with drag of magnitude k (b) Symbols used to describe the stepped detachment surface which is comprised of a dipping ramp segment connecting the upper and lower flat segments. Heavy line is segment with free slip (lower flat segment and ramp segment). Drag on upper flat segment of magnitude k

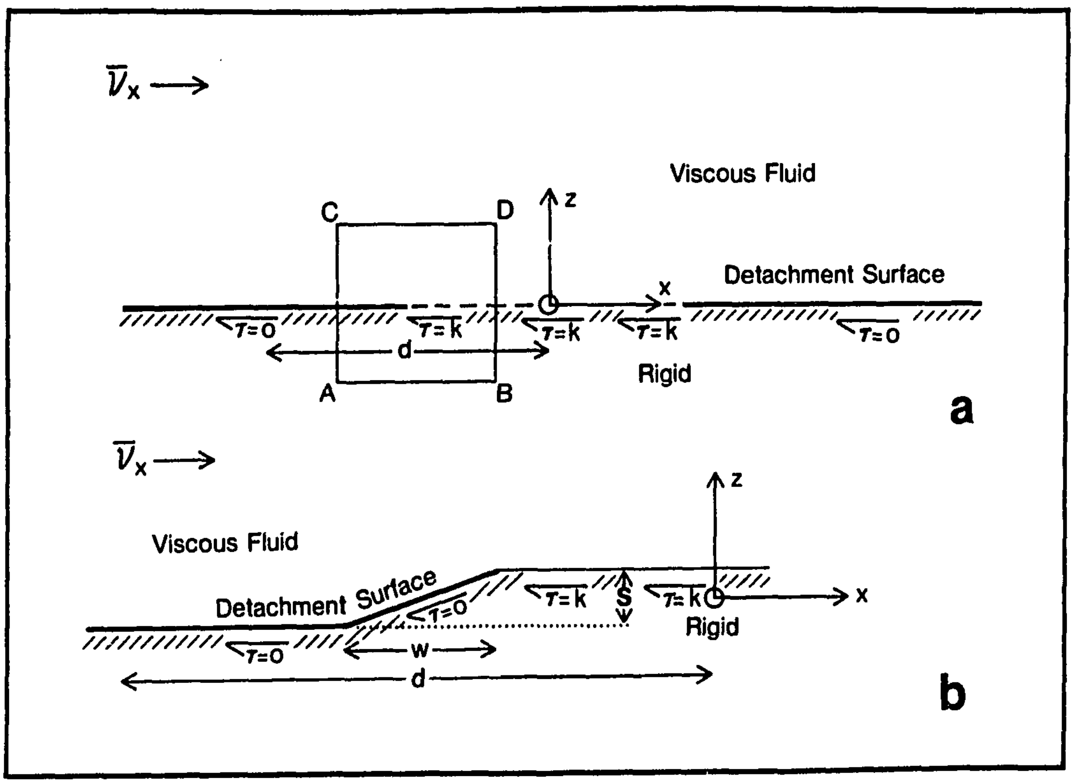

$\overline{V}_x$
Viscous Fluid
C
D
z
x
Detachment Surface
τ=0
τ=k
τ=k
τ=k
τ=0
d
Rigid
A
B
a
$\overline{V}_x$
z
Viscous Fluid
Detachment Surface
τ=0
τ=k
S
τ=k
x
Rigid
τ=0
w
d
b

$$v_x = \bar{v}_x + (kz/2\eta) + \sum_{m=1}^{\infty} (R_m/2\eta\, l_m)(l_m z - 1)\exp(-l_m z)\cos(l_m x) \tag{1a}$$

$$v_z = -\sum_{m=1}^{\infty} (R_m/2\eta\, l_m)(l_m z)\exp(-l_m z)\sin(l_m x) \tag{1b}$$

in which

$$l_m = m\pi/d \tag{1c}$$

Equations (1a) and (1b) are valid for any distribution of adhesional drag that can be expressed by a Fourier cosine series. For constant adhesional drag, we have assumed,

$$R_m = (2k/m\pi)\sin(m\pi/2);\ \text{odd } m \tag{1d}$$

The velocity in the x-direction (v_x), equation (1a), is the sum of three contributions. The first term in equation (1a), ($\bar{v}_x$), is a constant and defines uniform translation of the fluid. The other two contributions are the result of the drag along the detachment surface.

The drag causes a mean shear flow [second term in equation (1a)] and a perturbed shear flow (third term). The mean shear flow $(kz/2\eta)$, where η is the viscosity of the fluid, is produced by the average stress, $k/2$, along the interface between the fluid and the rigid substratum. I assume that the mean shear flow is zero at the detachment. It increases linearly with z so that far from the interface the velocity is a combination of the uniform translation and the mean shear flow. The perturbed shear flow, the third contribution to the velocity, decreases exponentially with increasing z and is required to satisfy the boundary conditions along the detachment surface. The velocity in the z-direction (v_z) is solely a result of the perturbed shear flow. It decreases exponentially with increasing z.

In evaluating the solution I determine displacements of points by integrating numerically over time. I introduce a drag parameter, K which is proportional to the ratio of the adhesional drag, k and a characteristic shear stress in the fluid, $(\overline{V}_x / d)\eta$, such that

$$K = (kFd / \overline{V}_x \eta) \tag{2a}$$

where F is a factor, the value of which is determined as follows. For $K = 1$, I set the velocity equal to zero at $x = 0$, $z = 0$, in equation (1a).

$$v_x = \sum_{m=1}^{\infty} (R_m/2\pi l_m). \qquad (2)$$

Substituting (2b) and (1d) into (2a),

$$F = \sum_{m=1}^{\infty} (1/m\pi)^2 \sin(m\pi/2); \quad m \text{ odd} \qquad (2c)$$

Thus, for $K = 1$ there is no slippage at point (0, 0), but there is slippage everywhere else along the interface. For K less than one there is slippage everywhere, and for $K = 0$ there is zero adhesional drag everywhere. I considered a range of K-values in Chapter I (Berger and Johnson, 1980), but here I will assume $K = 1$ for all calculations.

The solution is for a homogeneous viscous fluid, but I can qualitatively use the solution to determine types of minor folds and local faults that might develop in the stress field produced by termination of the detachment surface. I compute the stress difference and shear stress by means of the velocities, equations (1):

$$(\sigma_{xx} - \sigma_{zz}) = 4\eta(\partial v_x/\partial x) \tag{3a}$$

$$\sigma_{xz} = \eta[(\partial v_x/\partial z) + (\partial v_z/\partial x)]. \tag{3b}$$

The mean pressure is

$$p = -(\sigma_{xx} + \sigma_{zz})/2$$

$$= -\sum_{m=1}^{\infty} R_m \exp(-l_m z) \sin(l_m x) \tag{3c}$$

assuming a zero value at $x = 0$.

In order to discuss possible orientations of minor faults in the material I assume that the condition of faulting is described by the generalized Coulomb criterion (Rudnicki and Rice, 1975):

$$\sqrt{J_2} - p\tan(\phi) \leq C + p_0\tan(\phi) \tag{4a}$$

according to which yielding (faulting) occurs if the equality is satisfied. Here tan (ϕ) is the coefficient of friction, and ϕ is the friction angle, which we assume to be 30 degrees for the computations. J_2 is the second invariant of the deviatoric stress which, for plane strain, is,

$$J_2 = [(\sigma_{xx} - \sigma_{zz})/2]^2 + (\sigma_{xz})^2 \tag{4b}$$

and p_o is the overburden mean pressure, which must be added to the mean pressure computed via equation (3c).

In order to discuss where minor kink bands and drag folds might form in the fluid, I assume that a layered fluid is subjected to the stresses computed for the homogeneous fluid. The relevant stresses for folding are the normal stresses parallel, σ_{ss}, and normal, σ_{nn}, to markers between layers, and shear stress, σ_{ns}, parallel to layers. If θ is the slope angle of layering,

$$\sigma_{ss} - \sigma_{nn} = (\sigma_{xx} - \sigma_{zz})\cos(2\theta) + 2\sigma_{xz}\sin(2\theta) \tag{4c}$$

$$\sigma_{ns} = [(\sigma_{zz} - \sigma_{xx})/2]\sin(2\theta) + \sigma_{xz}\cos(2\theta). \tag{4d}$$

This completes the set of equations required to compute velocities, displacements, strains and stresses in the viscous fluid in the vicinity of the termination of a detachment surface.

Deformation near the termination of a detachment surface

Now let us examine results of computations of displacements, strains and stresses in a viscous fluid with passive layering near the termination of a flat detachment surface. There is zero drag along the detachment surface but along the extension of the detachment surface there is sufficiently great adhesional drag to prevent the fluid at the origin of coordinates (Fig. 1a) from moving. In the results presented in Fig. 2, the viscous fluid has been translated one-tenth of the length of the frictionless detachment surface (0.1 unit).

Figure 2(a) shows final positions of interfaces between passive layers in the viscous fluid that were originally horizontal. The interfaces have been deformed into a broad, low amplitude fold as a result of translation and drag. The drag itself is reflected in the tilting of the steeply inclined lines at either end of the figure; these lines originally were vertical. The layer-parallel shear increases from zero at the frictionless detachment surface at the left-hand end

Figure 2. Deformation in a thrust block that has been translated 0.1 unit. Markers originally horizontal and end lines originally vertical. Heavy line at base is frictionless segment. (a) Folding of passive markers. (b) Contours of finite compressive strain and magnitudes in per cent (see text for definition). Arrows show orientations of the maximum principal compressive strain. (c) Contours of normalized buckling stress $(\sigma_{ss} - \sigma_{nn}) / k$, and senses of monoclinal kinkbands and drag folds that should form. (d) Contours of yield function $(c + p_0\mu)/ k$, and senses of minor conjugate faults that should form (here $\mu = \tan \phi$).

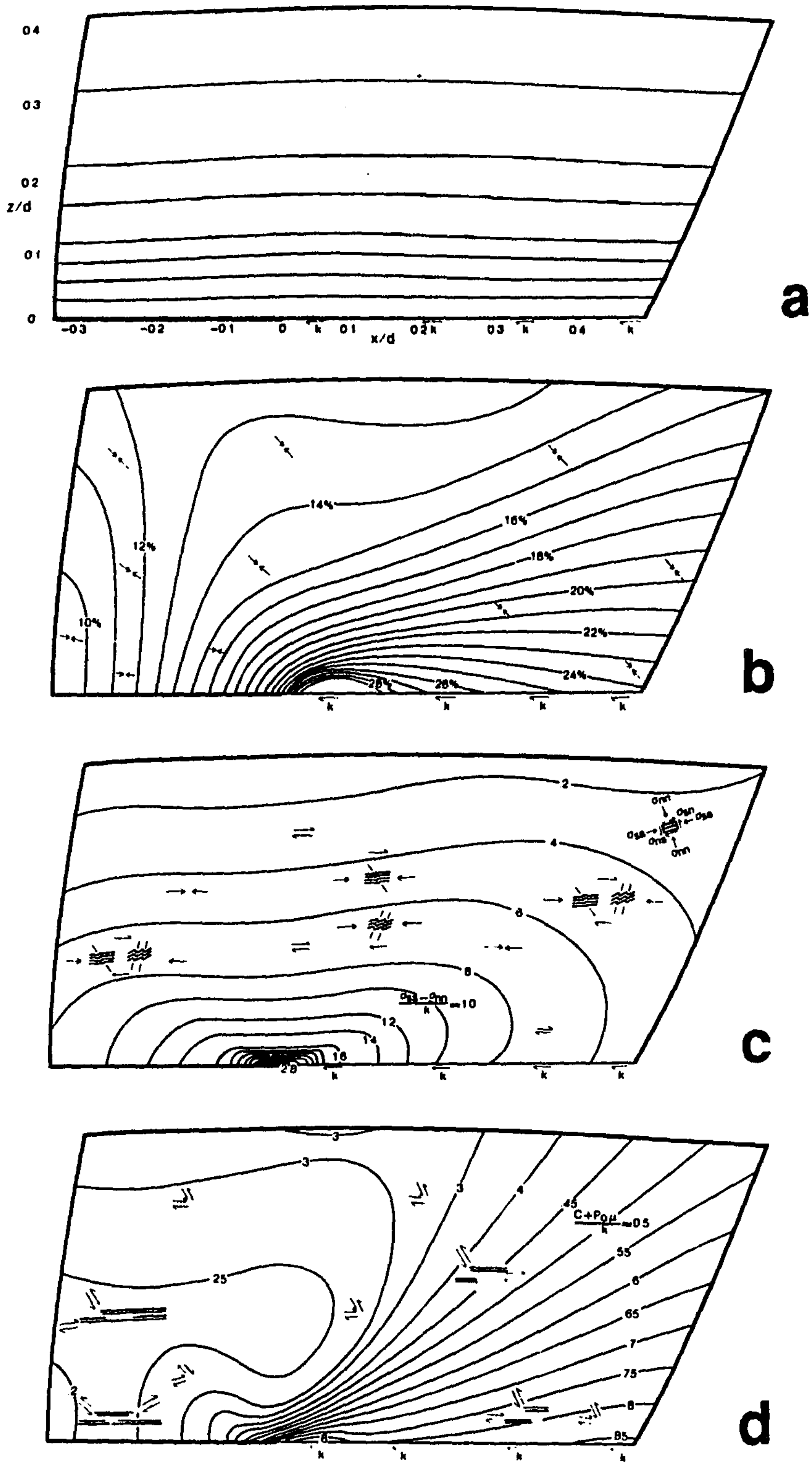
z/d
x/d
a
10%
12%
14%
16%
18%
20%
22%
24%
26%
28%
b
c
d

of the figure to a larger value at the top of the figure, as reflected in the tilt of the end line. In contrast, the layer-parallel shear decreases from a maximum value at the surface with large adhesional drag at the right-hand side of the figure, to a smaller value at the top of the figure.

The amplitude of the fold in the passive layering increases from zero at the detachment surface to a maximum value at some distance above the detachment surface, and then decreases to zero at very large distances above the detachment surface.

The distance above the detachment surface at which folding will be negligible will depend upon the amount of displacement on the detachment surface; the greater the displacement, the greater the distance of significant folding above the detachment surface.

The width of the fold increases upward, above the detachment surface, so that the width will increase and the amplitude will decrease with increasing distance above the detachment surface. Finally, the culmination of the fold shifts in the direction of transport with increasing displacement and with increasing distance above the detachment surface.

The mechanism of the folding in the passive layers shown in Fig. 2(a) is the reduction in horizontal velocity near the termination of the detachment surface. The formation of the fold reflects the gradient in shear stresses in the vertical direction; the equation of equilibrium indicates that a change in shear stress in the vertical direction is counteracted by a change in normal stress in the horizontal direction. Thus, the drag causes the viscous fluid to be compressed parallel to layering in the vicinity of the termination so that the viscous fluid thickens there, producing the fold. The folding in this case is a result of a fundamentally different mechanism than that described by Rich (1934), where folding is caused by repetition of stratigraphic section over detachment surfaces and ramps (Fig. 3a).

Directions and magnitudes of maximum finite compressive strains are shown in Fig. 2(b). The directions range from being parallel to the detachment surface at the detachment surface itself to being at an angle of slightly greater than 45°, plunging distally, in the overburden overlying the surface of high drag. The magnitude of the finite compressive strains are indicated in per cent, that is, in terms of $(1 - \mathcal{L}_f/\mathcal{L}_0) \times 100$, where $\mathcal{L}_f$ is the final length and $\mathcal{L}_0$ is the original length of a line element.

For far-field translation of one-tenth of the length of the detachment surface, the maximum finite shortening is about 30% near the termination. The compressive strains are larger in the fluid over the surface of high drag than they are over the detachment surface.

Magnitudes of the difference between layer-parallel and layer-normal stresses, divided by adhesional drag, k, and senses of layer-parallel shear are indicated in Fig. 2(c). Positive values of the stress difference indicate layer-parallel compression. The solution, of course, was derived for an homogenous, isotropic fluid, so that buckle folding cannot occur. However, I can use the solution to extrapolate where buckle folds would form and to indicate the sense of asymmetry of minor buckle folds if the fluid were layered. The sense of asymmetry of drag folds and monoclinal folds are opposite for the same state of deformation (Reches and Johnson, 1976; Ramberg and Johnson, 1976). Asymmetric chevron folds and drag folds will form with their short limbs facing distally, and monoclinal kink bands will form with their short limbs facing proximally, as shown in the inset sketches in Fig. 2(c). The stress difference is maximal near the termination of the detachment surface, so the strongest tendency for minor folds to form is there.

Figure 2(d) shows directions of minor faulting and magnitudes of a yield function, which is based on the generalized Coulomb law of failure and is the value of the cohesive strength plus the overburden mean pressure times the coefficient of friction. The friction angle is assumed to be 30° for all our computations. The cohesive strength and the mean pressure are normalized by k, so that the contours in Fig. 2(d) are in terms of values of the quantity, equation (4c),

$$[(C + p_0 \tan(30^\circ))]/k = \text{yield function} \tag{5}$$

required to prevent local faulting. The larger the value, the greater the tendency for faulting according to the yield criterion, so that the contours shown in Fig. 2(d) are considered to be contours of equal tendency to fault locally.

As shown in the figure, the tendency for faulting to occur is maximal near the extension of the detachment surface where adhesional drag is large. The orientations and senses of minor faulting, according to the idealized model, are shown by inset figures in Fig. 2(d). Near the detachment surface (lower left in Fig. 2d) the ideal faults are conjugate relative to the orientation of the surface and are reverse faults. In most places one fault is a low-angle thrust fault and the other is a high-angle reverse fault dipping in the direction of transport; that is, they are 'back thrusts'.

Deformation near a ramp fault

Deformation patterns of viscous overburdens moving over ramp faults are shown in Figs. 3 and 4 in order to compare deformation caused solely by repetition of strata (Fig. 3a) with that caused by a combination of repetition and of termination of slippage along the upper detachment surface (Fig. 3b). The solution for these cases is presented in the Appendix. In both cases, the inclined fault has a slope of 0.2, and the amount of horizontal translation is equal to one-fourth the height (S) of the inclined fault segment (0.25 units). The relative amounts of layer-parallel shear are indicated by the lines bounding the figure which were vertical before deformation. Where there was

Figure 3. Folding of passive markers and strain in the region above detachment surfaces and ramp subjected to translation of 0.5 units. (a) and (c): Frictionless detachment surfaces and ramp. (b) and (d): Terminating detachment surface and ramp. In (a) and (b), the markers were originally horizontal and the endlines vertical. (c) and (d) show the contours of finite compressive strain for (a) and (b), repectively.

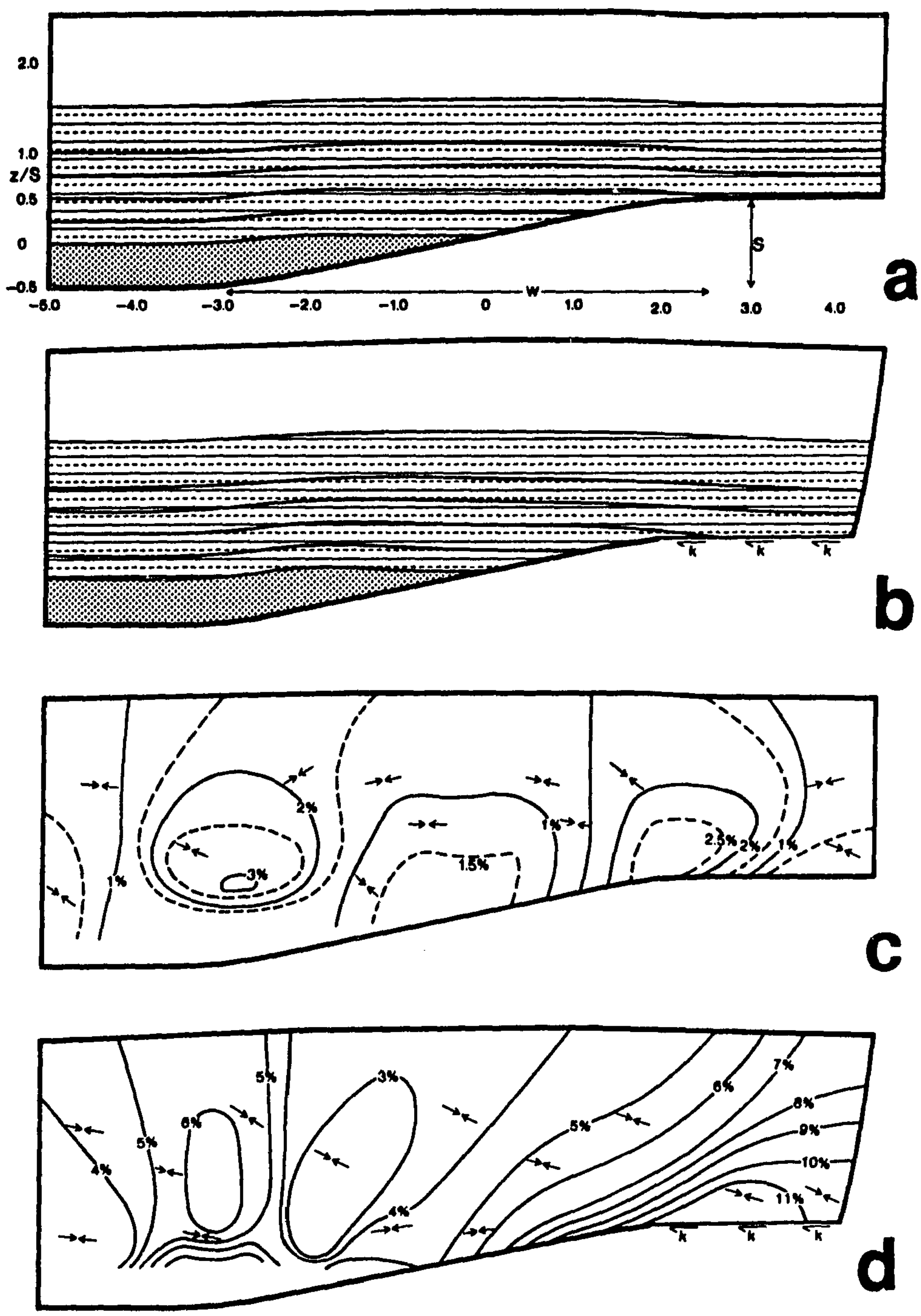
2.0
1.0
z/S
0.5
0
-0.5
S
w
-5.0
-4.0
-3.0
-2.0
-1.0
0
1.0
2.0
3.0
4.0
a
b
2%
3%
1%
1%
1.5%
2.5%
2%
1%
c
5%
3%
6%
5%
4%
5%
6%
7%
8%
9%
10%
11%
4%
d

Figure 4. Minor structures that should from in the region above detachment surfaces and ramp subjected to translation of 0.25 units. (a) and (c): Frictionless detachment surfaces and ramp. (b) and (d): Terminating detachment surface and ramp. (a) and (b) show the contours of normalized buckling stress $(\sigma_{ss} - \sigma_{nn})/k$ Monoclinal kink bands and drag folds may form in regions of positive stress difference, and pinch and swell structures in regions of negative stress difference. (c) and (d) show contours of yield function $(c + p_0\mu)/k$ and patterns of minor conjugate faults (here $\mu = \tan \Phi$).

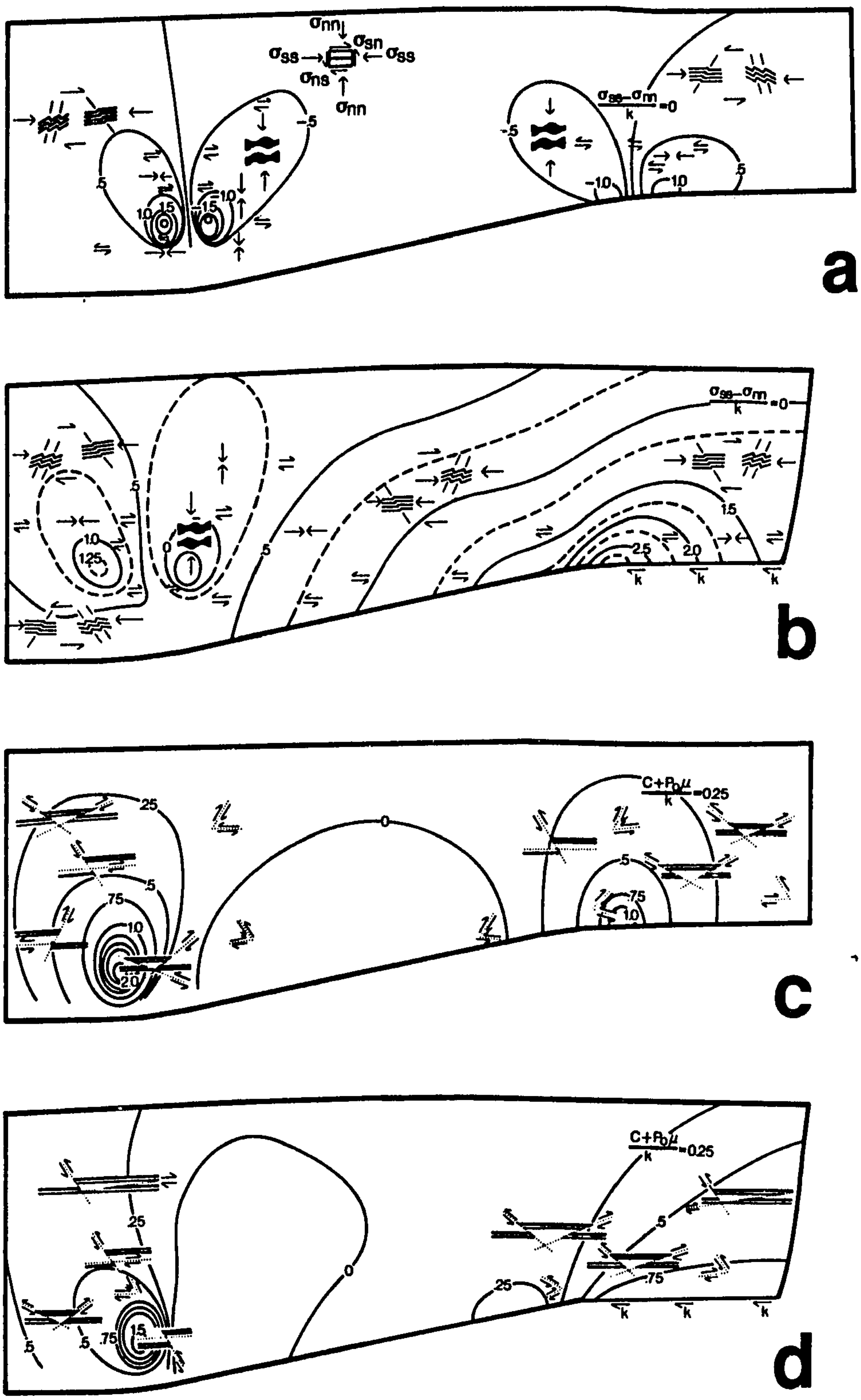
σnn
σsn
σss
σns
σss−σm / k =0
a
b
C+P0μ / k =0.25
c
d

zero drag, the lines are essentially vertical (Fig. 3a) and where there was drag, the line is tilted in the area of drag (right-hand side of Fig. 3b) and is nearly vertical in the area of zero drag (left-hand side).

In both examples, broad folds develop in the passive layering, but the forms of the fold are slightly different. For the ramp fault with zero drag, the fold is flat-topped with monoclinal flexures near the foot of the ramp and near the top of the ramp (Fig. 3a). The amplitude of folding is about the same for the passive interface at midheight on the ramp, $z = 0$, and for the interface at $z = S$. The amplitude at $z = 2.5S$ is slightly lower, so amplitude decreases upwards at large distances from the ramp. For the terminating ramp fault (Fig. 3b), however, a small anticline develops over the foot of the ramp near midheight of the fault. At intermediate levels ($z = 0.5S$ to $0.75S$) the fold is flat-topped but slightly asymmetric. The proximal limb is slightly steeper than the distal limb. At higher levels ($z = 2.5S$), the fold is rounded and its width increases with height, but the fold is still asymmetric.

The asymmetry is a result of adhesional drag along the upper detachment surface. As discussed in connection with the terminating detachment surface (Fig. 2a), the drag causes thickening in the vicinity of the termination of the ramp fault. The thickening reduces the dip of passive layering at the distal edge of the fold, whereas it has a minor effect on passive layering at the proximal edge of the fold, so that the proximal edge is steeper than the distal.

Directions and magnitudes of maximum compressive strains are shown in Figs. 3(c) and (d). There is a zone of relatively high compressive strain in the vicinity of the foot of the ramp. For the terminating ramp fault (fig. 3d), there is a zone of higher compression near the upper end of the ramp fault. This zone corresponds with that near the termination of a flat detachment surface (Fig. 2b).

Patterns of ideal minor folds and faults associated with a ramp fault and detachment surfaces without adhesional drag are shown in Figs. 4(a) and (c), those associated with the terminating ramp fault are shown in Figs. 4(b) and (d). The senses of asymmetry of drag folds and monoclinal kink bands are the same everywhere except near the head (Fig. 4a) or near the foot (Fig. 4b) where the sense of shear is reversed. Over the head and foot of the ramp fault connecting frictionless detachments, and over the foot of the terminating ramp fault, the layer-normal compression is larger than the layer-parallel compression, so pinch-and-swell structures or other extensional phenomena rather than folds should form there. For both ramp faults there is a strong tendency for minor faults to form near the foot of the ramp (Figs. 4c and d). For the ramp fault connecting frictionless detachments there is a secondary maximum of the yield function [equation (5)], at the top of the ramp. For the terminating ramp fault the yield function is large along the upper detachment surface where addhesional drag is great.

The orientation and sense of displacement for the minor faults are shown in Figs. 4(c) and (d). For the case of a frictionless detachment surface and ramp, the overall pattern of minor faults is diverse, whereas for the case of a terminating ramp, back thrust would predominate. At the foot of the ramp, for example, where the tendency for faulting is greatest, back thrusts occur in the case of a terminating detachment surface (Fig. 4d), whereas a more complex set of conjugate faults occur in the case of the frictionless detachment surface and ramp (Fig. 4c).

Discussion

I can compare the style of minor faulting derived analytically with faulting observed in field studies of Serra (1977) and the faulting observed in experiments by Morse (1977). Serra examined beds duplicated by thrusting over ramp faults and recognized three main structural styles in the upper thrust plate (Fig. 5). Serra observed that the lower beds in the hanging wall could be subjected to thickening by imbricate faulting (Fig. 5a) or by flowage (Fig. 5b), or could be offset by backthrusts (Fig. 5c).

The thickening in the upper plate can be a result of buckle folding of a multilayer (Sherwin, 1972; Wiltschko and Chapple, 1977; Fletcher, 1981) or of drag at the ramp as in Chapter I (Berger and Johnson, 1980). Both folding mechanisms can produce the geometry and internal deformation observed by Serra and shown in Figs. 5(a) and (b). In the case of buckling, a soft layer will thicken due to a decrease in vertical stress beneath anticlines, resulting in flowage (Sherwin 1972) or in faulting (Fletcher, 1981). Drag at the ramp could also cause the thickening.

Figure 5. Structural styles observed in ramp regions of small-scale overthrust faults (after Serra, 1977). (a) Imbricate faulting in upper thrust plate. (b) Flowage in upper thrust plate. (c) Backthrusts in upper thrust plate.

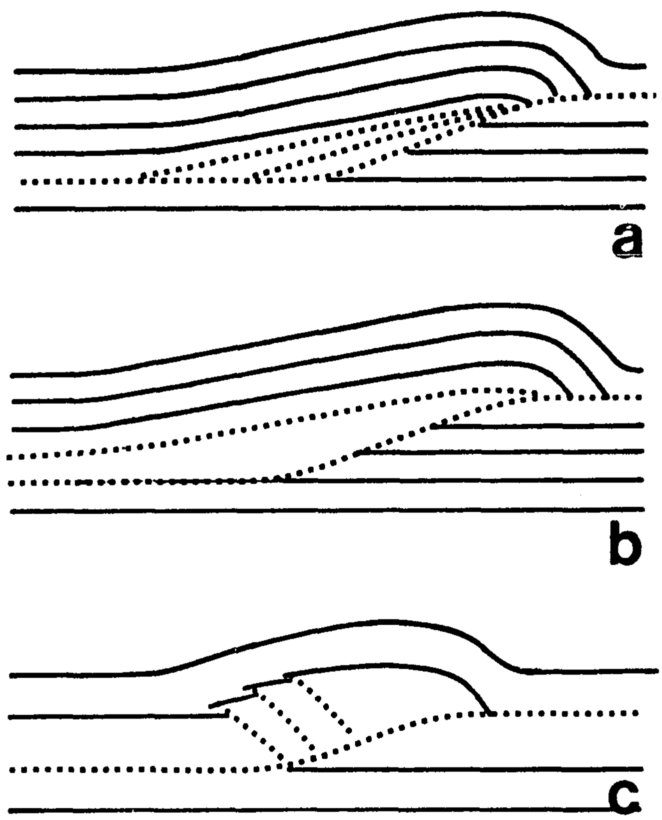
a
b
c

Serra (1977) reported that backthrusts commonly form in outcrops where the thickness of mechanical units was approximately equal to the height of the ramp. Morse (1977) experimentally produced backthrusts in folds formed by duplication of rock layers that were thrust over lubricated ramps. Morse noted that the backthrusts formed near the foot of the experimental ramp faults. In my analytical results, backthrust also form at the foot of the ramp (Fig. 4d). However, backthrusts are possible everywhere along the terminating detachment surface (Fig. 2d). It is likely that they are a result of the frictional drag as well as the presence of a thrust ramp.

Conclusion

Analysis of the deformation in the vicinity of the termination of a flat detachment surface clarifies a fundamental mechanism of folding. The mechanism is differential local thickening and layer-parallel compression produced by increased drag distally along a detachment surface. As translation continues, the fold will increase in amplitude and become asymmetric, with a steep distal limb, as a result of the mean shear caused by drag. Further, large translation can produce a nappe-shaped structure, as shown in Chapter I (Berger and Johnson, 1980, fig. 5d).

Accordingly, known mechanisms of folding include lateral termination of a detachment surface, draping over a fault (Powell, 1875; Reches and Johnson, 1978), intrusion of magma (Gilbert, 1877; Pollard and Johnson, 1973; Koch et al., 1981), bed-dupication (Rich, 1934; Wiltschko, 1979; Berger and Johnson, 1980), density instability (e.g. Ramberg, 1967), and buckling (e.g. Biot, 1961; Currie et al., 1962; Fletcher, 1977). Some folds appear to have been produced predominantly by one of these mechanisms, but others apparently are caused by a combination of mechanisms.

The Burning Springs anticline is probably an example of a fold produced by several mechanisms. Rodgers (1963) presents evidence that salt in Silurian rocks pinches out in the vicinity of the anticline, so that it is possible that the salt behaved as a viscous material with little drag and that the adjacent rock to the west behaved as a material with greater drag, much as in the idealized model of a terminating detachment surface. I would suggest that the termination of the detachment surface or a splay fault produced a low-amplitude fold which subsequently became amplified by buckling as the multilayered rocks were shortened further. Thus I suggest that the Burning Springs anticline is similar to most of the other folds on the Allegheny Plateau, west of the Valley and Ridge Province, which, according to Sherwin (1972) and to Wiltschko and Chapple (1977), are primarily a result of buckling of multilayers above zones of decollement. The most important difference would be that the Burning Springs Anticline is not part of a wave train, but rather is an isolated fold localized by a peculiarity of the stratigraphic section.

CHAPTER III

KINEMATICS OF FAULT-BEND FOLDING

INTRODUCTION

In 1934, John L. Rich suggested that folding would result from duplication of beds above a thrust ramp connecting detachments at different horizons, and since that time his conceptual model has been applied to explain many folds in the Appalachian and Rocky mountains.

A few mechanical and geometrical analyses have been devoted to elucidating Rich's model of bed-duplication folding. Thus, John Suppe (1983) has developed a geometrical construction that produces a bed-duplication fold closely resembling the one proposed by Rich. Wiltschko (1979a 1979b) has mechanically analyzed the energetics of thrust sheets moving over ramps. In Chapter I I have analyzed the folding of passive markers due to translation of a thrust sheet over a frictionless thrust ramp. I also have incorporated adhesional drag on the ramp and on the detachments, and have investigated the folding, stresses and strains within the thrust sheet.

In this Chapter, I introduce a simple kinematical[1] model for bed-duplication folds that reproduces the forms of folds constructed geometrically by Suppe (1983), and then compare the kinematical model with results derived from the mechanical model of bed-duplication folding developed in Chapters I and II.

KINEMATICAL MODEL OF THE FAULT-BEND FOLD

In the form proposed by Rich (1934), bed-duplication folding requires: 1) Translation of hanging-wall rocks subparallel to the thrust surface. 2) Steps or curves in the thrust surface. 3) Continuous contact between hanging-wall and footwall across the detachment surface. 4) Stiff (or rigid) footwall.

---

[1]Kinematics deals with the motion of particles, lines and bodies without consideration of the forces required to produce or maintain the motion.

Suppe (1983) added three requirements to constrain the geometry of bed-duplication folds. These are: 5) Constant length of beds. 6) Planar fold limbs. 7) Constant thickness of beds within planar fold limbs. Suppe assumed that the folds obey most of the geometric rules identified by Paterson & Weiss (1966) for ideal kink bands. In Suppe's terminology, the bed-duplication folds that satisfy his assumptions constitute "fault-bend folds."

Velocity Domains and Velocity Discontinuities

In my kinematical model (Fig. 1a), I divide the area above the thrust surface into three velocity domains, I, II, and III, separated by two velocity discontinuities that form domain boundaries. Within each domain, the velocities are constant. One velocity discontinuity forms the domain boundary at the base of the thrust ramp and is inclined at a clockwise angle of $90^{\circ} - \theta/2$ (Fig. 1a). This domain

Fig. 1. Velocities, displacement paths and fold form of kinematical model. (a) Velocity vectors (heavy arrows) and velocity domains (I, II and III) separated by domain boundaries (steep dashed lines). V_0 is uniform velocity and θ is dip of ramp. (b) Displacement paths of selected points, for a horizontal translation of $1.0\mathcal{S}$ where $\mathcal{S}$ is height of thrust ramp and θ is 20°. (c) Fold form produced by horizontal translation of $0.5\mathcal{S}$ with superimposed selected displacement paths.

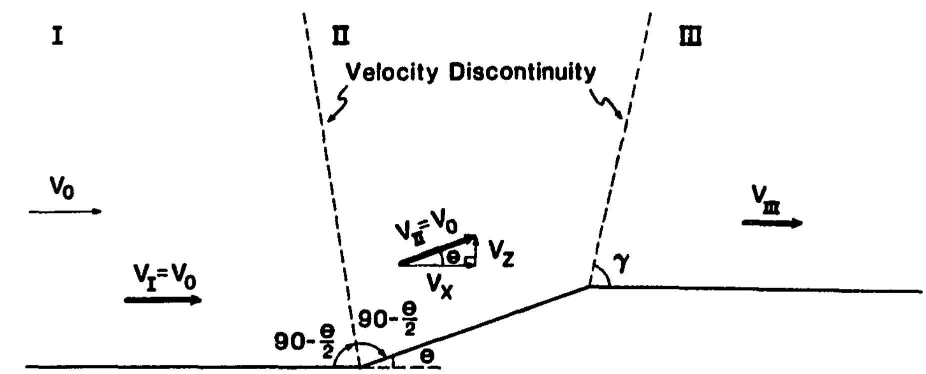
I
II
III
Velocity Discontinuity
V_0
$V_I = V_0$
$V_{II} = V_0$
V_Z
V_X
θ
$90-\frac{\theta}{2}$
$90-\frac{\theta}{2}$
γ
V_{III}

a.

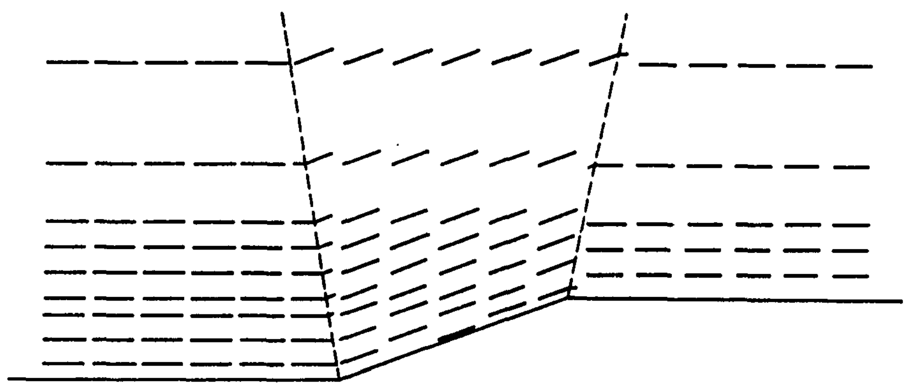

b.

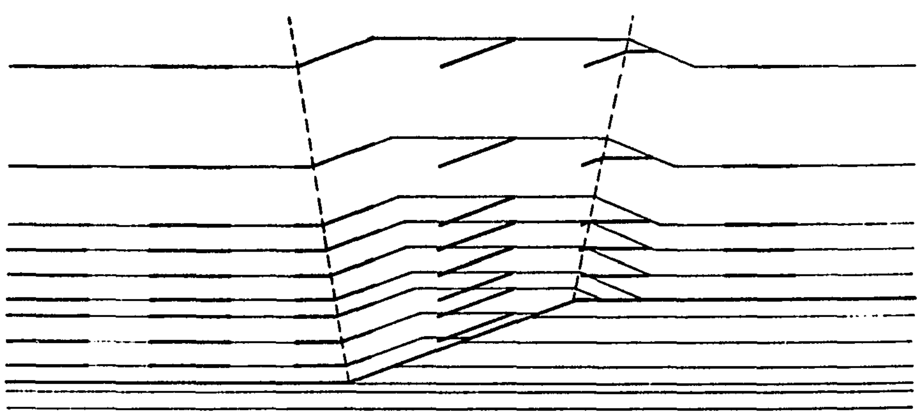

c.

boundary is fixed in all the kinematical models discussed herein. The other discontinuity forms the domain boundary at the top of the thrust ramp and is initially inclined at a counterclockwise angle, γ, of somewhat less than 90°. As we shall see below, this velocity domain boundary changes in orientation to $90^\circ + \theta/2$ as the bed-duplication fold stops growing vertically.

In each domain, the velocity vector is parallel to the detachment surface. Thus, in domain I, the velocity (V_I) is parallel to the lower detachment; in domain II, the velocity is redirected parallel to the thrust ramp; and in domain III, it is redirected parallel to the upper detachment. The velocity vectors change abruptly at domain boundaries.

The magnitudes of the velocity vectors are equal to V_0 within domains I and II because the vectors and bedding in both domains parallel the detachment surface near the domain boundary, and bed length is assumed to be conserved. In domain III, the magnitude of the velocity vector is slightly less than $V_0\cos(\theta)$, as I shall show below.

As shown in Fig. 2, each velocity vector in domains I and II can be decomposed into a component normal to the domain boundary (V_{nI} and V_{nII}) and a component tangential to the domain boundary (V_{sI} and V_{sII}). The normal components match at the domain boundary. The tangential components, however, are mismatched, and there is a change in magnitude of the tangential velocity equal to

$$V_{sII} - V_{sI} = 2V_0\sin(\theta/2) \qquad (1a)$$

which is approximately proportional to the slope of the ramp for small slopes,

$$V_{sII} - V_{sI} \approx V_0\tan(\theta); \quad \text{small } \theta \qquad (1b)$$

For small slopes, therefore, the magnitude of the vertical velocity over the ramp is merely equal to the velocity required to lift the material up the ramp as the material is translated horizontally

Fig. 2. Magnitude and orientation of velocity discontinuities at domain boundaries. Heavy arrows are velocity vectors. Light arrows are normal (subscript n) and tangential (subscript s) components of velocity vectors. Dashed lines are domain boundaries. Note change in magnitude of tangential velocity component at domain boundary.

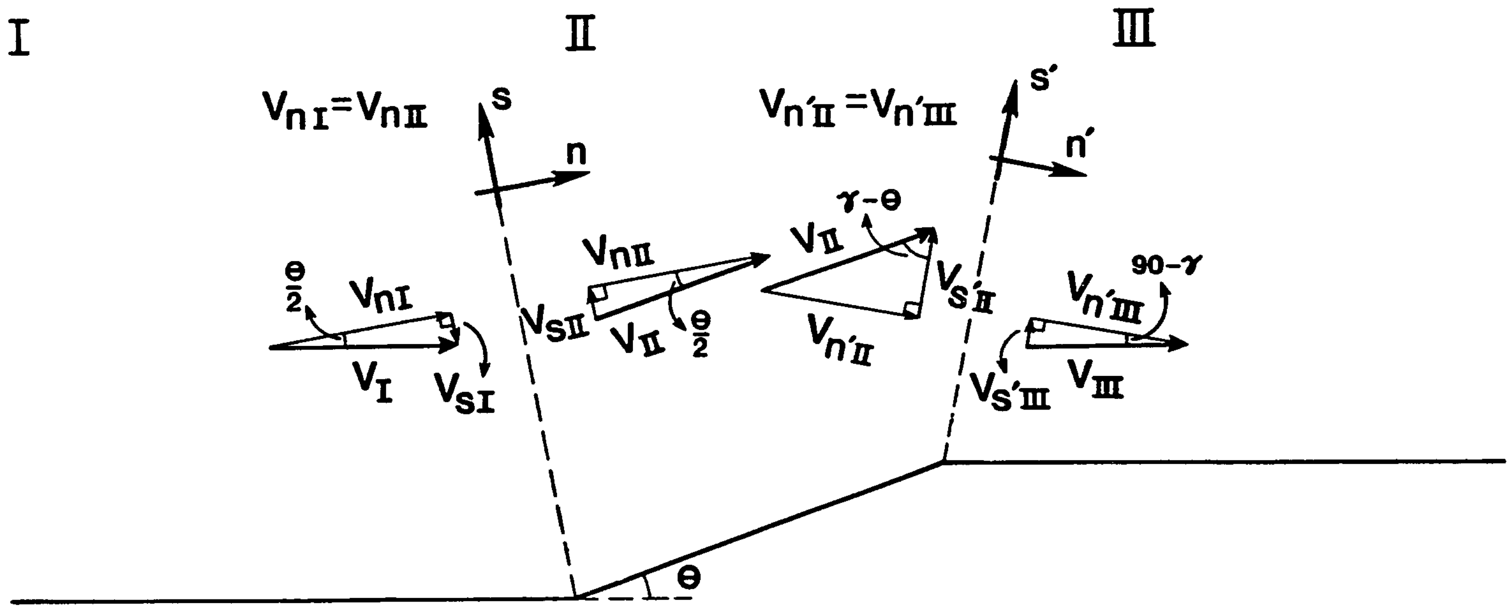

I
II
III
$V_{nI}=V_{nII}$
$V_{n'II}=V_{n'III}$
s
n
s'
n'
$\frac{\theta}{2}$
V_{nI}
V_I
V_{sI}
V_{nII}
V_{sII}
V_{II}
$\frac{\theta}{2}$
$\gamma-\theta$
V_{II}
$V_{s'II}$
$V_{n'II}$
90−γ
$V_{n'III}$
$V_{s'III}$
V_{III}
θ

toward the ramp.

I wish to emphasize that eq. (1a) is the magnitude of the discontinuity in velocity that occurs at the boundary between domains I and II and that there is no displacement discontinuity. Therefore, the domain boundary is a hinge, not a fault. A fault would require two closely spaced velocity discontinuities, with opposite sense, or else a displacement discontinuity. However, the pair of velocity discontinuities, one at each side of the ramp, behave much like the boundaries of a fault zone.

Within domain III, the velocity vector is parallel to the upper detachment, so at the boundary between domains II and III there is a change from a field of horizontal and vertical velocities to a field of horizontal velocity. The elimination of the vertical velocity component as beds cross the domain boundary causes tilting of the beds and the formation of the distal limb of a fold.

The magnitude of the velocity discontinuity at the boundary between domains II and III is determined in the same way as described above. Each vector is decomposed into normal and tangential components (Fig. 2). As a consequence of the reorientation of the velocity vector at the domain boundary, there is a discontinuity of the tangential velocity equal to

$$V_{sIII} - V_{sII} = V_{III}\cos(\gamma) - V_0\cos(\gamma-\theta) \qquad (2a)$$

For small slope angles, eq. (2a) is approximately

$$V_{sIII} - V_{sII} \approx -V_0\tan(\theta); \quad \text{small } \theta \qquad (2b)$$

Comparison of eqs. (1b) and (2b) shows that, for low ramp slopes, the first velocity discontinuity introduces and the second velocity discontinuity cancels the upward velocity component in the segment of material riding over the ramp fault. This is definitely consistent with the conceptual model of Rich (1934).

Relations between Velocities and Slopes of Velocity Discontinuities

The kinematical model provides enough information to trace marker lines as they are translated across the domains of the velocity field and through the velocity discontinuities. For example, a horizontal line segment that begins in domain I will deform into a dipping line segment as it enters domain II, with a dip equal to that of the thrust ramp. Similarly, a horizontal line segment that begins in domain II and enters domain III deforms into a line segment with a dip opposite to that of the thrust ramp.

The process is illustrated in Fig. 3(a), where a single line segment, *L*, moves with the flow, in five time steps, from domain II across the domain boundary into domain III. The two dashed lines in Fig. 3(a) show displacement paths of points that mark the ends of the line segment.

Figure 3(b) shows the initial and final positions of the line segment, *L*, as it begins (line AB), and completes (line CD), its passage through the velocity discontinuity (line BC). Points A, B, C,

Fig. 3. Initial and final positions of line segment that crosses domain boundary. (a) Five superimposed time steps showing displacement path of line segment, L as it crosses from domain II into domain III. Heavy arrows are velocity vectors and steep dashed lines are domain boundaries. (b) Initial and final positions of line segment, L as it intersects the domain boundary. Low angle dashed lines are displacement paths of points A and B.

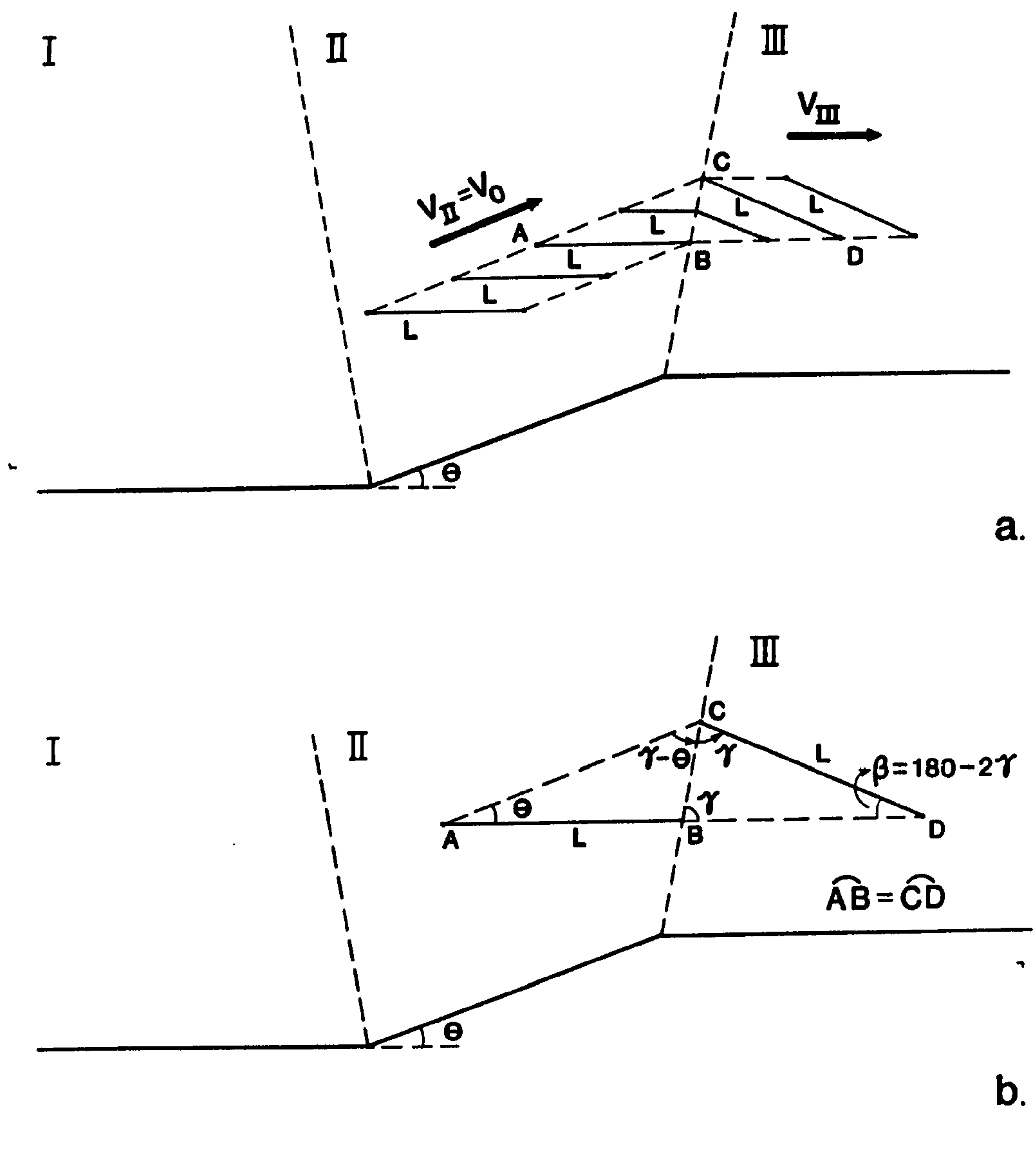
I
II
III
$V_{II}=V_0$
V_{III}
A
B
C
D
L
θ
a.
I
II
III
A
B
C
D
L
θ
γ-θ
γ
β=180-2γ
$\widehat{AB}=\widehat{CD}$
b.

and D are shown for reference in Fig. 3a. Note that point A, at the left-hand end of the line segment, remains in domain II and point B, at the right-hand end of the line segment, remains in domain III during the entire time period, t required for the line segment to pass through the discontinuity. As a result, the length of the dashed line, AC, is

$$AC = V_{II}t = V_0 t \tag{3a}$$

Similarly, the length of the dashed line BD is

$$BD = V_{III}t \tag{3b}$$

The value of V_{III} will be determined below in terms of the velocity V_0 and the slope angle, θ, of the ramp.

I first determine the angle, γ, the slope angle of the velocity discontinuity between domains II and III. Following Suppe (1983), I assume that line element $\mathcal{L}$ does not change length as it passes through the domain boundary, and thus,

$$AB = CD \tag{4a}$$

Following Paterson & Weiss (1966), I assume that beds are the same thickness on either side[1] of domain boundaries, or as shown in Fig. 3(b)

$$\text{angle (DBC)} = \text{angle (DCB)} \tag{4b}$$

The two assumptions stated above, (4a) and (4b) complete the definition of the geometry shown in Fig. 3, and from the geometry, I can eliminate the unknowns.

Considering triangle BCD, and using the law of sines,

$$[\sin(180^\circ - 2\gamma)/BC] = [\sin(\gamma)/L] \tag{5a}$$

Considering triangle ABC,

$$[\sin(\theta)/BC] = [\sin(\gamma - \theta)/L] \tag{5b}$$

I eliminate unknown length BC between eqs. (5), use trigonometric identities, and then use side lengths of a hypothetical right triangle containing γ in order to derive the following result,

$$\tan(\gamma) = \cot(\theta) \pm \sqrt{[\cot^2(\theta) - 3]}; \quad \theta \leq 30^\circ \tag{6}$$

Equation (6) generally has two real roots. For $\theta = 30^\circ$, however, it has

---

[1]Note that this assumption is independent of change of bed thickness within the discontinuity. In fact, as can be proved by considering the discontinuity to be represented by two smaller discontinuities bounding a thin zone, the thickness of layers increases and then decreases as the layers pass through the zone, even as the width of the zone is allowed to approach zero.

only one

$$\tan(\gamma) = \cot(\theta) = \tan(90 - \theta)$$

$$\gamma = 60^\circ; \quad \theta = 30^\circ$$

For ramp-fault angles greater than 30°, the roots of eq. (6) are imaginary, so there is no orientation of discontinuity that will satisfy the conditions of zero lengthening and thickening of beds.

The relation between the velocities in domains I and II on the one hand and domain III on the other can be derived with the law of sines, using angles ABC and BCA shown in Fig. 3(b):

$$[\sin(\gamma-\theta)/L] = [\sin(180-\theta)/AC] \tag{7a}$$

which, according to eqs. (3), can be written,

$$[\sin(\gamma-\theta)/V_{III}t] = [\sin(180-\gamma)/V_0 t] \tag{7b}$$

because BD = L.

Thus,

$$V_{III} = V_0[\sin(\gamma-\theta)/\sin(\gamma)] \tag{8a}$$

or

$$V_{III} = V_0[\cos(\theta) - \sin(\theta)\cot(\gamma)] \tag{8b}$$

Equation (8b) provides information about the range of velocities for domain III. For small ramp slope angles,

$$V_{III} \approx V_0\cos(\theta)$$

and $V_{III} \Rightarrow V_0$; $\theta \Rightarrow 0$.

For larger slope angles,

$V_{III} \Rightarrow V_0 \tan(30^\circ); \quad \theta \Rightarrow 30^\circ$

$\approx 0.5774\ V_0$

Accordingly, $\qquad 0.5774\ V_0 \leq V_{III} \leq V_0.$

Thus, eqs. (6) and (8) provide the necessary relations for determining the slope angle of the second discontinuity and the magnitude of the velocity vector within domain III.

Displacement Paths of Material Points

Figure 1(b) shows examples of displacement paths of many material points within the three domains associated with a ramp fault. The material points initially were situated along horizontal bedding planes. The left-hand end of each path is the initial position and the right-hand end is the final position of the material point, and the displacement paths show all intermediate positions occupied by the points. The nominal displacement of points, V_0t, was one half the height of the ramp.

Points originating and staying within domains I or III merely traced out straight, horizontal, line segments. Some points, however, were close to a discontinuity in velocity, so their displacement paths show bends.

If one ignores the points that passed through a velocity discontinuity, the displacement paths shown in Fig. 1(b) illustrate the three domains of the velocity field defined in Fig. 1(a). The velocity vectors in domains I and III are horizontal whereas those in domain II are inclined at the slope angle of the ramp fault. The magnitude of the velocity vector in domain III is somewhat less than that in domains I and II.

Fold Forms Predicted by the Kinematical Model

An example of a fold form predicted by the kinematical model is shown in Fig. 1(c), for a thrust ramp inclined at 20° and for horizontal translation in the far field, $V_0 t$ of $1.0 S$, where S is step height. Superimposed on the fold form are displacement paths of a few points. The positions of many more points were determined in order to construct the folded form of the passive layers.

The fold produced by the kinematical model is typical of bed-duplication folds in that its amplitude near the ramp is equal to the thickness of section duplicated by faulting, and its crest is flat (Fig. 1c).

Some special features of the fold are the following. The shapes of kink-like bands at either edge of the anticline are independent of distance above the thrust surface. Thicknesses of beds are constant, except in the fold hinges. The fold form produced by the kinematical model is identical to the fold form constructed geometrically by Suppe (1983) and termed the "fault-bend fold."

Figure 4 shows differences of fold forms caused by differences of

Fig. 4. Fold form form for a horizontal translation of 1.0*S* over thrust ramps of 10° (Fig. 5a), 20° (Fig. 5b) and 30° (Fig. 5c). *S* is height of thrust ramp.

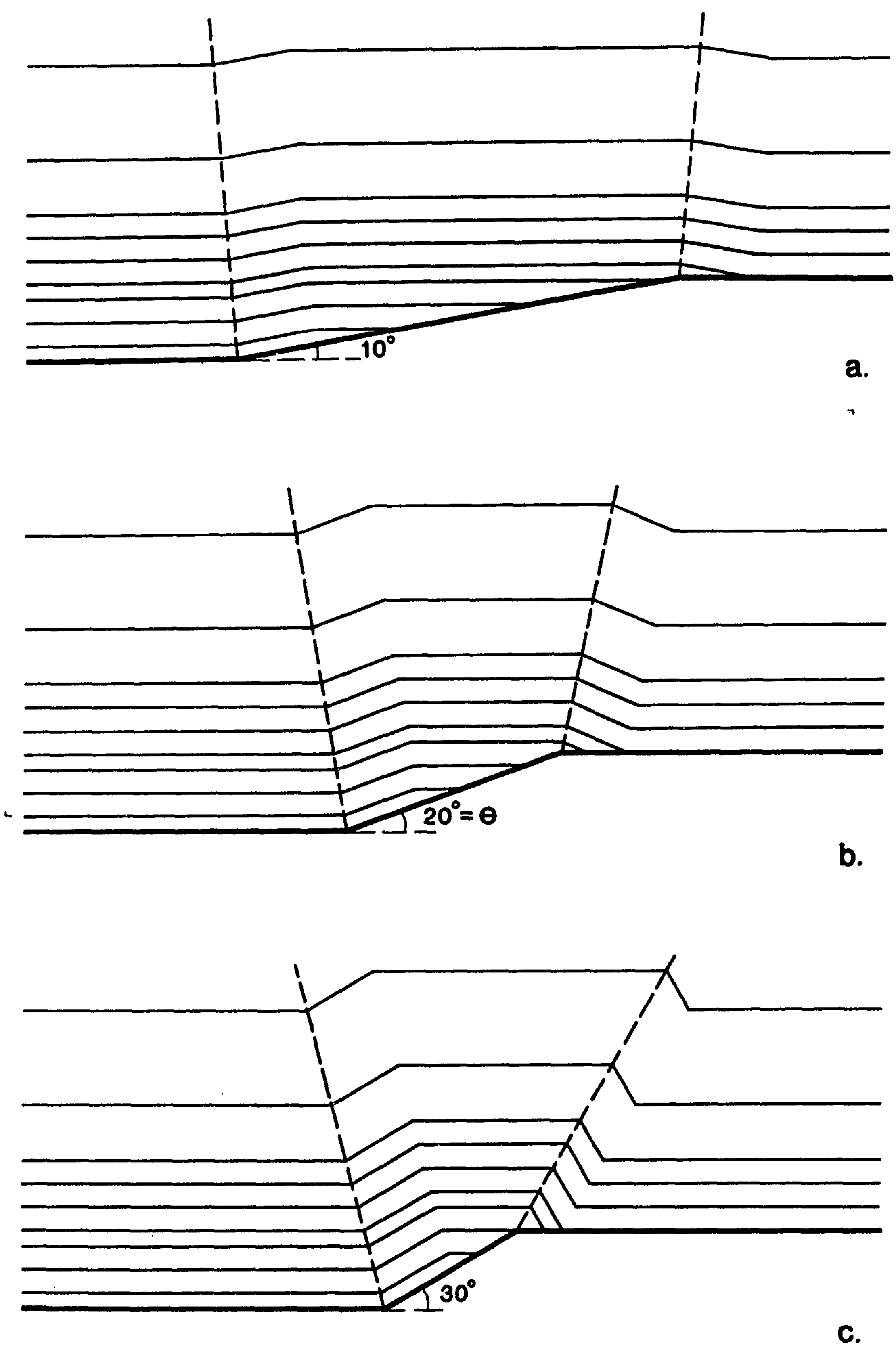

10°
a.
20°= θ
b.
30°
c.

ramp slope. The thrust ramps have dips of 10, 20 or 30°. The most obvious effect of increasing dip of the thrust ramp is to impart an asymmetry to the two limbs of the fold that is most apparent when the dip of the thrust ramp exceeds 20°.

Figure 5 shows changes of fold forms as results of changes in amounts of translation over a 20° ramp (0.2*S*, 1.0*S* and 2.9*S*, where *S* is the height of the thrust ramp). An increase in translation results in an increase in amplitude of the fold.

Kinematical Model for the Widening Stage

The fold cannot continue to grow in amplitude indefinitely with increasing translation. Duplication of beds at the ramp ceases and vertical fold growth ceases when the bottom of the lowest bed cut off at the base of the thrust ramp reaches the top of the ramp (Fig. 5c). Continued translation requires a new kinematical model that produces only widening of the flat, anticlinal crest.

Fig. 5. Fold form for horizontal translation of .2S (Fig. 4a), 1.0S (Fig. 4b), and 2.9S (Fig. 4c) over a 20° ramp. S is height of thrust ramp.

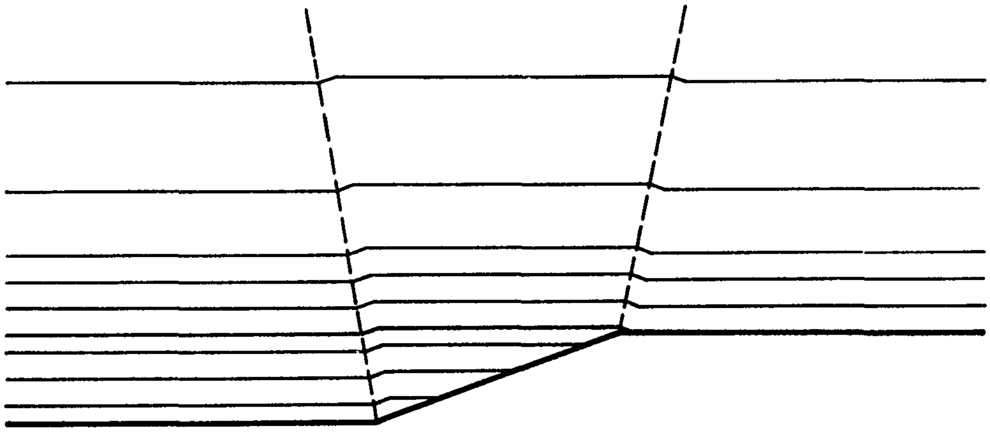
a.

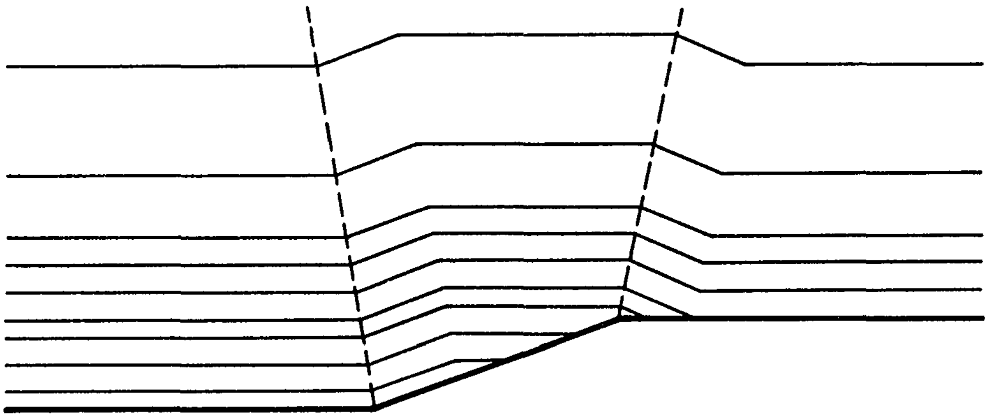
b.

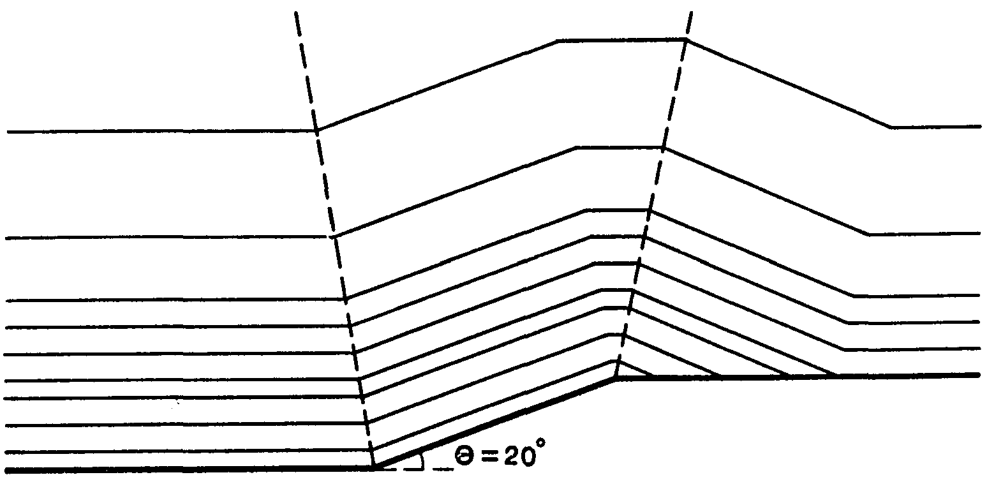

c.

In order for the assumptions of constant bed length and bed thickness to be maintained, the kinematical model must change when the bottom of the lowest bed reaches the crest of the ramp. The domain boundary oriented at angle, γ (less than 90°), ceases to be a velocity discontinuity, and a new domain boundary forms at a counterclockwise angle of 90° + $\theta/2$, such that the two velocity discontinuities become parallel (Fig. 6a).

The velocity in domain III changes from $V_{III} \leq V_0\cos(\theta)$ to $V_{III} = V_0$. Thus, the magnitude of the velocity vector becomes the same in all domains. The orientation of the velocity vector (V_{III}) remains parallel to the detachment surface. The magnitude of the discontinuity ($V_{S'III} - V_{S'II}$) decreases from the value given in eq. (2a) to the value given in eq. (1a), although of opposite sign.

An example of a fold constructed during the early stage according to the first kinematical model (Fig. 1a) and during the late stage according to the second kinematical model is shown in Fig. 6(a). The figure also shows the two velocity discontinuities of the second kinematical model. At large translation, a flat-crested fold is

Fig. 6. Fold form for a horizontal translation of $10.0S$ for two kinematical models. (a) Final fold form after translation of $10.0S$ using one velocity model for early folding and another for later folding. Bed length and thickness are constant. (b) Final fold form after translation of $10.0S$ using only onc velocity model [the model for late folding used in Fig. 6(a)]. V_0 is uniform velocity, S is height of thrust ramp, dashed lines are domain boundaries and heavy arrows are velocity vectors. θ is 20°.

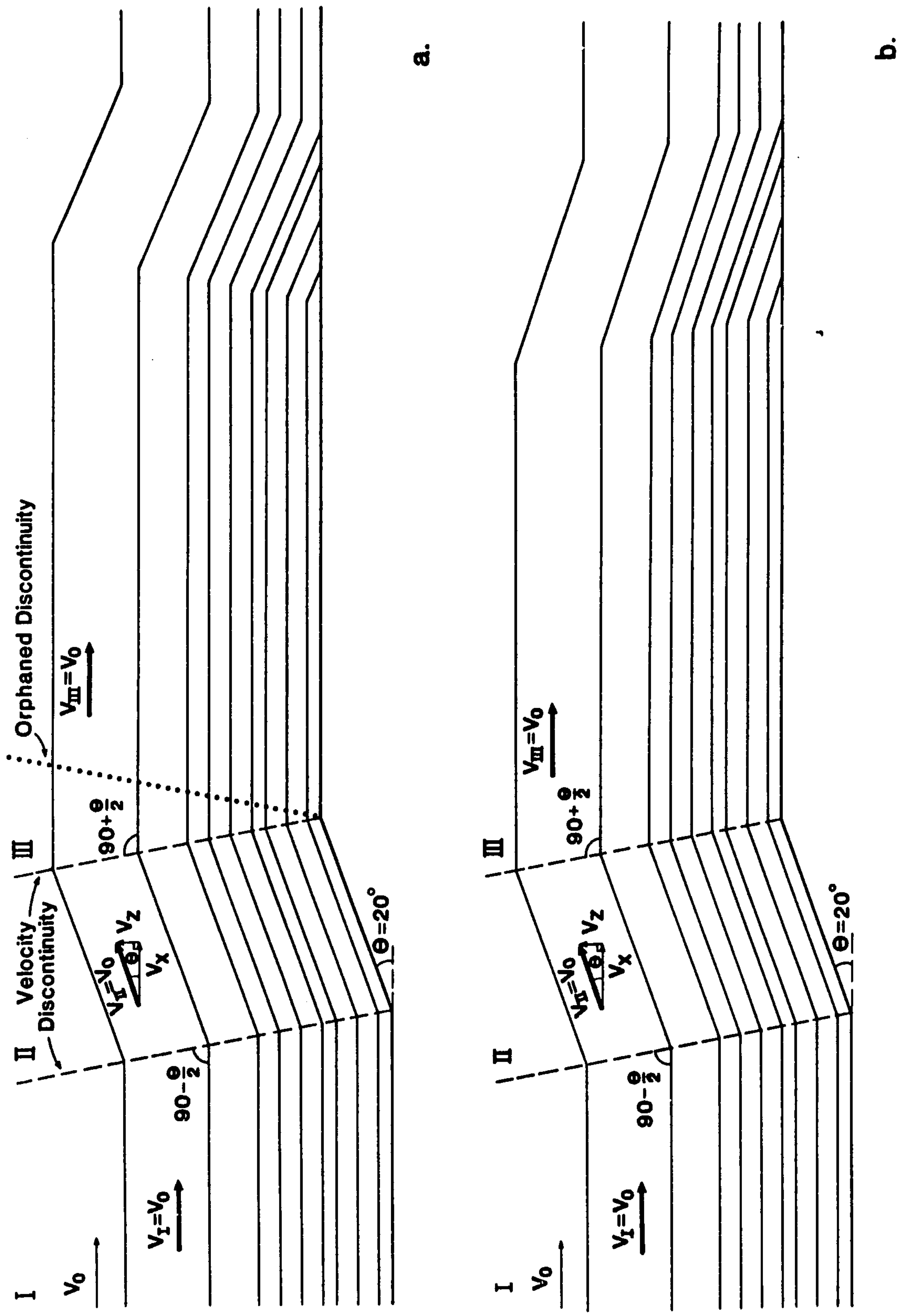
Orphaned Discontinuity
Velocity Discontinuity
I
II
III
V_0
$V_I = V_0$
$V_{II} = V_0$
$V_{III} = V_0$
V_Z
V_X
Θ
$90 - \frac{\Theta}{2}$
$90 + \frac{\Theta}{2}$
$\Theta = 20°$
a.
b.

produced, with an interlimb distance that increases with the amount of translation of the thrust block. Thus, during the late stage of fold growth, the distal fold limb is inactive and the fold is widening; deformation is occuring only at the edges to the proximal limb.

This completes the kinematical analysis of the geometric construction of bed-duplication folds proposed by Suppe (1983).

Other Kinematical Models

The introduction of two kinematical models has allowed me to investigate the essence of the kind of bed-duplication folds proposed by Suppe (1983). The kinematical models show that the number of fundamental variables that needs be specified is very small--a ramp slope, a velocity in each of three domains and slopes of two velocity discontinuities. Furthermore, identification of the fundamental variables allows me to change them and determine their effects on the form of bed-duplication folds. In this way, for example, one can determine which assumptions are essential to the kinematical description of a bed-duplication fold as described by Rich (1934).

The Suppe geometrical construction requires that bed thickness and bed length be constant. Even where the construction is applied to complex interactions of many ramp faults (Suppe 1980 1983), Suppe's construction maintains bed thickness and, perhaps, bed length. The resulting fold forms can be extremely complex, but perhaps some of the assumptions can be relaxed so the forms can be simplified.

Figure 7(a) shows a fold constructed using all the assumptions of the kinematical model (Fig. 1a), whereas Figs. 7(b) and 7(c) show examples of folds constructed for two kinematical models in which thicknesses and lengths of beds might change slightly. In the example shown in Fig. 7(b), the second velocity discontinuity is vertical, and the velocity in domain III is equal to the horizontal component of velocity in domain II. The beds on the distal limb thin slightly. A reason one might select this model is that it produces symmetric proximal and distal limbs. Another reason one might select this model is that, for low ramp slopes, it becomes identical to the first

Fig. 7. Fold forms and velocities resulting from three kinematical models after translation of 1.0S. (a) Fold form and velocities for early folding kinematical model. Thickness and length of beds is constant. (b) Fold forms and velocities for kinematical model that produces symmetric folds. (c) Fold form and velocities for late folding kinematical model. V_0 is uniform velocity, dashed lines are domain boundaries, and heavy arrows are velocity vectors. θ is 20°.

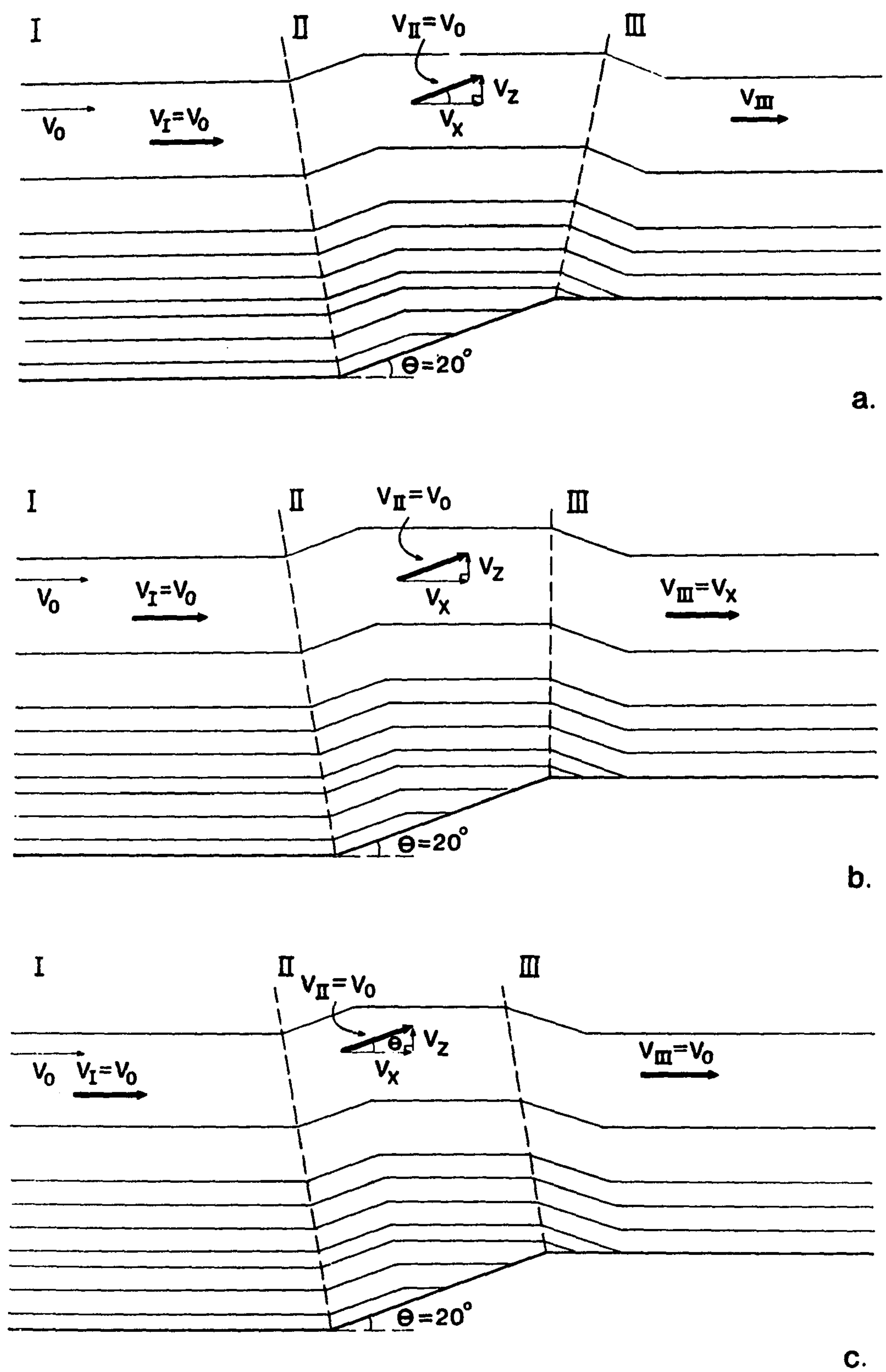

I
II
III
$V_{II}=V_0$
V_Z
V_X
V_0
$V_I=V_0$
V_{III}
$\Theta=20°$
a.
I
II
III
$V_{II}=V_0$
V_Z
V_X
V_0
$V_I=V_0$
$V_{III}=V_X$
$\Theta=20°$
b.
I
II
III
$V_{II}=V_0$
θ_F
V_Z
V_X
V_0
$V_I=V_0$
$V_{III}=V_0$
$\Theta=20°$
c.

kinematical model. In any case, the differences in fold form appear to be insignificant.

In the model shown in Fig. 7(c), I arbitrarily have inclined the second discontinuity even further, until the two velocity discontinuities are parallel. The velocity discontinuities, in fact, are the same as those that develop in the second stage of fold formation, shown in Fig. 6(a). The only difference, here, is that the velocity discontinuities are parallel throughout the folding history. The resulting fold for small translation is shown in Fig. 7(c) and for large translation is shown in Fig. 6(b). Comparison of Figs. 6(a) and 6(b) indicates that the model, which produces a distal limb in which beds have been slightly thinned (Fig. 6b) is virtually the same as the model that reproduces the Suppe geometric construction (Fig. 6a).

Because all these kinematical models produce essentially the same fold forms, the special assumptions of no change in thickness and no change in bed length must be inessential. Indeed, the only truely essential feature of the kinematical model appears to be that the folds are produced by fault duplication of beds, as indicated by Rich.

SUMMARY OF MECHANICAL MODEL OF BED-DUPLICATION FOLDING

The kinematical models were constructed to serve as a bridge between the geometrical constructions of Suppe (1983) and one of the mechanical models in Chapter I. Because the velocity distributions are presented in both the kinematical and the mechanical models, the models can be compared. In this section I review the mechanical model and present the velocities (Fig. 8a), displacement paths (Fig. 8b) and fold form (Fig. 8c).

The mechanical model in Chapter I presents the solution for the problem of uniform translation of a homogeneous, linearly viscous, infinite half-space containing passive bed-marker lines, over a stepped, rigid substratum. Here we select a step or ramp that is planar (Fig. 9a). In Chapter I, the ramp is a sinusoidal surface.

For the particular geometry chosen here (Fig. 9b), the step is one of a series, each connecting to a higher detachment. Thus, the x-axis

Fig. 8. Velocities, displacement paths and fold form for the mechanical model of Berger & Johnson (1980). (a) Velocity vectors within deforming thrust block. Note absence of velocity domains. Horizontal translation is $0.2S$, where S is height of thrust ramp. (b) Displacement paths of selected points. Horizontal translation is $1.0S$. (c) Fold form after translation of $1.1S$. θ is 20°.

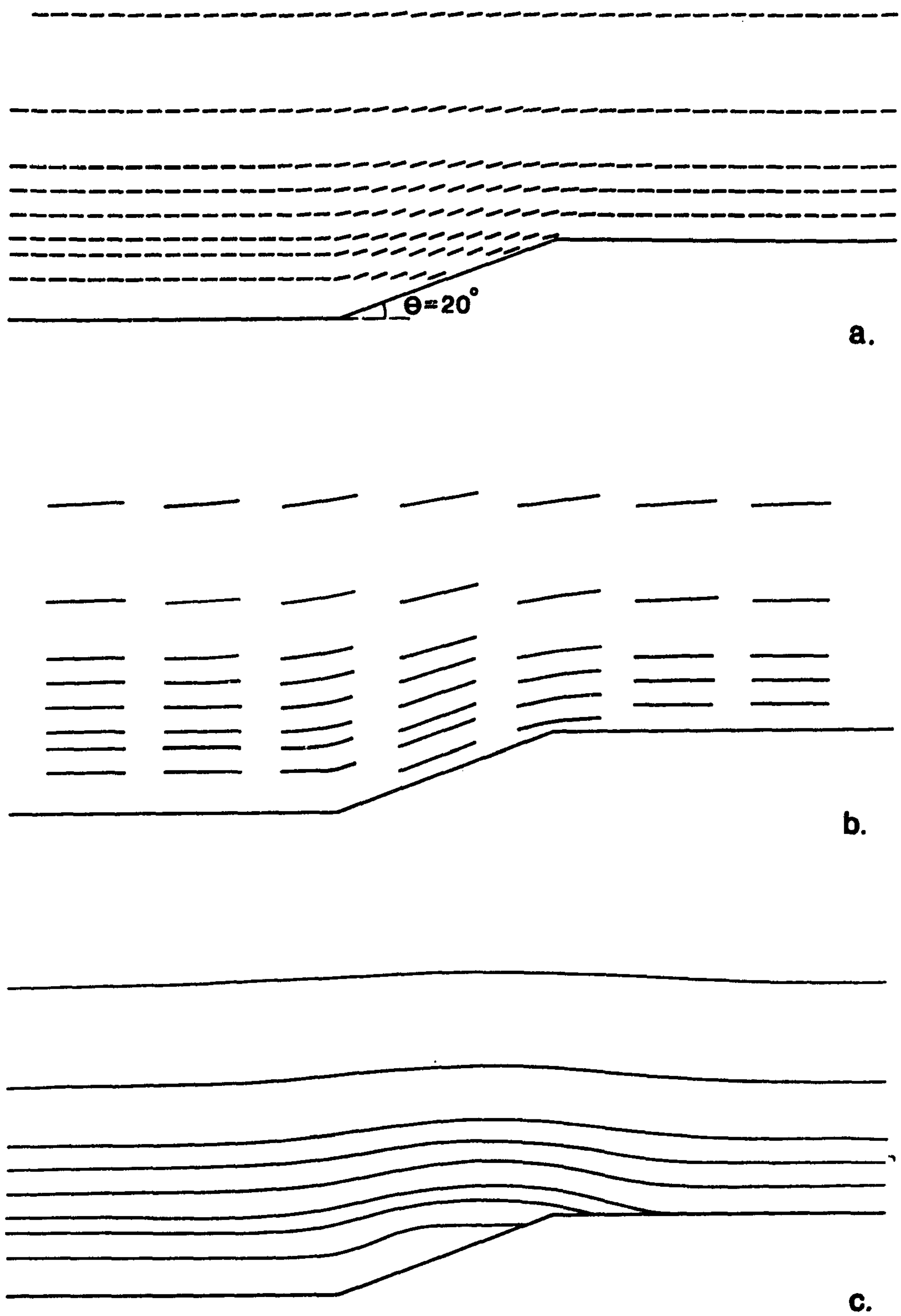
θ=20°
a.
b.
c.

Figure 9. Shape of detachment surface in second-order analysis of mechanical model. (a) Symbols used to describe a segment of the thrust surface, which is comprised of two detachment surfaces connected by a planar ramp. (b) Series of climbing, planar, thrust ramps connected by horizontal detachments.

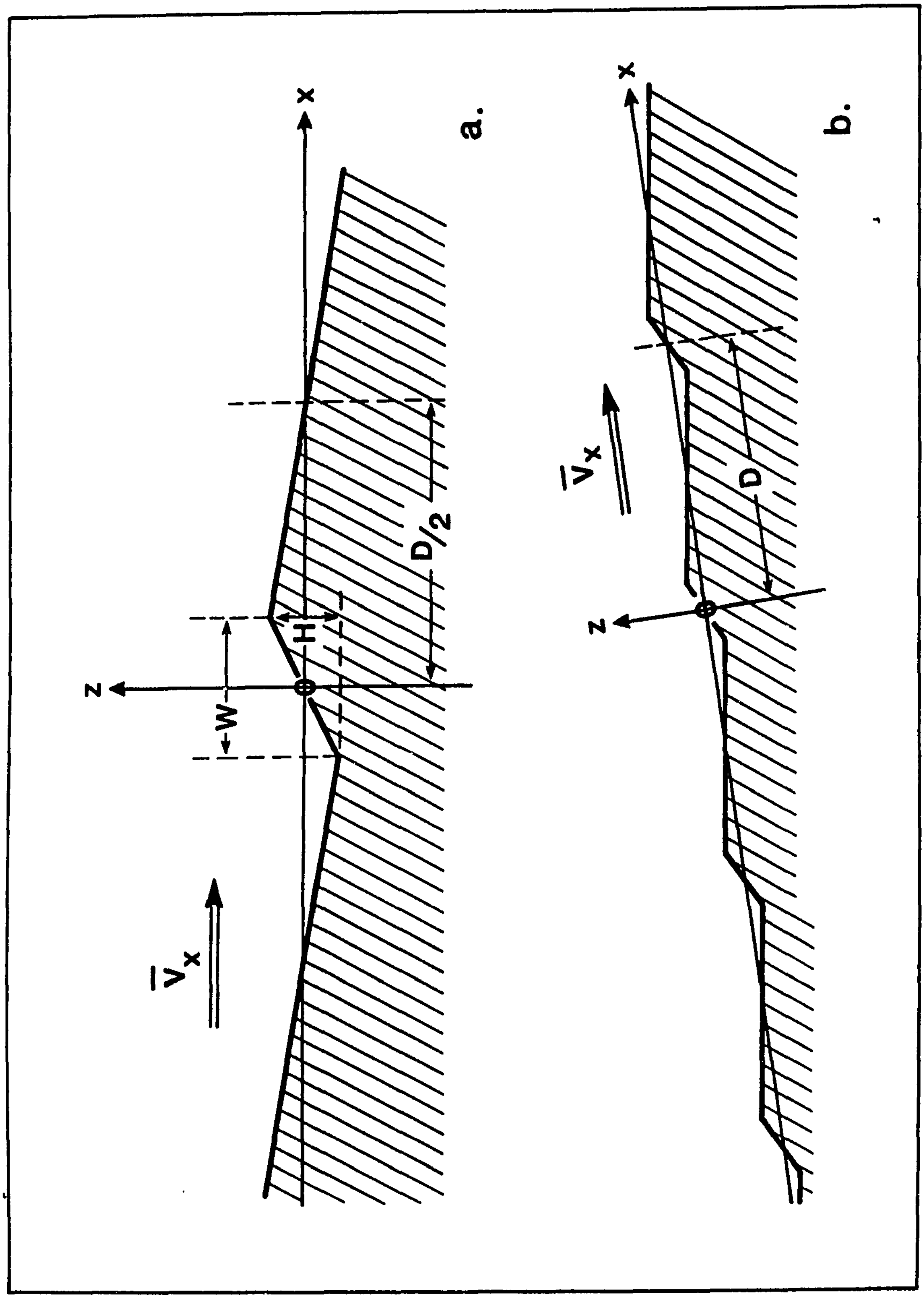
x
a.
z
W
H
D/2
$\bar{V}_x$
x
b.
z
D
$\bar{V}_x$

is inclined to the detachment surfaces, and parallel to the mean transport direction. In Chapter I and II, I chose a different series of steps, in which the x-axis is parallel to the detachment surfaces. Nevertheless, the forms of solutions for the velocity components are identical and are,

$$v_x = V_0[1 + \sum_{n=1}^{\infty} (A_n l_n)(l_n z)\exp(-l_n z)\sin(l_n x)] \tag{9a}$$

$$v_z = V_0 \sum_{n=1}^{\infty} (A_n l_n)(l_n z + 1)\exp(-l_n z)\cos(l_n x) \tag{9b}$$

Here

$$A_n = [H/(n\pi)^2][(D/w)[D/(D-w)]]\sin(l_n w) \tag{9c}$$

$$l_n = n\pi/D \tag{9d}$$

and

$$H = S[1-(w/D)] \tag{9e}$$

where S is step height, w is step width and D is spacing of the ramps (Fig. 9b).

To determine the final position of displaced points, the velocity components are integrated numerically with the Runge-Kutta technique.

Figure 8(a) shows displacement paths of particles originally uniformly spaced along passive, horizontal markers. The displacement paths are short, so they display the velocity field. The velocities are continuous throughout the thrust sheet and are of approximately uniform magnitude. In the vicinity of the thrust ramp, the velocities are perturbed from a horizontal orientation. The magnitude of the perturbation (i.e. the deviation from the horizontal) decreases exponentially upwards, so that at a distance, corresponding to several times the height of the ramp, the deviation is negligible.

Figure 8(b) shows longer displacement paths of selected particles. The paths are curved near the ramp as a result of the velocity perturbation there. Far above the ramp, the displacements approach uniformity.

Figure 8(c) presents the fold form for a translation of 1.1 S, where S is step height (defined in Fig. 9a). A symmetric fold is formed above the thrust ramp. The fold decreases in amplitude and increases in width with distance above the ramp. There is slight thickening or thinning of passive bedding.

DISCUSSION

Comparison of Models for Low Ramp Slopes

I have presented fold forms and velocity distributions assumed on the one hand in a kinematical model that reproduces the geometry of

Suppe's (1983) graphical construction, and derived on the other hand from a mechanical analysis of ramp folding. Fold forms produced by the kinematical and mechanical models of bed-duplication folding have the common property that, in the vicinity of the thrust ramp, the amplitude of the fold is equal to the amount of fault duplication of beds. This is the central concept of the folding model proposed by John L. Rich (1934), so both the kinematical and mechanical models include the essence of the Rich model. Furthermore, both types of analysis predict flat-crested folds where displacements are large, so both are consistent in this respect with the Rich conceptual model.

The velocity distributions and the fold forms constructed by the kinematical and mechanical models are similar, so the kinematical model appears to approximate the kinematics of the mechanical model, at least for low slopes. The geometrical construction of Suppe (1983) produces a reasonable, first estimate of the geometry of simple, bed-duplication folds.

Comparison of Models with High Ramp Slopes

The mechanical model can treat steeper thrust ramps if the problem is solved to second order, rather than to first order[1]. In eqs. (9), I have presented the first-order solution, which is valid if ramp slope is small. But the problem has been solved to second order, and I will present some results here for thrust ramps with slopes of 20° or 35°. These results from the mechanical model can be compared with those from the kinematical model.

The fold formed above a 20° ramp is slightly asymmetric according to the second-order analysis (Fig. 10a). For example, the

---

[1]The order of a solution reflects the extent to which the boundary conditions are matched. The analysis is accurate to first order if the slope of the thrust ramp, (A/l), is sufficiently small. It is accurate to first order if $(A/l)^2$ and higher powers are small compared to (A/l). The analyses are accurate to second order if $(A/l)^3$ is small compared to $(A/l)^2$.

Fig. 10. Fold forms produced by second order mechanical analysis. (a) Fold form produced after translation of 1.0S over a 20° ramp. Dashed lines remain steep after translation. (b) Fold form produced after translation of 1.0S over a 35° ramp. Tilted dashed lines were originally vertical. Note that bed dip does not exceed ramp dip. Beds are passive marker lines.

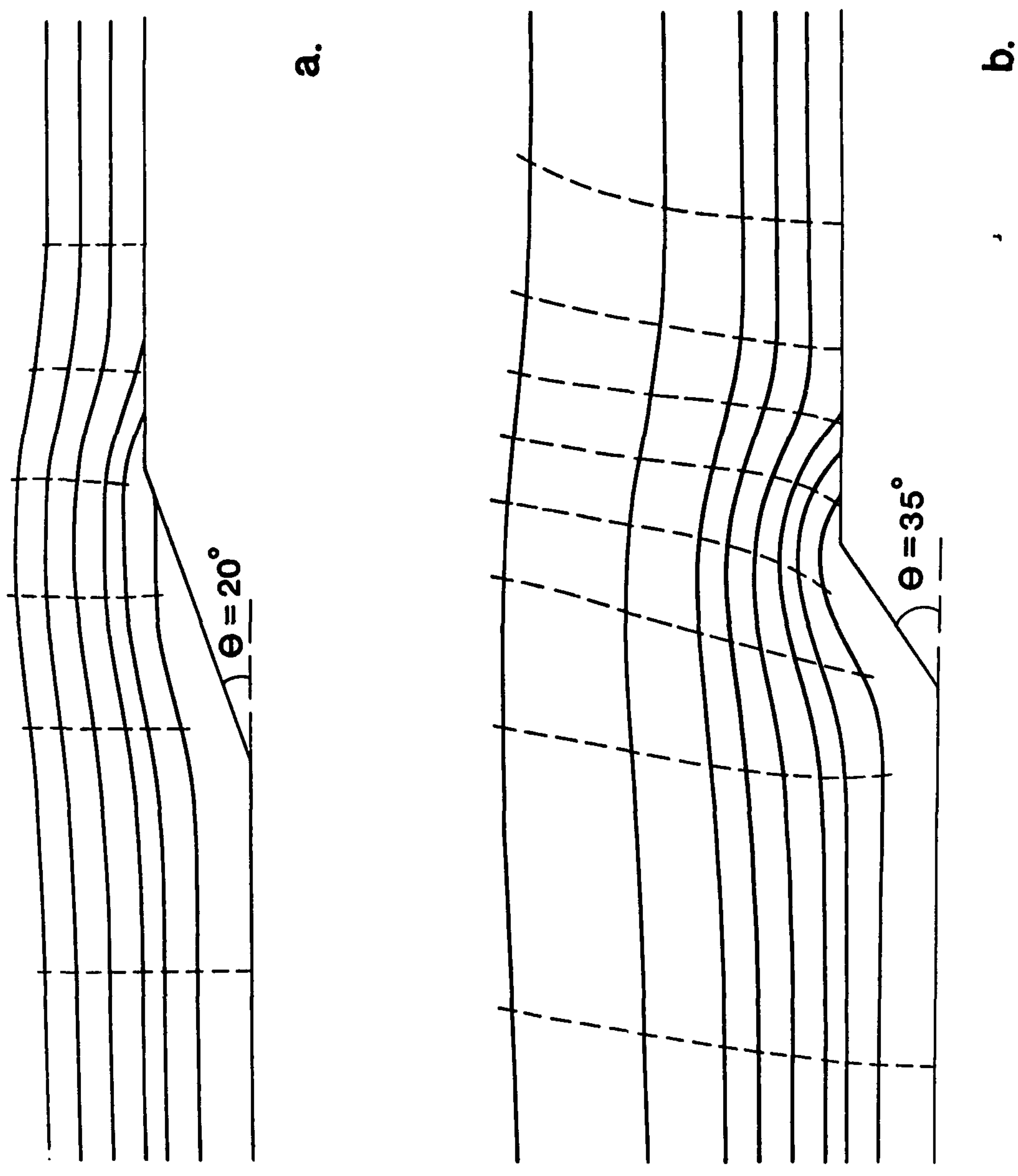
a.
θ=20°
b.
θ=35°

distal limb dips about 20° and the proximal limb dips about 15° in the second marker above the detachment surface shown in Fig. 10(a). The dip of both limbs is equal to or slightly less than the dip of the thrust ramp. The fold formed above the 35° ramp, Fig. 10(b), is distinctly asymmetric, again with a steeper distal limb. However, the dip of both limbs in markers above the upper detachment is less than the dip of the thrust ramp.

Another result of the second-order analysis is displayed by the distortion of the steep, dashed lines shown in Figs. 10(a) and 10(b). The dashed lines are passive markers that originally were vertical. Line segments far from the ramp remained nearly vertical during deformation for the the 20° ramp (Fig. 10a) but became distinctly tilted for the 35° ramp (Fig. 10b). The tilting of those vertical lines is a result of shearing set up by the interaction of the flow and the ramp--it reflects drag induced by the step. The shearing is zero in the first-order solution, and negligible in the second-order solution for the 20° ramp, but significant for the 35° ramp.

The fold forms derived with the second-order, mechanical analysis will now be compared with the fold forms produced by the kinematical model for thrust ramps with similar slopes. For a 20° ramp, the first-order mechanical model (Fig. 8c), the second-order mechanical model (Fig. 10a) and the kinematical model (Figs. 1c and 5b) all produce folds with approximately the same form. The asymmetry is absent in the first-order model, insignificant in the kinematical model, and moderate in the second-order model.

For a large ramp slope (30°), the kinematical model (Fig. 4c) produces a fold with profound asymmetry (Fig. 10b) and with a dip of the distal limb (60°) that is twice that of the thrust ramp. In contrast, at the slightly higher angle of 35°, the second-order mechanical model produces a fold form in which the limb dips are less than or equal to the dip of the thrust ramp. Furthermore, the velocities in the kinematical model do not account for the overall shearing which tilts steep markers. These problems of the kinematical model at high slopes-- the excessively steep distal limb, the lack of overall shearing, and gross failure of the model for ramp slopes greater than 30°--suggest that the kinematical model approximates the mechanical model only for low ramp slopes, slopes up to 20° or perhaps 25°. Nevertheless, the kinematical model qualitatively does predict the result that bed-duplication folds will be asymmetric.

Extension of the Mechanical Model

Neither the mechanical model, consisting of an homogeneous viscous fluid, nor the kinematical model (of an unknown kind of material), adequately describes folding near thrust ramps. The basic approach used to develop the mechanical model, however, can investigate a wide range of conditions and properties.

For example, one can investigate mechanical models with rheological properties that would duplicate closely the flow assumed in the kinematical model. Analysis by Raymond Fletcher (personal communication 1986) indicates that sharp hinges can be produced in extremely anisotropic materials. A similar analysis has been performed to show that flow patterns will change markedly in an anisotropic material, somewhat as assumed in the kinematical models, when the anisotropic material truncated at the ramp has been pushed over the top of the ramp. This is an example where an interesting mechanical result was anticipated by a geometric analysis of fold form.

The mechanical model has been extended in other ways in order to investigate various aspects of bed-duplication folding. For example, in Chapter I, I developed a mechanical model involving adhesional drag along a thrust ramp in order to investigate possible causes of the marked asymmetry of flat-crested, Powell Valley anticline in the southern Appalachians. According to cross-sections by Harris & Milici (1977) and by Wiltschko (1979a), the distal limb has dips on the order of 70° whereas the proximal limb has dips of about 20°.

Three of the fold forms developed where adhesional drag on the ramp ranged from very low (K=0) to high (K=1) are shown in Fig. 11. Figure 11 shows that, even to first order, the folds can become asymmetric and the distal limb can have a larger dip than the thrust ramp, if drag is moderately large on the ramp.

Fig. 11. Fold forms produced after translation of 10.0S with various amounts of drag along the ramp (First-order solution after Berger & Johnson 1980). (a) Zero drag. (b) Moderate drag (K less than one). (c) High drag. Beds are passive marker lines. θ is 17°.

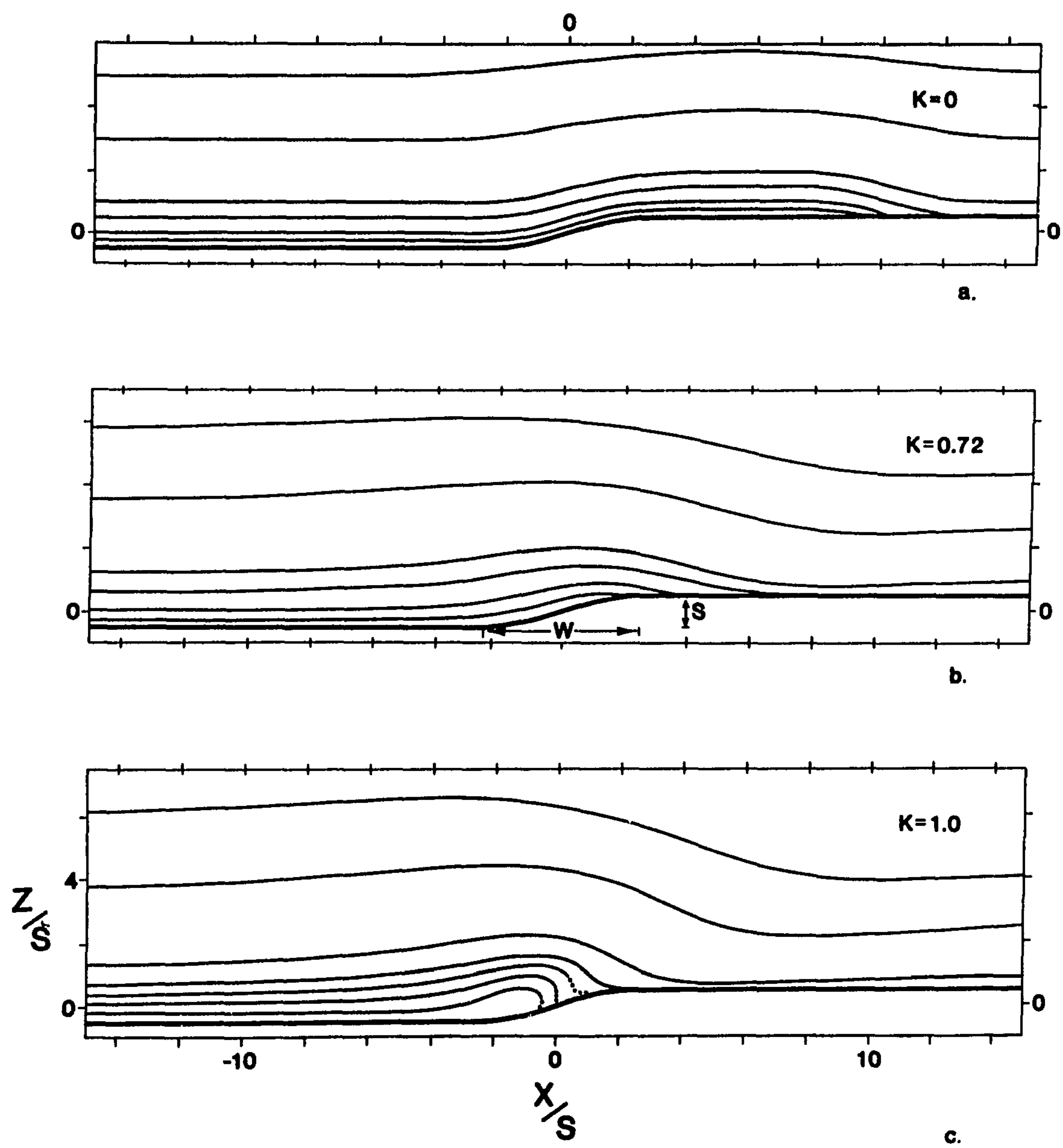

0
K=0
0
0
a.
K=0.72
0
0
S
W
b.
K=1.0
4
Z/S
0
0
-10
0
10
X/S
c.

In fact, Fig. 11(c) shows that, if adhesional drag is very large, such that slippage is prevented at midlength along the ramp, the folding process that produces a bed-duplication fold can initiate a nappe.

In Chapter I, I show that a flat-crested form, with a steep distal limb, can be produced by initially high drag on the ramp and then subsequently low drag, so the asymmetric distal limb becomes translated along the upper detachment. The most important effect of high drag on the thrust ramp is to produce an anticline at the thrust ramp. Translation of the anticline over the ramp produces much of the asymmetry and, of course, the flat-crested form is a result of translation onto the upper detachment.

There are other processes by which folding might occur at the thrust ramp prior to translation, and each can be studied via mechanical analysis. For example, if buckle folding occurs, as suggested by Hayes (1891), it can be treated by the introduction of mechanical layers. If the early folding is a result of lateral termination of easy slip on the lower detachment, it can and has been treated by the introduction of adhesional drag on the horizontal extension of the lower detachment surface as in Chapter II.

I have not investigated effects of a deformable substratum on bed-duplication folding. Such problems, however, can be solved by extensions of the analyses completed to date. I also have not modeled the formation of several ramp faults, such as those responsible for duplexes. However, at the most elementary level, duplexes could be modeled by sequentially forming and activating two or more ramp faults, using the first-order analysis. In fact, the first-order solution for the velocities for such problems has been presented herein, in eqs. (9).

In this way, the mechanical model can be extended widely in order to investigate many more conditions of bed-duplication folding.

References

Berger, P. and Johnson, A., 1982, Folding of passive layers and form of minor structures near terminations of blind thrust faults-application to the central Appalachian blind thrust, J. Struct. Geol., 4,343-353.

Biot, M., 1961, Theory of folding of stratified viscoelastic media and it implications in tectonics and orogenesis, Bull. Geol. Soc. Amer., 72, 1595-1620.

Budd, W., 1970, Stress variations with flow over undulations, J. Glaciol., 9, 29-48.

Butts, C., 1927, Fensters in the Cumberland overthrust block of southwestern Virginia, Va. Geol. Surv. Bull., 28, 1-12.

Cardwell, D., Erwin, R. and Woodward, H., 1968, Geologic Map, West Virginia, West Virginia Geologic and Economic Survey, Morgantown.

Chamberlin, R. and Miller, W., 1918, Low-angle faulting, J. Geol., 26, 1-44.

Chapple, W., 1978, Mechanics of thin-skinned fold and thrust belts, Geol. Soc. Am. Bull., 89, 1189-1198.

Cooper, B., 1964, Relation of stratigraphy to structure in the southern Appalachians in Tectonics of the Southern Appalachians (edited by Lowry, W.), Va. Poytech. Inst. Dep. Geol. Soc. Mem., 1, 81-114.

Currie, J., Patnode, H., and Trump, R., 1962, Development of folds in sedimentary strata, Geol. Soc. Am. Bull., 73, 655-674.

Douglas, R., 1950, Callum Creek, Langford Creek and Gap Map areas, Alberta, Geol. Surv. Can. Mem., 225, 1-124.

Elliott, D., 1976a, The motion of thrust sheets, J. Geophys. Res., 81, 949-963.

Elliott, D., 1976b, The energy balance and deformation mechanisms of thrust sheets, Phil. Trans. R. Soc., A283, 289-312.

Faill, R., 1969, Kink band structures in the Valley and Ridge province, Pennsylvania, Geol. Soc. Am. Bull., 2539-2550.

Faill, R., 1973, Kink-band folding, Valley and Ridge province, Pennsylvania, Geol. Soc. Am. Bull., 84, 1289-1314.

Fletcher, R., 1977, Folding of a single viscous layer: Exact infinitesimal-amplitude solution, Tectonophysics, 39, 593-606.

Fletcher, R., 1981, Mechanics of folding above a decollement (abstr.), Geol. Soc. Amer. Abstr. with Prog., 13, 453.

Gilbert, G., 1877, Report on the Geology of the Henry Mountains, U.S.

Government Printing Office, Washington.

Gwinn, V., 1964, Thin-skinned tectonics in the Plateau and northwestern Valley and Ridge provinces of the central Appalachians, Geol. Soc. Amer. Bull., 863-900.

Gwinn, V., 1970, Kinematic patterns and estimates of lateral shortening, Valley and Ridge and Great Valley Provinces, central Appalachians , south-central Pennsylvania *in* Studies of Appalachian Geology: Central and Southern (edited by Fisher, F., Pettijohn, F., Reed, J. and Weaver, K.), Interscience, New York, 127-146.

Harris, L., 1970, Details of thin-skinned tectonics in part of Valley and Ridge and Cumberland Plateau provinces of the southern Appalachians *in* Studies of Appalachian Geology: Central and Southern (edited by Fisher, F., Pettijohn, F., Reed, J. and Weaver, K.), Interscience, New York, 161-173.

Harris, L. and Milici, R., 1977, Characteristics of thin-skinned style of deformation in the southern Appalachians, and potential hydrocarbon traps, U.S. Geological Survey Prof. Pap. 1018, 1-40.

Hayes, C., 1891, The overthrust faults of the southern Appalachians, Bull. Geol. Soc. Amer., 2, 141-154.

Hsu, K., 1969, Role of cohesive strength in the mechanics of overthrust faulting and of landsliding, Geol. Soc. Amer. Bull., 80, 927-952.

Hubbert, M. and Rubey, W., 1959, Role of fluid pressure in mechanics of overthrust faults, I. Mechanics of fluid-filled porous solids and its application to overthrust faulting, Bull. Geol. Soc. Amer., 70, 115-206.

Johnson, A., 1977, Styles of Folding, Elsevier, Amsterdam, 1-406.

Kamb, B., 1970, Sliding motion of glaciers: theory and observations, Rev. Geophysics and Space Phys., 8, 673-728.

Kehle, R., 1970, Analysis of gravity sliding and orogenic translation, Geol. Soc. Am. Bull., 81, 1641-1663.

Keith, A., 1896, Briceville Folio, Tennessee, Geologic Atlas of the United States, Folio 33, 1-9.

Keith, A., 1901, Maynardville Folio, Tennessee, Geologic Atlas of the United States, Folio 75, 1-11.

Koch, F., Johnson, A., and Pollard, D., 1981, Monoclinal bending of strata over laccolithic intrusions, Tectonophysics, 74, T21-31.

McClung, D., 1981, A physical theory of snow gliding, Canadian Geotechnical Journal, 18, 86-94.

Milici, R., 1970, The Allegheny structural front in Tennessee and its regional tectonic implications, Am. J. Sci., 268, 127-141.

Morse, J., 1977, Deformation in the ramp regions of overthrust faults-experiments with small-scale rock models, Wyo. Geol. Assoc. Guidebook, Casper, 457-470.

Nickelsen, R., 1963, Fold patterns and continuous deformation mechanisms of the central Pennsylvania folded Appalachians *in* Guidebook to Tectonics and Cambrian-Ordovician Stratigraphy in the Central Appalachians of Pennsylvania, Pittsburgh Geological Society and Appalachian Geological Society, 13-30.

Paterson, M. and Weiss, L., 1966, Experimental deformation and folding of phyllite, Geol. Soc. Amer. Bull., 77, 343-374.

Perry, W., 1975, Tectonics of the western Valley and Ridge foldbelt, Pendleton County, West Virginia, a summary report, U.S. Geological Survey J. Res., 3, 583-588.

Pollard, D. and Johnson, A., 1973, Mechanics of growth of some laccolith intrusions in the Henry Mountains, Utah, II. Bonding and failure of overburden layers and sill formation, Tectonophysics, 18, 311-354.

Powell, J., 1875, Exploration of the Colorado River of the West and its Tributaries, U.S. Government Printing Office, Washington.

Raleigh, C. and Griggs, D., 1963, Effect of the toe in the mechanics of overthrust faulting, Geol. Soc. Amer. Bull., 74, 819-830.

Ramberg, H., 1967, Gravity, Deformation and the Earth's Crust, Academic Press, London.

Ramberg, I. and Johnson, A., 1976, A theory of concentric, kink and sinusoidal folding and of monoclinal flexuring of compressible elastic multilayers. V. Asymmetric folding and monoclinal kinking, Tectonophysics, 35, 295-334.

Reches, Z. and Johnson, A., 1979, Development of monoclines: Part II. Theoretical analysis of monoclines *in* Laramide Folding Associated with Basement Block Faulting in the Western United States (edited by Matthews, V.), Geol. Soc. Amer. mem., 151, 273-311.

Rich, J., 1934, Mechanics of low-angle overthrust faulting as illustrated by Cumberland thrust block, Virginia, Kentucky and Tennessee, Bull. Am. Assoc. Pet. Geol., 18, 1584-1596.

Rodgers, J., 1949, Evolution of thought on structure of middle and southern Appalachians, Am. Assoc. Pet. Geol. Bull., 33, 1643-1654.

Rodgers, J., 1963, Mechanics of Appalachian foreland folding in Pennsylvania and West Virginia, Am. Assoc. Pet. Geol. Bull., 47, 1527-1536.

Royse, F., Warner, M. and Reese, D., 1975, Thrust belt structural geometry and related stratigraphic problems, Wyoming, Idaho, and northern Utah, *in* Deep Drilling Frontiers of the Central Rocky Mountains (edited by Bolyard, D.), Rocky Mountain Association of Geologist, 1975 Symposium, Denver, Colorado, 41-54.

Rudnicki, J. and Rice, J., 1975, Conditions for the localization of deformation in pressure-sensitive dilatant materials, J. Mech. Phys. Solids, 23, 371-394.

Rutten, M., 1969, The Geology of Western Europe, Elsevier, Amsterdam, 1-520.

Seguret, M., 1972, Etude tectonique des Nappes et Series decollees de la Partie centrale du Versant sud des Pyrenees: Caractere synsedimentaire, role de la Compression et de la Gravite, These Fac. Sci., Montpellier, Publ. U.S.T.E.L.A., Ser. Geol. Struct., 2, 1-155.

Serra, S., 1977, Styles of deformation in the ramp regions of overthrust faults, *in* Wyoming Geologic Association Guidebook, Casper, 487-498.

Sherwin, J., 1972, Decollement Folding, Ph.D. thesis, Brown University (University microfilms, Ann Arbor, Michigan), 1-150.

Suppe, J., 1979, Fault-bend folding (abstr.), Geol. Soc. Amer., Abstr. Progr., 11, 525.

Suppe, J., 1980, Imbricated structure of western Foothills belt, southcentral Taiwan, Petroleum Geology of Taiwan, 17, 1-16.

Suppe, J., 1983, Geometry and kinematics of fault-bend folding, Am. J. Sci., 283, 684-721.

Thompson, R., 1979, A structural interpretation across part of the northern Rocky Mountains, British Columbia, Canada, Can. J. Earth Sci., 16, 1228-1241.

Willis, B., 1893, The Mechanics of Appalachian Structure // Thirteenth Annual Report of the United States Geological Survey to the Secretary of the Interior, 1891-92, Part 2-Geology, 211-289.

Wiltschko, D., 1979a, A mechanical model for thrust sheet deformation at a ramp, J. Geophys. Res., 84, 1091-1104.

Wiltschko, D., 1979b, Partitioning of energy in a thrust sheet and implications concerning driving forces, J. Geophys. Res., 84, 6050-6058.

Wiltschko, D. and Chapple, W., 1977, Flow of weak rocks on Appalachian Plateau folds, Am. Assoc. Pet. Geol. Bull., 61, 653-670.

Woodward, H., 1959, Structural interpretations of the Burning Springs anticline in Symposium on Sandhill Deep Well, Wood County, West

Virginia (edited by Woodward, H.), West Virginia Geological and Economic Survey, Rept. of Investigation, 18, 159-168.

APPENDIX

SUMMARY OF THEORETICAL ANALYSES

Uniform shear resistance along ramp. Zero elsewhere.

In the analysis of folding, the components of stress and velocity are separated into mean values and perturbed values. The mean values of stress and velocity are those that solve the problem describing the uniform translation over a planar interface (no thrust ramp) without shear resistance. The mean values are exact. The perturbed stresses and velocities are the values that must be added to the mean values in order to describe stresses and velocities in the material above the non-planar interface (the detachment surface and thrust ramp) or material that is subjected to shear resistance. The perturbed values are exact only if the boundary conditions are satisfied exactly, and the order of approximation of a solution reflects the extent to which the boundary conditions are satisfied exactly. The mean values are uniform whereas the perturbed values are nonuniform--they vary from place to place and time to time.

The components of velocity and stress for a point are sums of the mean (bar over symbol) and perturbed (tilda over symbol) values:

$$v_x = \bar{v}_x + \tilde{v}_x \tag{1a}$$

$$v_z = \bar{v}_z + \tilde{v}_z \tag{1b}$$

$$\sigma_{xx} = \bar{\sigma}_{xx} + \tilde{\sigma}_{xx} \tag{1c}$$

$$\sigma_{zz} = \bar{\sigma}_{zz} + \tilde{\sigma}_{zz} \tag{1d}$$

$$\sigma_{xz} = \bar{\sigma}_{xz} + \tilde{\sigma}_{xz} \tag{1e}$$

The mean velocities and mean stresses are given by the relations

$$\bar{v}_x = (\partial \bar{v}_x/\partial x)x + V_0 \tag{1f}$$

$$\bar{v}_z = (\partial \bar{v}_z/\partial z)z \tag{1g}$$

$$\bar{\sigma}_{xx} = 2\mu(\partial \bar{v}_x/\partial x) - p_0 \tag{1h}$$

$$\bar{\sigma}_{zz} = 2\mu(\partial \bar{v}_z/\partial z) - p_0 \tag{1i}$$

$$p_0 = -(\bar{\sigma}_{xx} + \bar{\sigma}_{zz})/2 \tag{1j}$$

For the problems treated here, all mean values except the mean horizontal velocity and mean shear stress are zero. p_0 is the mean pressure and μ is the coefficient of viscosity. Plain strain is assumed.

A general solution for the perturbed velocities, $\tilde{v}_x$ and $\tilde{v}_z$ is derived from the velocity potential

$$\psi = (1/l)[[c + d(lz)]\exp(lz) + [a + b(lz]\exp(-lz)]\cos(lx) \tag{2a}$$

where l is the wave number which will be defined below, and a, b, c and d are constants to be determined later

$$\tilde{v}_x = -\partial\psi/\partial z \tag{2b}$$

$$\tilde{v}_z = \partial\psi/\partial x \tag{2c}$$

$$\tilde{\sigma}_{xx} = 2\mu(\partial v_x/\partial x) - p \tag{2d}$$

$$\tilde{\sigma}_{zz} = 2\mu(\partial v_z/\partial z) - p \tag{2e}$$

$$\tilde{\sigma}_{xz} = \mu(\partial v_z/\partial x + \partial v_x/\partial z) \tag{2f}$$

In the following derivations, all solutions for stresses and velocities refer to the perturbed values unless explicitly described otherwise. All solutions are solved to first order in the slope of the interface (A/l).

The non-planar interface ζ, is described by means of the Fourier, sine series:

$$\zeta = \sum_{m=1}^{\infty} A_m \sin(l_m x) \tag{3a}$$

in which x is the horizontal coordinate and A_m is amplitude of a sine wave and,

$$l_m = m\pi / d \tag{3b}$$

where m is an integer and d is the spacing of adjacent ramps.

One boundary condition is that the interface does not move,

$$\partial\zeta/\partial t = 0 = [v_z]_\zeta - [v_x]_\zeta(\partial\zeta/\partial x) \tag{4}$$

(the brackets with the subscript implies "evaluated at the position of the subscript"--in this case, at the interface, ζ).

The other boundary condition is that the shear stress, σ_{ns}, parallel to the interface, is of the form of a Fourier cosine series:

$$\sigma_{ns} = \sum_{m=1}^{\infty} R_n \cos(m\pi x/d) = [\sigma_{zz} - \sigma_{xx}]_\zeta (\partial\zeta/\partial x) + [\sigma_{xz}]_\zeta \qquad (5)$$

in which R_n is determined by the shear-stress distribution at the detachment surface.

The Fourier series approximation demands a mean shear stress and implies that the velocities far from the interface will be equal to the velocity due to the perturbed mean shear. Consideration of this boundary condition indicates that ψ must be chosen so that the σ_{xz} is a cosinusoidal function of x.

The Fourier series coefficients, A_m and R_n, which describe the interface and the shear stress distribution are presented in Chapter I [equations (8)] and will not be repeated here.

The general solution for the velocity potential ψ [equation (2)] was adequate to determine the inital form of the velocity equations, but is inadequate to determine the form of the velocity equations with the added complications of the two Fourier series that describe the interface and shear stress distribution. The new form of the velocity potential is derived as follows.

Substituting equation (3a) into equation (4), using (2b) and (2c) for the velocities (assuming c=d=0 for a half-space), equation (4) becomes,

$$0 = \sum_{m=1}^{\infty} [-a_n \sin(l_n x) - [(a_n - b_n)/2]\, l_n \sum_{m=1}^{\infty} [A_m r \cos(l_r x)$$

$$+ A_m q \cos(l_q x)]] \qquad (6a)$$

in which

$$r = (m/n) - 1; \quad q = (m/n) + 1 \qquad (6b)$$

$$l_r = r l_n; \qquad l_q = q l_n \qquad (6c)$$

Two things should be noted. First, m and n are odd, because odd values of m are required to describe the interface and even values of n give zero values for the shear at the interface. Second, r can be negative.

For all values of m and n (odd and greater than zero), the three terms in equation (6) are orthogonal, so more terms are need in equation (2) which describes the general solution. To be a solution, ψ, must have the form,

$$\psi = \sum_{n=1}^{\infty} \{(1/l_n)\,[a_n + b_n(l_n z)]\exp(-l_n z)\cos(l_n x)$$

$$+ \sum_{m=1}^{\infty} (1/l_q)\,[a_{m,n} + b_{m,n}(l_q z)]\exp(-l_q z)\sin(l_q x)$$

$$+ \sum_{m=1}^{\infty} (1/l_r)\,[c_{m,n} + d_{m,n}(l_r z)]\exp(-l_r z)\sin(l_r x)\}\ ;\ r \geq 0 \qquad (7a)$$

If r is less than zero, the last term in equation (7a) becomes

$$+ \sum_{m=1}^{\infty} (1/l_r)\,[c_{m,n} + d_{m,n}(l_r z)]\exp(l_r z)\sin(l_r x)\ ;\ r < 0$$

Using equations (2b) and (2c), the expressions for the velocities can now be written.

$$v_x = \sum_{n=1}^{\infty} \{[a_n + b_n(l_n z - 1)]\exp(-l_n z)\cos(l_n x)$$

$$+\sum_{m=1}^{\infty} [a_{m,n}+ b_{m,n}(l_q z- 1)]\exp(- l_q z)\sin(l_q x)$$

$$+\sum_{m=1}^{\infty} [c_{m,n}+ d_{m,n}(l_r z- 1)]\exp(- l_r z)\sin(l_r x)\} \; ; \quad r \geq 0 \qquad (7b)$$

If r is less than zero, the last term in equation (7b) becomes

$$-\sum_{m=1}^{\infty} [c_{m,n}+ d_{m,n}(l_r z+ 1)]\exp(l_r z)\sin(l_r x)\}; \quad r < 0$$

$$v_z = \sum_{n=1}^{\infty} \{-[a_n+ b_n(l_n z)]\exp(- l_n z)\sin(l_n x)$$

$$+\sum_{m=1}^{\infty} [a_{m,n}+ b_{m,n}(l_q z)]\exp(- l_q z)\cos(l_q x)$$

$$+\sum_{m=1}^{\infty} [c_{m,n}+ d_{m,n}(l_r z)]\exp(- l_r z)\cos(l_r x)\} \; ; \quad r \geq 0 \qquad (7c)$$

If r is less than zero, the last term in equation (7c) becomes

$$+\sum_{m=1}^{\infty} [c_{m,n}+ d_{m,n}(l_r z)]\exp(l_r z)\cos(l_r x)\} \; ; \quad r < 0$$

Substituting the velocities into the interface equation [equation

(4)], expressions for the constants are derived,

$$a_n = 0 \tag{8a}$$

$$a_{m,n} = -(b_n/2)\, l_q A_m \tag{8b}$$

$$c_{m,n} = -(b_n/2)\, l_r A_m;\ \text{for all } r \tag{8c}$$

To determine the other two constants requires determination of the shear stress at the interface, $[\sigma_{xz}]_\zeta$, [equation (2f)], and the normal stress difference at the interface, $[\sigma_{zz} - \sigma_{xx}]_\zeta$ [equations (2d) and (2e)]. Substituting equations (2d, e and f), evaluated at the interface ζ, into equation (5) yields,

$$\sum_{n=1}^{\infty} R_n \cos(l_n x) = \sum_{n=1}^{\infty} [2\mu\, l_n b_n \cos(l_n x)$$

$$- 4\mu \sum_{m=1}^{\infty} l_n b_n (A_m\, l_n) \cos(l_n x) \sin(l_m x)$$

$$-4\mu \sum_{m=1}^{\infty} l_n b_n (l_m A_m) \sin(l_n x) \cos(l_m x)$$

$$-2\mu \sum_{m=1}^{\infty} l_q (a_{m,n} - b_{m,n}) \sin(l_q x)$$

$$-2\mu \sum_{m=1}^{\infty} l_r (c_{m,n} - d_{m,n}) \sin(l_r x)) \; ; \; r \geq 0 \tag{9}$$

If r is negative, then the last term in equation (9) is replaced by

$$-2\mu \sum_{m=1}^{\infty} l_r (c_{m,n} + d_{m,n}) \sin(l_r x)) \; ; \; r < 0$$

Using trigonometric identities, and solving for constants,

$$b_n = R_n / 2\mu l_n \tag{10a}$$

$$b_{m,n} = b_n (l_n A_m) + a_{m,n} \tag{10b}$$

$$d_{m,n} = c_{m,n} - b_n (l_n A_m) \; ; \; r \geq 0 \tag{10c}$$

If r is negative, then equation (10c) is replaced by,

$$d_{m,n} = b_n(l_n A_m) - c_{m,n}; \; r < 0$$

This completes the solution for the constants. They are substituted into the equations for the perturbed velocities [equations (7b and 7c)]. The above derivation presents the contribution of the frictional drag to the velocities and stresses. A complete solution to the problem posed in Chapter I must include a mean rate of translation and a perturbed velocity set up by the interaction of the mean flow and the ramp. This solution will be presented later.

```
1.05 T !,"STORED UNDER <RAMP.NSF>"
1.08 A !,"RATIO OF SHEAR STRENGTH*TIME TO VISCOSITY?",K1
1.09 S NX=31;X FPRM(2,120)
1.10 S  PI=3.14159265536;S T=10;S WD=.1;S SW=0.2;S SD=SW*WD
1.11 T !,"D/W",1/WD,"    W/S",1/SW,"     D/S",1/(SW*WD)
1.12 A !,"MAXIMUM DISPLACEMENT FACTOR (FRACTION OF S)?",ST
1.13 A !,"NUMBER OF TIME INCREMENTS?(>10)",T
1.14 S EX=-5*SD;T !,"EXX",EX;A !,"EXX?",XE;F J=1,2,NX;D 9
1.15 S L=PI*SD;A !,"WANT INTERFACE? YES PLUS NO.",OO
1.16 I (OO)1.17,1.17;T !,"INTERFACE,X,ZETA";S XM=1/SW;S XI=XM/10;D 8
1.17 D 1.95;I (OO)10.1;A !,"X-LEFT?",XL;I (XL)1.2,1.9,1.2
1.19 T !!,"TIME STEP   OLD POSITIONS,X,Z   NEW POSITIONS,XX,ZZ"
1.20 A !,"X-RIGHT?",XR,"  NUMBER OF POINTS?",IM
1.25 S XI=(XR-XL)/(IM-1);S X=XL-XI
1.30 T !,"POSITION OF BASE IS -0.5"
1.40 A !,"Z-POSITION OF LAYER?",Z
1.45 D 1.19
1.60 S X=X+XI;I (X-XR)3.1,3.1,1.7
1.70 G 1.4
1.90 Q
1.95 T !,"W",1/SW;T !,"DO A SINGLE POINT? Y=NEG. NO.";A OO

3.10 S XX=X;S ZZ=Z
3.12 T !,"TIME STEPS",!
3.16 F I=1,T;T %3.01,I;D 4
3.30 T !,%8.04,X,Z,"      ",XX,ZZ
3.90 G 1.6

4.05 S DX=0;S DZ=0
4.10 F N=1,2,NX;S LN=N*L;D 5
4.20 S XX=XX+DX+(1+XE*XX)*ST/T;S ZZ=ZZ+DZ-(XE*ZZ)*ST/T

5.07 S CS=FCOS(LN*XX);S AN=AN(N)
5.10 S TP=FEXP(-LN*ZZ);S SN=FSIN(LN*XX)
5.12 S T1=LN*ZZ
5.14 S R=R(N);S T1=LN*ZZ;S TR=TP^2
5.16 S MM=R*(T1-1)*TP*CS
5.17 S P=-R*T1*TP*SN
5.18 F M=1,2,NX;D 6
5.20 S T2=LN*(XX*XE+1)
5.30 S DX=DX+AN*(ST/T)*(T2*T1*SN-XE*(2-T1^2)*CS)*TP+MM
5.40 S DZ=DZ+AN*(ST/T)*(T2*(1+T1)*CS+XE*(1-T1-T1^2)*SN)*TP+P
```

```
 6.10 S RR=(M/N)-1;S QQ=(M/N)+1
 6.13 I (RR)6.14,6.15,6.15
 6.14 S IZ=-1;G 6.2
 6.15 S IZ=1
 6.20 S LR=LN*RR;S LQ=LN*QQ
 6.30 S AA=-(R/2)*LQ*AN(M);S CC=-(R/2)*LR*AN(M)
 6.40 S BB=CC;S DD=IZ*AA
 6.50 S TR=FEXP(-FABS(LR)*ZZ);S TQ=FEXP(-LQ*ZZ)
 6.60 S MM = MM+(AA+BB(LQ*ZZ-1))*TQ*FSIN(LQ*XX)
 6.62 S MM=MM+IZ*(CC+DD*(LR*ZZ-IZ))*TR*FSIN(LR*XX)
 6.70 S P=P+(AA+BB*(LQ*ZZ))*TQ*FCOS(LQ*XX)
 6.73 S P=P+(CC+DD*(LR*ZZ))*TR*FCOS(LR*XX)

 8.05 F X=-XM,XI,XM;S ZT=0;D 8.1;T !,X,ZT
 8.07 R
 8.10 F N=1,2,NX;S AN=AN(N);D 8.2
 8.15 R
 8.20 S ZT=ZT+AN*FSIN(L*N*X)

 9.02 S T4=FSIN((J*PI/2)*WD)
 9.03 S R(J)=2*K1*T4/(((J*PI)^2)*SD*T)
 9.05 I (J*WD-1)9.1,9.9,9.1
 9.10 S T1= FCOS(J*PI*WD/2);S T2=FCOS(J*PI/2)
 9.20 S T3=(1/(PI*(1/WD-J)))*FSIN((1-J*WD)*PI/2)
 9.30 S T4=(1/(PI*(1/WD+J)))*FSIN((1+J*WD)*PI/2)
 9.40 S AN(J)=(2/(J*PI))*(T1-T2)+T3-T4
 9.80 R
 9.90 S AN(J)=-(2/(J*PI))*FCOS(J*PI/2)

10.10 D 1.3;A !,"X/S?",X,"   Z/S?",Z
10.15 F J=1,2,NX;D 9
10.17 D 1.19
10.20 S XX=X;S ZZ=Z;F I=1,T;D 4
10.30 T !,%8.04,X,Z,"        ",XX,ZZ
10.40 Q
*
```

Uniform shear resistance along part of flat detachment. Zero elsewhere.

In this problem, the interface is flat, so one boundary condition is that ζ, is constant,

$$\zeta = A_m \tag{11}$$

Note that in this problem, A_m is a constant and is not the expression given in equation (8c) of chapter I. The other boundary conditions are those of the previous problem and are given in equations (4) and (5). R_m is presented in equation (1d) of chapter 2. The velocity potential ψ is given in equation (2a). Using equations (2), the velocities are

$$v_x = -[a + b(lz-1)]\exp(-lz)\cos(lx) \tag{12a}$$

$$v_z = [a + b(lz)]\exp(-lz)\sin(lx) \tag{12b}$$

in which the wave number l is

$$l = \pi / d$$

Using the boundary condition expressed in equation (5), at $z = 0$,

$$\sigma_{ns} = [\sigma_{xz}]_{\zeta=0} \tag{13}$$

and solving for the constants,

$$a - b = [\sum_{m=1}^{\infty} R_m \cos(l_m x)]/2\mu l \tag{14}$$

Using the boundary condition expressed in equation (4), at $z = 0$, and the condition that the vertical velocity must vanish at the interface,

$$[v_z]_{\zeta=0} = 0 = a\sin(lx) \tag{15}$$

Accordingly,

$$a = 0; \quad b = -[\sum_{m=1}^{\infty} R_m \cos(l_m x)]/2\mu l \tag{16}$$

Substituting equations (16) into equations (12) and adding the mean horizontal velocity, $\bar{v}_x$, and the mean shear flow, v, yields,

$$v_x = \bar{v}_x + v + (1/2\mu)\sum_{m=1}^{\infty}(1/l_m)\, R_m(l_m z - 1)\exp(-l_m z)\cos(l_m x) \tag{17a}$$

$$v_z = -(1/2\mu)\sum_{m=1}^{\infty}(1/l_m) R_m(l_m z)\exp(-l_m z)\sin(l_m x) \tag{17b}$$

This completes the solution for the velocities due to drag on a flat detachment surface. Note that a mean shear flow contribution is required, because in this case, the origin of coordinates is picked such that σ_{ns} is always greater than zero. Thus, the average shear flow is not zero as it was in the previous problem.

```
1.05 T !,"STORED UNDER <SUR.FLT>"
1.08 A !,"RATIO OF SHEAR STRENGTH/VISCOUS SHEAR STRESS?",KK
1.09 S NX=31;X FPRM(2,120);S SP=1
1.10 S  PI=3.14159265 36;S T=10
1.11 S SD=SP/4;T !,"P/S",1/SP
1.12 A !,"MAXIMUM DISPLACEMENT FACTOR (FRACTION OF P)?",ST
1.15 S L=2*PI*SD;S BQ=0;F J=1,2,NX;D 11
1.16 S R=KK*ST*SP/(BQ*T);F N=1,2,NX;D 12
1.17 D 1.95;I (WW)10.1;A !,"X-LEFT?",XL;I (XL)1.2,1.9,1.2
1.19 T !!,"TIME STEP   OLD POSITIONS,X,Z   NEW POSITIONS,XX,ZZ"
1.20 A !,"X-RIGHT?",XR,"  NUMBER OF POINTS?",IM
1.22 A !,"MIN Z?",ZM,!,"MAX Z?",ZX,!,"INTERVAL?",ZI
1.25 S XI=(XR-XL)/(IM-1)
1.30 S Z=ZM-ZI
1.40 S X=XL-XI;S Z=Z+ZI;I (Z-ZX)1.45,1.45;Q
1.45 D 1.19
1.60 S X=X+XI;I (X-XR)3.1,3.1,1.7
1.70 G 1.4
1.90 Q
1.95 T !,"DO A SINGLE POINT? Y=NEG. NO.";A WW

3.10 S XX=X;S ZZ=Z;F I=1,T;D 4
3.30 T !,%8.04,X,Z,"      ",XX,ZZ
3.90 G 1.6

4.10 S MM=0;S P=0;F N=1,2,NX;S LN=N*L;D 5
4.15 S T4=R*2*ZZ*SD/SP
4.20 S ZZ=ZZ+P
4.25 S XX=XX+MM+T4+ST/T

5.07 S CS=FCOS(LN*XX)
5.10 S TP=FEXP(-LN*ZZ);S SN=FSIN(LN*XX)
5.12 S T1=LN*ZZ
5.16 S MM=MM+R(N)*(T1-1)*TP*CS
5.17 S P=P-R(N)*T1*TP*SN

10.10 A !,"X/S?",X,"   Z/S?",Z
10.17 D 1.19
10.20 S XX=X;S ZZ=Z;F I=1,T;D 4
10.30 T !,%8.04,X,Z,"        ",XX,ZZ
10.40 G 1.17

11.10 S BQ=BQ+(1/SD)*(SP/2)*(1/(PI^2))*((1/J)^2)*FSIN(2*J*(PI/SP)*SD)

12.10 S LN=N*L
12.20 S R(N)=(R/(2*SD))*((1/(N*PI)^2))*FSIN(LN/SP)
12.30 S RN(N)=(2/(N*PI))*FSIN(LN)
```

```
18.05 A !,"X?",XX,"    Z?",ZZ
18.10 S SS=0;S BQ=0;S GQ=0;S P=0
18.20 F N=1,2,NX;S LN=N*L;D 19
18.25 S SH=2*SD/SP+BQ
18.30 T "    SH STR. FROM B.C.",SS+2*SD/SP
18.40 T "    SH STR. FROM SOLUT.",SH
18.60 R

19.05 S TP=(1-LN*ZZ);S T1=FEXP(-LN*ZZ)
19.08 S CN=FCOS(LN*XX)
19.09 S SN=FSIN(LN*XX)
19.20 S BQ=BQ+RN(N)*TP*T1*CN
19.30 S SS=SS+RN(N)*CN
19.40 S GQ=RN(N)*TP*T1*SN+GQ
19.50 S P=P-RN(N)*T1*SN

21.10 T !,"COMPUTE STRESSES"
21.15 A !!!,"X1?",X1,"    Z1?",Z1
21.20 D 22
21.30 D 18.1
21.40 F N=1,2,NX;S LN=N*L;D 19
21.50 S SX=GQ;S SS=2*SD/SP+BQ
21.60 T !," SXX",SX,"    SXZ",SS
21.70 I (FABS(SX))21.71,21.72;T "      TAN 2THETA(SIG 1)",SS/SX
21.71 G 21.73
21.72 T !,"THETA IS + OR - 45 DEGREES"
21.73 S J2=FSQT((SX^2)+(SS^2));T !,"J2",J2
21.74 T "     YIELD FUNCTION",J2-P*0.5774,"    P",P
21.78 S SN=TN/FSQT(1+TN^2);S CN=1/FSQT(1+TN^2)
21.80 S DS = 2*SX*CS+2*SS*SN;S SH = -SX*SN+SS*CN
21.85 T "    SSS-SNN",DS,"   SNS",SH
21.90 G 21.2

22.10 S X2=X1;S Z2=Z1
22.20 A !!,"X1?",X1,"  Z1?",Z1
22.30 S DX=X1-X2;S DZ=Z1-Z2;S TN=DZ/DX
22.40 S XX=X1-DX/2;S ZZ=Z1-DZ/2;T "X POS",XX,"   Z POS",ZZ
*
```

```
1.05 T !,"PROGRAM FOR COMPUTING FINITE STRAINS OF A DEFORMED"
1.07 T !,"RECTANGLE---STORED UNDER STRAIN.BER"
1.10 A !,"DELTA X?", DX,"    DELTA Z?",DZ
1.15 T !,"PT. A IS IN SW CORNER, B IN SE, C IN NW, & D IN NE"
1.20 F I=1,30;D 2;D 3
1.30 Q

2.10 A !,"XA",XA,"  ZA",ZA,"  XB",XB,"  ZB",ZB
2.20 A !,"XC",XC,"  ZC",ZC,"  XD",XD,"  ZD",ZD
2.30 S A1(2)=(1/2)*(XC-XA+XD-XB)/DZ
2.40 S A1(1)=(1/2)*(XB-XA+XD-XC)/DX
2.50 S A2(1)=(1/2)*(ZB-ZA+ZD-ZC)/DX
2.60 S A2(2)=(1/2)*(ZC-ZA+ZD-ZB)/DZ
2.70 S I1=(A1(1)^2)+(A2(1)^2)+(A1(2)^2)+(A2(2)^2)
2.80 S I2=((A1(1)^2)+(A2(1)^2))*((A2(2)^2)+(A1(2)^2))
2.85 S I2=I2-(A1(1)*A1(2)+A2(2)*A2(1))^2
2.88 S S1=(1/2)*(I1+FSQT((I1^2)-4*I2))
2.89 S S1=FSQT(S1);S S2=(1/2)*(I1-FSQT((I1^2)-4*I2));S S2=FSQT(S2)
2.90 S TN=2*(A1(1)*A2(1)+A2(2)*A1(2))
2.91 S TN=TN/((A1(1)^2)+(A1(2)^2)-(A2(1)^2)-(A2(2)^2))

3.10 T !,"X AND Z FOR PTS A,B,C,D",!,XA,ZA,!XB,ZB,!,XC,ZC,!,XD,ZD
3.20 T !,"FINITE STRETCHES--S1",S1,"     S2,S2," D VOL",S1*S2
3.30 T !,"TANGENT TWO THETA",TN,!!
```

Uniform shear resistance on upper flat segment of detachment surface. Zero elsewhere.

In this problem, the detachment surface is not represented by a simple sinusoidal, Fourier series. Instead, a cosinusoidal, Fourier series is used that approximates a planar ramp segment. Thus, the boundary condition that describes the interface is

$$\zeta = \sum_{m=1}^{\infty} A_m \cos(l_m x) \tag{18}$$

where A_m is presented in equation (A3) of chapter 2. The other boundary conditions are those presented in equations (4) and (5) with the exception that σ_{ns} is redefined

$$\sigma_{ns} = \sum_{n=1}^{\infty} R_n \cos(l_n x) \tag{19}$$

where R_n is defined in equation (A4) of chapter 2.

The change in the boundary condition neccessitates a change in the velocity potential ψ, from that shown in equation (7). However, the method to determine the form of the velocity potential is exactly that as described in the derivation of equation (6). Substitute equation (18) into equation (4), using equations (2b and 2c). Equation (4) becomes

$$0 = \sum_{n=1}^{\infty} [-a_m \sin(l_m x) + (a_n - b_n) l_n \sum_{m=1}^{\infty} A_m \sin(l_n x)\cos(l_m x)$$

$$- (a_n - b_n) \sum_{m=1}^{\infty} l_m A_m \cos(l_n x)\sin(l_m x)] \qquad (20)$$

The three terms in equation (20) are orthogonal so the velocity potential, ψ, must have the form

$$\psi = \sum_{n=1}^{\infty} [(1/l_n)[a_n + b_n(l_n z)]\exp(-l_n z)\cos(l_n x)$$

$$+ \sum_{m=1}^{\infty} (1/l_q)[a_{m,n} + b_{m,n}(l_q z)]\exp(-l_q z)\cos(l_q x)$$

$$+ \sum_{m=1}^{\infty} (1/l_r)[c_{m,n} + d_{m,n}(l_r z)]\exp(-l_r z)\cos(l_r x)]; \quad r \geq 0 \qquad (21)$$

If r is less than zero, the last term in equation (21) becomes

$$+\sum_{m=1}^{\infty}(1/l_r)[c_{m,n}+d_{m,n}(l_r z)]\exp(l_r z)\cos(l_r x)] \ ; \ r<0$$

Using equations (2b and 2c) the expressions for the velocities can now be written

$$v_x = \sum_{n=1}^{\infty}\{[a_n+b_n(l_n z-1)]\exp(-l_n z)\cos(l_n x)$$

$$+\sum_{m=1}^{\infty}[a_{m,n}+b_{m,n}(l_q z-1)]\exp(-l_q z)\cos(l_q x)$$

$$+\sum_{m=1}^{\infty}[c_{m,n}+d_{m,n}(l_r z-1)]\exp(-l_r z)\cos(l_r x)\} \ ; \ r\geq 0 \qquad (22a)$$

If r is less than zero, the last term in equation (22a) becomes

$$-\sum_{m=1}^{\infty}[c_{m,n}+d_{m,n}(l_r z+1)]\exp(l_r z)\cos(l_r x)] \ ; \ r<0$$

$$v_z = -\sum_{n=1}^{\infty}\{[a_n+b_n(l_n z)]\exp(-l_n z)\sin(l_n x)$$

$$-\sum_{m=1}^{\infty}[a_{m,n}+b_{m,n}(l_q z)]\exp(-l_q z)\sin(l_q x)$$

$$- \sum_{m=1}^{\infty} [c_{m,n} + d_{m,n}(l_r z)]\exp(-l_r z)\sin(l_r x)\} ; \quad r \geq 0 \tag{22b}$$

If r is less than zero, the last term in equation (22b) becomes

$$- \sum_{m=1}^{\infty} [c_{m,n} + d_{m,n}(l_r z)]\exp(l_r z)\sin(l_r x)\} ; \quad r < 0$$

Substituting the velocities [equations (22)] into the interface equation [equation (4)], produces expressions for the constants,

$$a_n = 0 \tag{23a}$$

$$a_{m,n} = -b_n l_q A_m/2 \tag{23b}$$

$$c_{m,n} = -b_n l_r A_m/2 ; \quad \text{for all } r \tag{23c}$$

The other constants are determined using the boundary condition that describes the shear stress distribution on the interface, equations (5 and 19). As in the first problem presented in this section, the stresses are evaluated at the interface, $z = \zeta$. The shear stress on the interface is

$$\sigma_{ns} = \sum_{n=1}^{\infty} \{-2\mu l_n[(a_n - b_n)\cos(l_n x)$$

$$+ \sum_{m=1}^{\infty} (2b_n - a_n)(A_m l_n)\cos(l_n x)\cos(l_m x)]$$

$$-4\mu \sum_{m=1}^{\infty} l_n(a_n - b_n)(l_m A_m)\sin(l_n x)\sin(l_m x)]$$

$$-2\mu \sum_{m=1}^{\infty} l_q(a_{m,n} - b_{m,n})\cos(l_q x)$$

$$-2\mu \sum_{m=1}^{\infty} l_r(c_{m,n} - d_{m,n})\cos(l_r x)\} \; ; \; r \geq 0 \qquad (24)$$

If r is negative, then the last term in equation (24) is replaced by

$$-2\mu \sum_{m=1}^{\infty} l_r(c_{m,n} + d_{m,n})\cos(l_r x)\} \; ; \; r < 0$$

Using trigonometric identities and solving for the constants,

$$b_n = R_n / 2\mu l_n \tag{25a}$$

$$b_{m,n} = b_n l_n A_m + a_{m,n} = c_{m,n} \tag{25b}$$

$$d_{m,n} = b_n l_n A_m - c_{m,n} = a_{m,n}\ ;\ r \geq 0 \tag{25c}$$

If r is negative, then equation (25c) is replaced by

$$d_{m,n} = -b_n l_n A_m + c_{m,n} = -a_{m,n}\ ;\ r < 0$$

This completes the solution for the constants. They are substituted into equations (22) in order to compute the perturbed velocities. The problem posed in Chapter II is not complete without the mean horizontal flow, $\bar{v}_x$, and the mean shear flow, v. The mean flow and the perturbed flow set up by the interaction of the mean flow and the ramp will be presented next. The mean shear flow is presented in the next paragraph; it's form depends on the choice of R_r.

.The derivation is valid for any shear stress distribution that can be described using a Fourier cosinusoidal series, i.e. any R_n.

Solution

Here I present the solution for velocities for the problem illustrated in Fig. 1(b) of Chapter II, where there is a detachment surface and a ramp fault with zero drag and a higher detachment surface with adhesional drag, k. This problem is similar to those discussed in Chapter I, except in the previous solutions there was zero drag on the ramp. Further in Chapter I, I assumed a sinusoidal ramp fault, whereas, here I assume a straight ramp fault. For the present problem, I can identify four contributions to the velocities and stresses within the viscous fluid. One is the mean rate of translation, $\bar{v}_x$. Another is the velocity gradient set up by the average shear stress acting over the interface between the fluid and the rigid substratum,

$k(z-S/2)(1-w/d)(1/2\eta)$

in which I have set this component equal to zero along the upper detachment surface, and S is ramp height, w is ramp width.

The third component is a perturbed velocity set up by the interaction of the mean flow and the ramp, and the fourth component is the perturbed flow required to satisfy the stress boundary conditions along the surface. The components are arranged in the order just described in the expression for the velocity in the x-direction:

$$
\begin{aligned}
v_x = \bar{v}_x &+ k(z-S/2)(1-w/d)(1/2\eta) \\
&+ [\bar{v}_x - kz(1-w/d)(1/2\eta)] \sum_{m=1}^{\infty} A_m l_m (l_m z)\exp(-l_m z)\cos(l_m x) \\
&+ (1/2\eta) \sum_{n=1}^{\infty} (R_n/l_n)[(l_n z-1)\exp(-l_n z)\cos(l_n x) \\
&- \sum_{m=1}^{\infty} (A_m/2)[(l_q + l_r(l_q z-1))\exp(-l_q z)\cos(l_q x)
\end{aligned}
$$

$$\pm(l_r \pm l_q(l_r z \mp 1))\exp(\mp l_r z)\cos(l_r x))] \qquad (26a)$$

$$v_z = -[\bar{v}_x - kz(1 - w/d)(1/2\eta)] \sum_{m=1}^{\infty} A_m l_m (1 + l_m z)\exp(-l_m z)$$

$$\sin(l_m x) - (1/2\eta) \sum_{n=1}^{\infty} (R_n/l_n)[l_n z \exp(-l_n z)\sin(l_n x)$$

$$- \sum_{m=1}^{\infty} (A_m/2)[l_q(1 + l_r z)\exp(-l_q z)\sin(l_q x)$$

$$+ l_r(1 \pm l_q z)\exp(\mp l_r z)\sin(l_r x))]. \qquad (26b)$$

Here

$$A_m = (4S/w)d(1/m\pi)^2\cos[m\pi(1 - w/d)/2];\ \text{for all } m \qquad (26c)$$

$$R_m = (2k/n\pi)\sin[n\pi(1 - w/d)/2];\ \text{odd n} \qquad (26d)$$

$$q = [(m/n)+1]; \quad r = [(m/n)-1]; \quad l_q = ql_n; \quad l_r = rl_n \qquad (26e)$$

The upper signs in eqs. (26a) and (26b) are selected for $m > n$, and the lower signs are selected for $m < n$

The derivation of expressions for stresses and the drag parameter, K, is similar to that discussed in connection with equations (2)-(4) in Chapter II. I introduce a drag parameter, K,

$$K = (F - s/d)kp/\bar{v}_x\mu \tag{27}$$

where $p = 2s/(d-w)$, k is the adhesional drag and F is a factor, the value of which is determined as follows. For $K = 1$, I set the velocity equal to zero at $x = 0$, $z = 1$, in eq. 26a. Substituting eq. 27 into (eq. 26a)$_{x=0,\ z=1}$ and solving for F

$$F = \sum_{n=1}^{\infty} \sum_{m=1}^{\infty} \{ [(l_n - 1)\exp(-l_n) + A_m[-l_q - l_r(l_q - 1)]\exp(-l_q)$$

$$\pm A_m[-l_r \mp l_q(l_r \mp 1)]\exp(\mp l_r)][-2d/(d-w)](1/n\pi)^2 \sin[l_n(d-w)/2]$$

$$+ A_m/d(l_m)^2\exp(-l_m)\} / 1 + A_m(l_m)^2\exp(-l_m) \tag{28}$$

Thus, for $K = 1$ there is no slippage at point (0,1), but there is slippage everywhere else along the interface.

The normalized shear stress σ_{ns}/k is

$$\sigma_{ns}/k = p/d$$

$$+\sum_{n=1}^{\infty}\sum_{m=1}^{\infty}[(2/n\pi)\sin(n\pi p/d)[(l_n z-1)\exp(-l_n z)\cos(l_n x)$$

$$+(A_m/2)q[-l_q - l_r(l_q z-1)]\exp(-l_q z)\cos(l_q x)$$

$$+(A_m/2)r[-l_r \mp l_q(l_r z \mp 1)]\exp(\mp l_r z)\cos(l_r x) \qquad (29)$$

where $p = (d+w)/2$.

The expressions for stresses and velocities converge for large m and n if z is positive; that is, for points in the fluid that lie above midheight on the ramp. The expressions for stresses converge more slowly than those for velocities, because the Fourier components of the velocities converge according to $1/m$ and $1/n^2$ whereas those for the stresses converge according 1 and $1/n$. Equation (26a) and (26b) diverge for z negative, that is, for points in the fluid that lie below midheight on the ramp. I have elected not to compute velocities and stresses for points below midheight on the ramp, but I could have performed the computations by using plus and minus options as I did for parameter r in equations (26a) and (26b).

```
1.05 T !,"STORED UNDER <SPLAY.BAL>"
1.08 A !,"RATIO OF SHEAR STRENGTH/VISCOUS SHEAR STRESS?",KK
1.09 S MX=31;S NX=(MX+1)/2;X FPRM(2,120);D 1.97
1.10 S  PI=3.141592653б;S T=10;A !,"SLOPE OF RAMPS?, 2S/W", SW
1.11 D 1.96;T "    P/S",1/SP,"      W/S",1/SW, "  2P/W",2*SW/SP
1.12 A !,"MAXIMUM DISPLACEMENT FACTOR (FRACTION OF S)?",ST
1.13 S L=PI*SD;A !,"NO. TIME INCR.?",T;F N=1,NX;S LN=L*N;D 12.4
1.14 T !,"RAMP IS AT 0,0 COORDS";S SL=0;S JQ=0;F M=1,2,MX;D 9
1.15 T !,"MAX SLOPE",SL;A !,"WANT INTERFACE? YES=PLUS NO.",WW
1.16 I (WW)1.17,1.17;T !,"INTERFACE,X,ZETA";S XM=5/SW;S XI=5;D 8
1.17 D 11;D 1.95;I (OO)10.1;A !,"X-LEFT?",XL;I (XL)1.2,1.9,1.2
1.19 T !!,"TIME STEP   OLD POSITIONS,X,Z   NEW POSITIONS,XX,ZZ"
1.20 A !,"X-RIGHT?",XR,"  NUMBER OF POINTS?",IM
1.21 S AF=KK*ST*SP/((BQ)*T);F N=1,NX;S LN=N*L; D 12
1.23 S V=-AF*SD/SP
1.25 S XI=(XR-XL)/(IM-1);S X=XL-XI
1.30 T !,"POSITION OF BASE IS -1.0"
1.40 A !,"Z-POSITION OF LAYER?",Z
1.45 D 1.19;T "  DX        DZ      DZ/DX"
1.60 S X=X+XI;I (X-XR)3.1,3.1,1.7
1.70 G 1.4
1.90 Q
1.95 T !,"DO A SINGLE POINT? Y=NEG. NO.";A OO
1.96 S SD=1/SD;S SW=SW/2;S SP=2/(1/SD-1/SW);T !,"  D/W",SW/SD
1.97 A !,"SPACING OF RAMPS? D/S",SD

3.10 S XX=X;S ZZ=Z
3.12 T !,"TIME STEPS",!
3.16 F I=1,T;T %3.01,I;D 4
3.30 T !,%8.04,X,Z,"      ",XX,ZZ
3.90 G 1.6

4.05 S DX=0;S DZ=0;S SX=0;S SZ=0
4.11 F M=1,2,MX;S LM=L*M;D 5
4.12 F N=1,NX;S LN=L*N;D 7;F M=1,2,MX;S LM=L*M;D 6
4.15 S T4=AF*(ZZ-1)*SD/SP
4.18 S BZ=SZ+DZ;S BX=DX+SX+T4+ST/T
4.20 S ZZ=ZZ+BZ;S XX=XX+BX

5.10 S TT=FEXP(-LM*ZZ)
5.14 S T2=LM*ZZ
5.30 S DX=DX+(ST/T+V)*AM(M)*LM*T2*TT*FCOS(LM*XX)
5.40 S DZ=DZ-(ST/T+V)*AM(M)*LM*(T2+1)*TT*FSIN(LM*XX)
```

```
6.12 S RR=(M/N)-1;S QQ=(M/N)+1;S LQ=LN*QQ;S LR=LN*RR;S IY=1
6.13 I (RR)6.14,6.16,6.17
6.14 S IZ=-1;G 6.25
6.16 S IZ=1;S IY=0;G 6.25
6.17 S IZ=1
6.25 S ER=FEXP(-FABS(LR)*ZZ);S EQ=FEXP(-LQ*ZZ)
6.27 S JN=B(N)*(AM(M)/2)
6.30 S SX=SX+JN*(-LQ-LR*(LQ*ZZ-1))*EQ*FCOS(LQ*XX)
6.35 S SX=SX-JN*IZ*(LR+IZ*LQ*(LR*ZZ-IZ))*ER*FCOS(LR*XX)*IY
6.40 S SZ=SZ-JN*(-LQ-LR*(LQ*ZZ))*EQ*FSIN(LQ*XX)
6.45 S SZ=SZ+JN*(LR+IZ*LQ*(LR*ZZ))*ER*FSIN(LR*XX)*IY

7.10 S TP=FEXP(-LN*ZZ);S T1=LN*ZZ
7.20 S SX=SX+B(N)*(T1-1)*TP*FCOS(LN*XX)
7.30 S SZ=SZ-B(N)*T1*TP*FSIN(LN*XX)

8.05 F X=-XM,XI,XM;S ZT=0;D 8.1;T !,X,ZT;D 18
8.07 R
8.10 F M=1,2,MX;S LM=M*L;S AM=AM(M);D 8.2
8.15 R
8.20 S ZT=ZT+AM*FCOS(LM*X)

9.10 S LM=M*L;S AM(M)=8*(1/SD)*(SW/((M*PI)^2))*FCOS(LM/SP)
9.20 S JQ=JQ+AM(M)*(LM^2)*FEXP(-LM)
9.30 S SL=SL+AM(M)*LM*FSIN(M*PI/2)

10.10 D 1.45
10.18 D 1.21;D 1.23;D 3.12
10.19 D 1.3;A !,"X/S?",X,"    Z/S?",Z
10.20 S XX=X;S ZZ=Z;F I=1,T;T %3.00,I;D 4;D 10.3
10.25 Q
10.30 T !,%8.04,X,Z,"        ",XX,ZZ,BX,BZ
10.40 I (BX)10.5,10.9,10.5
10.50 T BZ/BX
10.90 R

11.05 S BQ=0;F N=1,NX;S LN=N*L;D 14;F M=1,2,MX;S LM=M*L;D 13
11.10 S BQ=(BQ+SD*JQ)/(JQ+1)
11.20 T !,"FACTOR  F",BQ
11.30 R

12.20 S B(N)=(AF/SD)*(1/((N*PI)^2))*FSIN(LN/SP)
12.40 S RN(N)=(2/(N*PI))*FSIN(LN/SP)

13.10 S RR=(M/N)-1;S QQ=(M/N)+1;S IY=1
13.15 I (RR)13.16,13.17,13.19
13.16 S IZ=-1;G 13.2
13.17 S IZ=1;S IY=0;G 13.2
13.19 S IZ=1
13.20 S LQ=LN*QQ;S LR=LN*RR
13.30 S TQ=FEXP(-LQ);S TR=FEXP(-FABS(LR))
13.60 S GQ=(AM(M)/2)*(-LQ-LR*(LQ-1))*TQ
13.70 S HQ=-(AM(M)/2)*IZ*(LR+IZ*LQ*(LR-IZ))*TR*IY
13.80 S BQ=(GQ+HQ)*CQ+BQ
```

```
14.05 S DQ=(LN-1)*FEXP(-LN)
14.20 S CQ=(-SP/SD)*(1/((N*PI)^2))*FSIN(LN/SP)
14.30 S BQ=BQ+DQ*CQ

15.05 S DX=0;S DZ=0
15.07 A !,"XX?",XX,"    ZZ?",ZZ
15.10 F N=1,NX;S LN=N*L;D 16;F M=1,2,MX;S LM=M*L;D 17
15.20 T !,"DX,DZ,DZ/DX",DX,DZ,DZ/DX
15.30 Q

16.10 S DX=DX-B(N)*FCOS(LN*XX)

17.10 D 6.12
17.11 I (RR)17.12,17.13,17.14
17.12 S IZ=-1;G 17.16
17.13 S IZ=1;S IY=0;G 17.16
17.14 S IZ=1
17.16 S TP=B(N)*AM(M)/2
17.20 S DX=DX-(2*TP*LN)*FCOS(LQ*XX)
17.30 S DX=DX+IZ*TP*2*LN*FCOS(LR*XX)*IY
17.50 S DZ=DZ+TP*(LQ*FSIN(LQ*XX)+LR*FSIN(LR*XX))*IY

18.05 S XX=X;S ZZ=ZT
18.10 S AQ=0;S KQ=0;S SL=0;S SS=0;S BQ=0;S CQ=0;S DQ=0
18.15 F M=1,2,MX;S LM=M*L;S SL=SL-AM(M)*LM*FSIN(LM*XX)
18.20 F N=1,NX;S LN=N*L;D 19;F M=1,2,MX;S LM=M*L;D 20
18.25 S SH=AQ*SL+SD/SP+BQ+KQ+DQ
18.30 T "    SH STR. FROM B.C.",SS+SD/SP
18.40 T "    SH STR. FROM SOLUT.",SH
18.60 R

19.05 S TP=(1-LN*ZZ);S T1=FEXP(-LN*ZZ)
19.08 S CN=FCOS(LN*XX)
19.09 S SN=FSIN(LN*XX)
19.10 S AQ=AQ+2*RN(N)*TP*T1*SN
19.20 S BQ=BQ+RN(N)*TP*T1*CN
19.30 S SS=SS+RN(N)*CN
19.40 S GQ=RN(N)*TP*T1*SN+GQ
19.50 S P=P-RN(N)*T1*SN

20.05 D 6.12;I (RR)20.06,20.07,20.08
20.06 S IZ=-1;G 20.09
20.07 S IZ=1;S IY=0;G 20.09
20.08 S IZ=1
20.09 S T1=FEXP(-LQ*ZZ);S CQ=FCOS(LQ*XX)
20.10 S KQ=KQ+RN(N)*QQ*(LQ+LR*(LQ*ZZ-1))*(AM(M)/2)*T1*CQ
20.20 S T2=FEXP(-FABS(LR)*ZZ)*AM(M)/2;S CR=FCOS(LR*XX)
20.25 S SQ=FSIN(LQ*XX);S SR=FSIN(LR*XX)
20.30 S DQ=DQ+RN(N)*RR*(LR+IZ*LQ*(LR*ZZ-IZ))*T2*CR*IY
20.40 S HQ=HQ+RN(N)*QQ*(AM(M)/2)*(LQ+LR*(LQ*ZZ-1))*T1*SQ
20.50 S IQ=IQ+IY*RR*IZ*T2*(LR+IZ*LQ*(LR*ZZ-IZ))*SR
20.60 S P=P+RN(N)*QQ*(AM(M)/2)*LR*T1*SQ
20.70 S P=P+RN(N)*IY*RR*LQ*T2*SR*IY
```

```
21.10 T !,"COMPUTE STRESSES"
21.20 A !,"XX?",XX,"    ZZ?",ZZ
21.30 S AQ=0;S KQ=0;S P=0;S BQ=0;S CQ=0;S DQ=0;S HQ=0;S GQ=0;S IQ=0
21.40 F N=1,NX;S LN=N*L;D 19;F M=1,2,MX;S LM=M*L;D 20
21.50 S SX=GQ+H2+IQ;S SS=SD/SP+BQ+KQ+DQ
21.55 F M=1,2,MX;S LM=L*M;D 22
21.60 T !," SXX",SX,"     SXZ",SS
21.70 T !,"TAN 2THETA(SIG 1)",SS/SX
21.73 S J2=FSQT((SX^2)+(SS^2))
21.74 T !,"YIELD FUNCTION",J2+P*0.5774,"     P",P
21.76 A !,"ANGLE OF LAYERING + OR -?, DEGREES",AL
21.78 S SN=FSIN(2*AL*PI/180);S CN=FCOS(2*AL*PI/180)
21.80 S DS = 2*SX*CS+2*SS*SN;S SH = -SX*SN+SS*CN
21.85 T !,"SSS-SNN",DS,"    SNS",SH

22.10 S S T1=-2*(ST/T+V)*(LM^2)*AM(M)*(LM*ZZ/AF)*FEXP(-LM*ZZ)
22.20 S SS=SS+T1*FCOS(LM*XX);S SX=SX+T1*FSIN(LM*XX)
*
```

```
1.05 T !,"STORED UNDER <RAMP.STR>"
1.08 A !,"RATIO OF SHEAR STRENGTH*TIME TO VISCOSITY?",K1
1.09 S NX=31;X FPRM(2,120)
1.10 S PI=3.14159265536;S T=10;S WD=.1;S SW=0.2;S SD=SW*WD
1.11 T !,"D/W",1/WD,"   W/S",1/SW,"    D/S",1/(SW*WD)
1.12 A !,"MAXIMUM DISPLACEMENT FACTOR (FRACTION OF S)?",ST
1.13 A !,"NUMBER OF TIME INCREMENTS?(>10)",T
1.14 F J=1,2,NX;D 9
1.15 S L=PI*SD;A !,"WANT INTERFACE? YES PLUS NO.",OO
1.16 I (OO)1.17,1.17;T !,"INTERFACE,X,ZETA";S XM=1/SW;S XI=XM/10;D 8
1.17 D 1.95;I (OO)10.1;A !,"X-LEFT?",XL;I (XL)1.2,1.9,1.2
1.19 T !!,"TIME STEP   OLD POSITIONS,X,Z   NEW POSITIONS,XX,ZZ"
1.20 A !,"X-RIGHT?",XR,"  NUMBER OF POINTS?",IM
1.25 S XI=(XR-XL)/(IM-1);S X=XL-XI
1.30 T !,"POSITION OF BASE IS -0.5"
1.40 A !,"Z-POSITION OF LAYER?",Z
1.45 D 1.19
1.60 S X=X+XI;I (X-XR)3.1,3.1,1.7
1.70 G 1.4
1.90 Q
1.95 T !,"W",1/SW;T !,"DO A SINGLE POINT? Y=NEG. NO.";A OO

3.10 S XX=X;S ZZ=Z
3.12 T !,"TIME STEPS",!
3.16 F I=1,T;T %3.01,I;D 4
3.30 T !,%8.04,X,Z,"      ",XX,ZZ
3.90 G 1.6

4.05 S DX=0;S DZ=0;S UX=0;S UZ=0;S WX=0
4.10 F N=1,2,NX;S LN=N*L;D 5
4.20 S XX=XX+ST/T+DX;S ZZ=ZZ+DZ

5.07 S CS=FCOS(LN*XX);S AN=AN(N)
5.10 S TP=FEXP(-LN*ZZ);S SN=FSIN(LN*XX)
5.12 S T1=LN*ZZ
5.14 S R=R(N);S T1=LN*ZZ;S TR=TP^2
5.16 S MQ=R*(T1-1)*TP;S PQ=-R*T1*TP
5.17 S MM=MQ*CS;S P=PQ*SN;S UX=UX-LN*MQ*SN;S UZ=UZ-LN*R*(T1-2)*TP*CS
5.18 S WX=WX-PQ*LN*CS;F M=1,2,NX;D 6
5.20 S TX=AN*(ST/T)*LN*T1*TP
5.25 S TZ=AN*(ST/T)*LN*(T1+1)*TP
5.30 S DX=DX+MM+TX*SN;S DZ=DZ+P+TZ*CS
5.40 S UX=UX+TX*LN*CS;S UZ=UZ-LN*LN*AN*(ST/T)*(T1-1)*SN
5.60 S WX=WX-TZ*LN*SN
```

```
6.10 S RR=(M/N)-1;S QQ=(M/N)+1
6.13 I (RR)6.14,6.15,6.15
6.14 S IZ=-1;G 6.2
6.15 S IZ=1
6.20 S LR=LN*RR;S LQ=LN*QQ;S SQ=FSIN(LQ*XX);S CQ=FCOS(LQ*XX)
6.25 S SR=FSIN(LR*XX);S CR=FCOS(LR*XX)
6.30 S AA=-(R/2)*LQ*AN(M);S CC=-(R/2)*LR*AN(M)
6.40 S BB=CC;S DD=IZ*AA
6.50 S TR=FEXP(-FABS(LR)*ZZ);S TQ=FEXP(-LQ*ZZ)
6.52 S MQ=(AA+BB*(LQ*ZZ-1))*TQ
6.54 S MR=IZ*(CC+DD*(LR*ZZ-IZ))*TR
6.56 S PQ=(AA+BB*(LQ*ZZ))*TQ
6.58 S PR=(CC+DD*(LR*ZZ))*TR
6.60 S MM=MM+MQ*SQ+MR*SR
6.70 S P=P+PQ*CQ+PR*CR
6.80 S UX=UX+LQ*MQ*CQ+LR*MR*CR
6.90 S WX=WX-LQ*PQ*SQ-LR*PR*SR
6.95 S UZ=UZ-LQ*(AA+BB*(LQ*ZZ-2))*TQ*SQ
6.98 S UZ=UZ-IZ*LR*(CC+DD*(LR*ZZ-2*IZ))*TR*SR

8.05 F X=-XM,XI,XM;S ZT=0;D 8.1;T !,X,ZT
8.07 R
8.10 F N=1,2,NX;S AN=AN(N);D 8.2
8.15 R
8.20 S ZT=ZT+AN*FSIN(L*N*X)

9.02 S T4=FSIN((J*PI/2)*WD)
9.03 S R(J)=2*K1*T4/(((J*PI)^2)*SD*T)
9.05 I (J*WD-1)9.1,9.9,9.1
9.10 S T1= FCOS(J*PI*WD/2);S T2=FCOS(J*PI/2)
9.20 S T3=(1/(PI*(1/WD-J)))*FSIN((1-J*WD)*PI/2)
9.30 S T4=(1/(PI*(1/WD+J)))*FSIN((1+J*WD)*PI/2)
9.40 S AN(J)=(2/(J*PI))*(T1-T2)+T3-T4
9.80 R
9.90 S AN(J)=-(2/(J*PI))*FCOS(J*PI/2)
```

```
10.10 D 1.3;A !,"X/S?",X,"   Z/S?",Z
10.15 F J=1,2,NX;D 9
10.17 S A(1,1)=1;S A(2,2)=1;S A(2,1)=0;S A(1,2)=0
10.20 S XX=X;S ZZ=Z;F I=1,T;D 4;D 11
10.30 T !,%8.04,X,Z,"        ",XX,ZZ
10.40 Q

11.10 C COMPUTE FINITE STRAINS
11.20 S B(1,1)=1+UX;S B(1,2)=UZ;S B(2,1)=WX;S B(2,2)=1-UX
11.30 S C(1,1)=A(1,1)*B(1,1)+A(2,1)*B(1,2)
11.32 S C(1,2)=A(1,2)*B(1,1)+B(1,2)*A(2,2)
11.34 S C(2,1)=B(2,1)*A(1,1)+A(2,1)*B(2,2)
11.36 S C(2,2)=A(1,2)*B(2,1)+A(2,2)*B(2,2)
11.40 F J=1,2;F K=1,2;S A(J,K)=C(J,K)
11.50 F J=1,2;F K=1,2;S C(J,K)=A(J,K)^2
11.55 S I1=0;F J=1,2;F K=1,2;S I1=I1+C(J,K)
11.60 S I2=(C(1,1)+C(2,1))*(C(2,2)+C(1,2))
11.65 S I2=I2-(A(1,1)*A(1,2)+A(2,2)*A(2,1))^2
11.70 S S=(1/2)*(I1+FSQT((I1^2)-4*I2));S S=FSQT(S)
11.75 S TN=2*(A(1,1)*A(2,1)+A(2,2)*A(1,2))
11.76 S TN=TN/(C(1,1)+C(1,2)-C(2,1)-C(2,2))
11.80 S PH=(A(2,1)-A(1,2))/(A(1,1)+A(2,2))
11.82 S D=A(1,1)*A(2,2)-A(1,2)*A(2,1)
11.85 T !,"TIME STEP",I,"   MAX. STRETCH",S
11.90 T "   MIN STRETCH",1/S,"    TAN 2THETA",TN
11.95 T !, "   TAN ROTATION",PH,"  DILATION",D,"   I1,I2",I1,I2
11.96 D 10.3;T !
11.99 R
```

Translation over a frictionless detachment surface and ramp

In the preceding derivations, the solutions for drag are presented for the general case of drag applied to any boundary that can be described with a Fourier, sinusoidal series.The actual problems posed in Chapters I and II deal with detachment surfaces of different forms, although each is described with a Fourier, sinusoidal series. In the following derivation, the interface is described by ζ (equation 3a). However, A_m has one value in Chapter I and a different value in Chapter II. Either value is valid in the general solution.

The boundary conditions for the previous problems are given in equations (3a and 4). In this problem, however, the solution is for the perturbed velocity as a result of the interaction of the mean flow and the ramp. The mean flow must enter into the boundary condition given in equation (4). Thus, the position of the interface is

$$\partial\zeta/\partial t = 0 = [\tilde{v}_z]_\zeta - [\tilde{v}_x + \bar{v}_x]_\zeta(\partial\zeta/\partial x) \qquad (30)$$

Using equation (3a) and solving for the perturbed velocity in the z direction at the interface, to first order,

$$[\tilde{v}_z]_\zeta = \bar{v}_x A_m l_m \cos(l_m x) \qquad (31)$$

The velocity potential, ψ, which for the previous problems had been of the form of equation (2a) with added terms to include all the waveforms, is now of the form

$$\psi = (1/l)([c + d(lz)]\exp(lz)+[a + b(lz)]\exp(-lz))\sin(lx) \qquad (32)$$

The velocity potential, ψ is chosen with this form so that $\tilde{v}_z$ will be a cosinusoidal function of x as specified in equation (31).

Solving for the velocities and stresses using equations (2),

$$v_x = \sum_{m=1}^{\infty} [a_m + b_m(l_m z - 1)]\exp(-l_m z)\sin(l_m x) \qquad (32a)$$

$$v_z = \sum_{m=1}^{\infty} [a_m + b_m(l_m z)]\exp(-l_m z)\cos(l_m x) \tag{32b}$$

$$\sigma_{xz} = \sum_{m=1}^{\infty} -2\mu l_m[a_m + b_m(l_m z - 1)]\exp(-l_m z)\sin(l_m x) \tag{32c}$$

Because the interface is frictionless, the shear stress at the interface, σ_{ns} [equation (5)] is zero and to first order, at $z=\zeta$,

$$\sigma_{ns} = 0 = [\sigma_{xz}]_{z=\zeta} \tag{33}$$

Solving for the constants, using equations (32c and 33)

$$a_m = b_m \tag{34}$$

and equation (31)

$$a_m = \bar{v}_x A_m l_m \tag{35}$$

This completes the solution for the constants. They are substituted back into equations (32) to compute the perturbed velocities.

Translation over a frictionless thrust ramp with uniform shortening

In this problem, the addition of uniform shortening has altered the mean flow such that it is now described by the equations,

$$\bar{v}_x = \bar{v}_{0x} + (1/4\mu)(\bar{\sigma}_{xx} - \bar{\sigma}_{zz})x \tag{36a}$$

$$\bar{v}_z = -(\partial \bar{v}_x/\partial x)z \tag{36b}$$

The vertical velocity is assumed to be zero at the unperturbed, rigid interface. The position of zero horizontal velocity is determined by the value of $\bar{v}_{0x}$.

The position of the interface is modified from equation (30) to include a vertical mean flow

$$\partial\zeta/\partial t = 0 = [\tilde{v}_z + \bar{v}_z]_\zeta - [\tilde{v}_x + \bar{v}_x]_\zeta(\partial\zeta/\partial x) \tag{37}$$

where ζ is defined by equation (3a).

The other boundary equations are

$$\sigma_{nn} = \tilde{\sigma}_{zz} + \bar{\sigma}_{zz} \tag{38a}$$

$$\sigma_{ns} = \tilde{\sigma}_{xz} + (\bar{\sigma}_{zz} - \bar{\sigma}_{xx})\partial\zeta/\partial x \tag{38b}$$

Evaluating the vertical perturbed flow at the interface [substitute equation (3a) and equations (36) into equation (37) and solving for the vertical perturbed flow at the interface],

$$[\tilde{v}_z]_\zeta = \sum_{m=1}^{\infty} (\partial \bar{v}_x/\partial x)\, A_m \sin(l_m x)$$

$$+ [\bar{v}_{0x} + (\partial \bar{v}_x/\partial x)\, A_m\, l_m \cos(l_m x) \tag{39}$$

In order to determine the form of the velocity potential, ψ, a trial solution is selected of the form

$$\psi = F \cos(l_m x) + G\,(l_m x) \sin(l_m x) \tag{40}$$

Substituting equation (40) into the biharmonic equation

$$- l_m^4 [(4G-F)\cos(l_m x) - G(l_m x)\sin(l_m x)]$$

$$+ 2 l_m^2 (2d^2G/dx^2 - d^2F/dz^2)\cos(l_m x)$$

$$-2 l_m^2 (d^2G/dz^2)(l_m x)\sin(l_m x)$$

$$+ (d^4F/dz^4)\cos(l_m x) + (d^4G/dz^4)(l_m x)\sin(l_m x) = 0 \qquad (41)$$

The general solution to G is

$$G = [a + b(l_m z)]\exp(-l_m z) + [c + d(l_m z)]\exp(l_m z) \qquad (42a)$$

and F is

$$F = [A + B(l_m z)]\exp(-l_m z) + [C + D(l_m z)]\exp(l_m z)$$

$$+ b(l_m z)^2\exp(-l_m z) + d(l_m z)^2\exp(l_m z) \qquad (42b)$$

Using equations (42) to determine the form of ψ, assuming that the perturbed velocities vanish at plus infinity,

$$\psi = \{[(A + B(l_m z)) + b(l_m z)^2]\cos(l_m x)$$

$$+ [a + b(l_m z)](l_m x)\sin(l_m x)\}\exp(-l_m z) \qquad (43)$$

Solving for the velocities,

$$\tilde{v}_x = l_m\{[A+B(l_m z-1)+b[(l_m z)^2 - 2(l_m z)]]\cos(l_m x)$$

$$+ [a+b(l_m z-1)](l_m x)\sin(l_m x)\}\exp(-l_m z) \quad (44a)$$

$$\tilde{v}_z = -l_m\{[A+B(l_m z) + b(l_m z)^2 - [a+b(l_m z)]]\sin(l_m x)$$

$$- [a+b(1_m z)](l_m x)\cos(l_m x)\}\exp(-l_m z) \quad (44b)$$

$$\hat{\sigma}_{xz} = -2\mu l^2\{[A+B(l_m z-1)-a+b[(l_m z)^2-3(l_m z)+1]]\cos(l_m x)$$

$$+ [a+b(l_m z-1)](l_m x)\sin(l_m x)\}\exp(-l_m z) \quad (44c)$$

Solving for the constants, using equation (39) and assuming that the horizontal velocity is zero at $x = 0$,

$$A = 0 \quad (45a)$$

$$a = (\partial \bar{v}_x/\partial x)A_m/l_m \quad (45b)$$

In order for there to be free slip at the interface, the shear stress [equation (38b)] must be zero, which requires that

$$b = a \tag{45c}$$

$$B = 2(\partial \bar{v}_x / \partial x) A_m / l_m = 2a \tag{45d}$$

This completes the solution for the constants. These values are substituted back into the equations for the velocities [equations (44)]. To solve the problem completely, the solution must include a uniform translation term which is added to the solution.